communications materials

A Nature Portfolio journal

Review article

https://doi.org/10.1038/s43246-025-00976-z

Spin-modulated catalysis in sulfur cathodes for improved performance in lithium–sulfur batteries

Chao Yue Zhang[1,2,12], Jing Yu[1,3,12], Chen Huang[1], Gema Cabello[4], Xuede Qi[1,5], Guo Wen Sun[2], Chaoqi Zhang[6], Ren He[1], Dawei Yang[7], Canhuang Li[1], Junshan Li[8], Xueqiang Qi[5], Javier Rubio Garcia[4] ✉, Marta Estrader[9,10] ✉, Jordi Arbiol[3,11], Jin Yuan Zhou[2] ✉ & Andreu Cabot[1,11] ✉

The rapid growth of electric vehicles and the increasing integration of renewable energy into the grid have heightened the demand for high-capacity energy storage systems based on abundant, low-cost materials. To address the limitations of conventional ion-intercalation batteries, conversion-type electrodes have gained significant attention, as their energy storage relies on chemical redox reactions often requiring activation or acceleration via electrocatalysis. Recent studies reveal that electrocatalytic activity is governed not only by active-site density and charge-carrier availability, but also by the spin states of electrons within the catalyst. Consequently, understanding the role of electronic spin states in battery performance, and how to manipulate them to enhance energy storage, has become a critical research frontier. This review provides a comprehensive overview of current strategies to modulate spin states in electrocatalysts for conversion-type cathodes. While external magnetic fields remain the primary method to probe and control electron spin, more practical and scalable approaches, such as atomic coordination engineering and surface spin filters, are emerging. Particular focus is given to sulfur cathodes, which offer exceptional theoretical energy density and capacity but depend heavily on catalytic hosts to enable efficient sulfur redox reactions. The review also surveys experimental techniques for probing spin states and theoretical approaches for modeling spin-related phenomena at the atomic scale. Finally, it highlights emerging research directions, underscoring the potential of spin-state modulation as a transformative strategy for next-generation energy storage technologies.

The replacement of fossil fuels with renewable energy sources has emerged as a critical challenge in the pursuit of a sustainable energy future. One of the central obstacles in this transition is the development of clean, cost-effective, and scalable energy storage systems, which are essential not only for integrating intermittent renewable sources, such as solar and wind, into the power grid but also for the widespread electrification of transportation. In this context, electrochemical energy storage, particularly in the form of batteries, plays a pivotal role due to its ability to store and deliver electricity efficiently and on demand.

However, current electrochemical energy storage technologies still face limitations in terms of cost, performance, and long-term stability. Among them, lithium-ion batteries (LIBs), which dominate the market, rely on intercalation-type electrodes, such as graphite anodes and transition metal (TM) oxide or phosphate cathodes. While these systems offer good

[1]Catalonia Institute for Energy Research – IREC, Sant Adrià de Besòs, Barcelona, Spain. [2]School of Physical Science & Technology, Lanzhou University, Lanzhou, China. [3]Catalan Institute of Nanoscience and Nanotechnology (ICN2), CSIC and BIST, Campus UAB, Bellaterra, Barcelona, Spain. [4]Schlumberger Cambridge Research, Cambridge, United Kingdom. [5]College of Chemistry and Chemical Engineering, Chongqing University of Technology, Chongqing, China. [6]College of Materials Science and Engineering, Fuzhou University, Fuzhou, China. [7]Henan Key Laboratory of Quantum Materials and Quantum Energy, School of Quantum Information Future Technology, Henan University, Kaifeng, China. [8]Institute for Advanced Study, Chengdu University, Chengdu, PR China. [9]Departament de Química Inorgànica i Orgànica, Universitat de Barcelona, Martí i Franques 1, Barcelona, Spain. [10]Institute of Nanoscience and Nanotechnology (IN2UB), Universitat de Barcelona, Barcelona, Catalonia, Spain. [11]ICREA, Pg. Lluís Companys 23, Barcelona, Spain. [12]These authors contributed equally: Chao Yue Zhang, Jing Yu. ✉e-mail: jrubio@slb.com; martaestrader@ub.edu; zhoujy@lzu.edu.cn; acabot@irec.cat

reversibility and cycle life, they are fundamentally constrained by their limited gravimetric energy density, which typically does not exceed 400 Wh kg^{-1}.

To overcome this bottleneck, the development of novel electrode materials is urgently required. In particular, conversion-type cathodes, such as those based on oxygen, sulfur, and halide chemistries, offer significantly higher theoretical energy densities. These electrodes operate via a chemical transformation reaction between the migrating ions (e.g., Li^+) and the active cathode material, forming new compounds during charge and discharge. Despite their potential, such conversion reactions are often associated with sluggish kinetics, leading to limited rate capability and reduced energy efficiency in secondary battery systems.

As in the case of fuel cells, where catalytic enhancement is essential, electrocatalysts are increasingly recognized as crucial for activating and accelerating these chemical reactions in conversion-type batteries. Their incorporation holds promise for overcoming the inherent kinetic barriers, improving both the reaction reversibility and the overall performance of high-energy battery chemistries[1].

Sulfur cathodes, which operate based on the reaction of metal ions (e.g., Li^+) with sulfur to form metal sulfides (e.g., Li_2S), have attracted particular attention due to their exceptionally high theoretical energy density (~2600 Wh kg^{-1}) and specific capacity (1675 mAh g^{-1}), as well as the abundance and low cost of sulfur. Despite these appealing advantages, secondary sulfur-based batteries have yet to achieve widespread commercial deployment. This is primarily due to a number of performance limitations, including moderate rate capability, high self-discharge rates, low round-trip energy efficiency, and rapid capacity fading over repeated cycles. These issues become particularly severe under the lean-electrolyte and high-sulfur-loading conditions required to realize the high-energy densities that sulfur batteries promise[2,3].

This poor performance is largely attributed to the sluggish kinetics of the sulfur redox reactions (SRRs), which involve the formation of multiple metal polysulfide intermediates during the conversion of elemental sulfur (S_8) into metal sulfides. Figure 1a–c illustrates the specific case of lithium–sulfur batteries (LSBs), which follow a complex multistep pathway. In conventional ether-based electrolytes, this process combines electrochemical and chemical reactions, collectively converting S_8 into lithium sulfide (Li_2S) through a series of soluble lithium polysulfide (LiPS) intermediates, as represented by the overall reaction: $S_8 + 16Li \leftrightarrow LiPSs \leftrightarrow 8Li_2S$[4].

The intermediate polysulfide species generated during cycling are highly soluble in the electrolyte and can diffuse away from the cathode, where they undergo parasitic reactions at the metal anode. This process, known as the polysulfide shuttle effect, arises because reduced polysulfides at the anode migrate back to the cathode and are reoxidized at inappropriate stages of the charge–discharge cycle. Such shuttling, and more broadly the uncontrolled migration of polysulfides through the separator, results in irreversible sulfur loss, metal anode degradation, and a marked decline in charge–discharge capacity. Collectively, these effects compromise the energy efficiency, cycling stability, and self-discharge characteristics of metal–sulfur batteries. To suppress polysulfide migration, minimize self-discharge, enhance sulfur utilization, and support high-rate operation, particularly under the high sulfur loadings required for practical applications, highly active catalytic additives must be incorporated to accelerate SRRs.The electrocatalytic activity of an electrode is governed by several key factors, including its charge and mass transport properties, the density of active sites, and its ability to facilitate electron transfer and effectively interact with the reactant species[5]. Achieving efficient charge and mass transport requires the rational design and engineering of the electrode architecture, ensuring the presence of both continuous pathways for electron and ion transport and a large electrochemically active surface area. This typically involves creating structures with high porosity and extensive surface exposure. In metal–sulfur batteries, the incorporation of porous host materials, such as hollow nanospheres, nanowires[6], nanotubes[7], nanosheets[8], sandwich structures[9], monoatomic or diatomic materials[10], and metal-organic frameworks (MOFs)[11], has proven particularly effective. These structures not only enhance ion transport and active site accessibility but also offer physical confinement for the active material, improving sulfur utilization and stability. Furthermore, efficient charge transport also depends on the intrinsic structural and morphological properties of the electrode material. This can be further optimized through strategies, such as lattice distortion[12,13], the introduction of structural defects[14], heteroatom doping[15], and the construction of heterostructures[16].

The ability of a catalyst to interact with reactants and facilitate electron transfer is a fundamental determinant of its intrinsic activity and overall efficiency. This capability is governed by the position and occupancy of the catalyst's electronic energy levels, which in turn influence the binding energies of reaction precursors, intermediates, and products[17]. In a simplified framework, the most effective catalysts are those that exhibit intermediate adsorption strengths, strong enough to activate reactants but weak enough to allow facile desorption of products[15,18]. To accelerate the identification of promising catalytic materials, this concept can be further reduced to a single electronic descriptor: the position of the d-band center relative to the Fermi level[19]. This parameter has been widely adopted as a reliable predictor of catalytic activity, enabling the rapid screening of candidate materials[20–22].

Within this framework, efforts to optimize electrocatalytic reaction sites have focused primarily on modulating composition, atomic coordination, and local chemical environment to modulate the electronic energy levels and improve catalytic performance[23]. In this context, the interactions between various TM-based compounds and polysulfides have been extensively studied, including systems based on carbides[24], phosphides[7], sulfides[25], nitrides[18], selenides[26,27], and tellurides[28],

While these studies have extensively examined the electronic structure of various materials, they often overlook a fundamental electron property that plays a crucial role in defining electronic state occupation, charge transfer, chemical bonding, and reactivity: its intrinsic angular momentum, or spin. Despite its pivotal role in these processes, electron spin remains largely underexplored in the field of electrocatalysis[29,30].

Quantum mechanics has long established the profound impact of electron spin on molecular structures and the electronic and magnetic properties of materials[31–33]. The Pauli exclusion principle dictates that two electrons occupying the same spatial eigenstate must have opposite spins, a rule that is fundamental to the formation of chemical bonds. Additionally, the interaction of electrons with nuclei, influenced by the electrons' intrinsic charge and angular momentum, is key in defining a material's electronic structure[34]. The interaction between the electron spin and its orbital angular momentum also affects charge transport[35].

Despite being fundamental to our understanding of material structure, properties, and reactivity, the critical role of electron spin in electrochemical reactions has only begun to receive significant attention over the past decade, and even more recently within the field of electrochemical devices, such as batteries. It is only in recent years that the spin configuration of catalytically active sites has been recognized as a key factor influencing both the thermodynamics and kinetics of electrochemical processes[36].

A notable example can be found in the oxygen cathode of metal–air batteries, where the spin state of the active site has been shown to affect electron transfer spin pairing, thereby modulating both the reaction rate and product selectivity[37]. In such systems, the effect is closely related to the selective formation of triplet oxygen, the ground-state configuration of O_2, through spin alignment of unpaired electrons in intermediate radical species adsorbed on the catalyst surface[38,39]. This alignment facilitates spin-conserved pathways, improving catalytic efficiency and selectivity.

Emerging from the principles of spin chemistry, the field of spin catalysis is gaining increasing attention as a novel approach to controlling chemical reactivity. It is founded on the fundamental principle that chemical reactions are spin-selective, that is, reactions are only allowed (or proceed efficiently) when the total spin state of the products matches that of the reactants, whereas those involving a spin transition are forbidden or significantly slowed down[35].

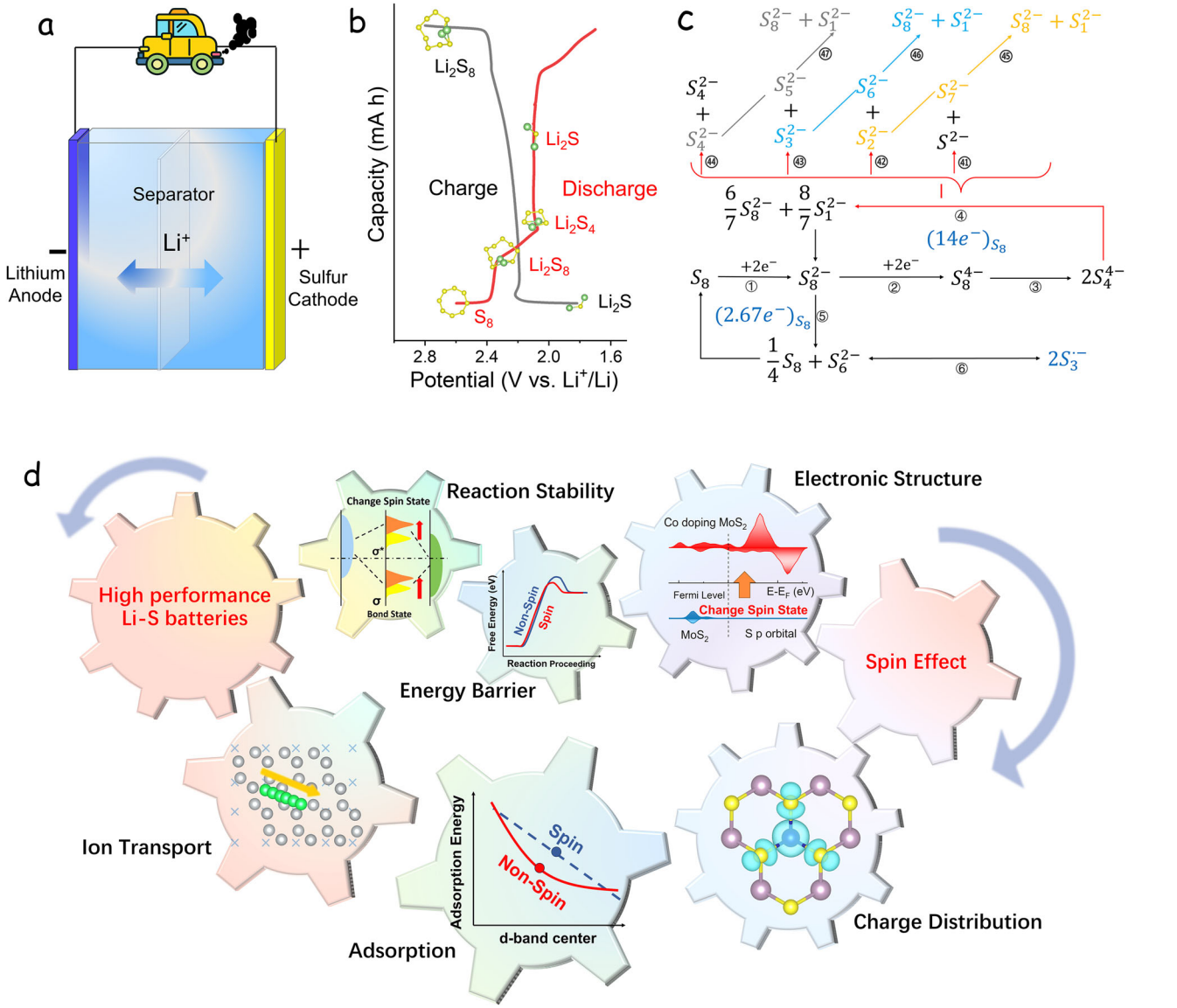

Fig. 1 | The effect of spin catalysis in LSBs. a Schematic illustration of an LSB. **b** Typical charge-discharge voltage curves of an LSB in an ether-based electrolyte. **c** Scheme of one of the complex sulfur reduction reaction mechanisms proposed. **d** Schematic diagram of the spin effect for realizing high-performance LSBs.

Spin catalysis introduces new paradigms and methodologies into electrocatalysis research by enabling the manipulation of reaction pathways through control of the spin states of the catalyst. This can be achieved by modifying the coordination environment of metal active sites to tune their spin configuration, incorporating magnetic materials, applying external magnetic fields, or integrating chiral components that promote spin-selective electron transfer[40–42].

To harness these effects, spin catalysis demands the rational design and precise engineering of catalyst crystal structures and chemical compositions, with careful consideration of the spin configuration as a critical performance factor[43]. This emerging strategy holds significant potential for advancing the design of next-generation electrocatalysts, particularly for complex multi-electron conversion reactions.

In the field of metal-sulfur batteries, various innovative approaches have been recently proposed to tune the electronic structure and manipulate the spin of TM-based materials to improve the reactivity of polysulfides in SRR catalytic conversion, including tuning the catalyst coordination environment or applying an external magnetic field to the material[44–50]. As schematized in Fig. 1d, the electron spin can influence the catalyst surface electronic structure and charge distribution, which can alter the ion transfer ability, energy barrier, adsorption capacity, and stability of reaction intermediates, ultimately controlling the reaction rate and selectivity[37,51–55]. Additionally, as later detailed in this review, spin alignment in ferromagnetic (FM) materials can locally generate magnetic fields and field gradients in the volume of electrolyte close to the electrode that can improve ion diffusion and concentration, reduce the interface diffusion layer, and even block the transport of polysulfides in sulfur cathodes and the growth of dendrites in metal anodes[44,56–59].

These pioneering studies highlight how robust theoretical frameworks, combined with advanced synthetic strategies, can be leveraged to modulate catalyst spin states and develop more effective materials for metal–sulfur batteries. Yet, this research field remains in its infancy, with many promising approaches still unexplored and countless others yet to be discovered. Realizing the potential of spin-state engineering for the systematic design of catalytic materials across diverse elements, structures, and compositions requires a deeper understanding of the interplay between electron spin states and SRR mechanisms. Equally critical is the ability to synthesize catalysts with strong spin polarization effects, materials capable of modulating the spin configuration of reaction intermediates to enhance both catalytic activity and selectivity[60].

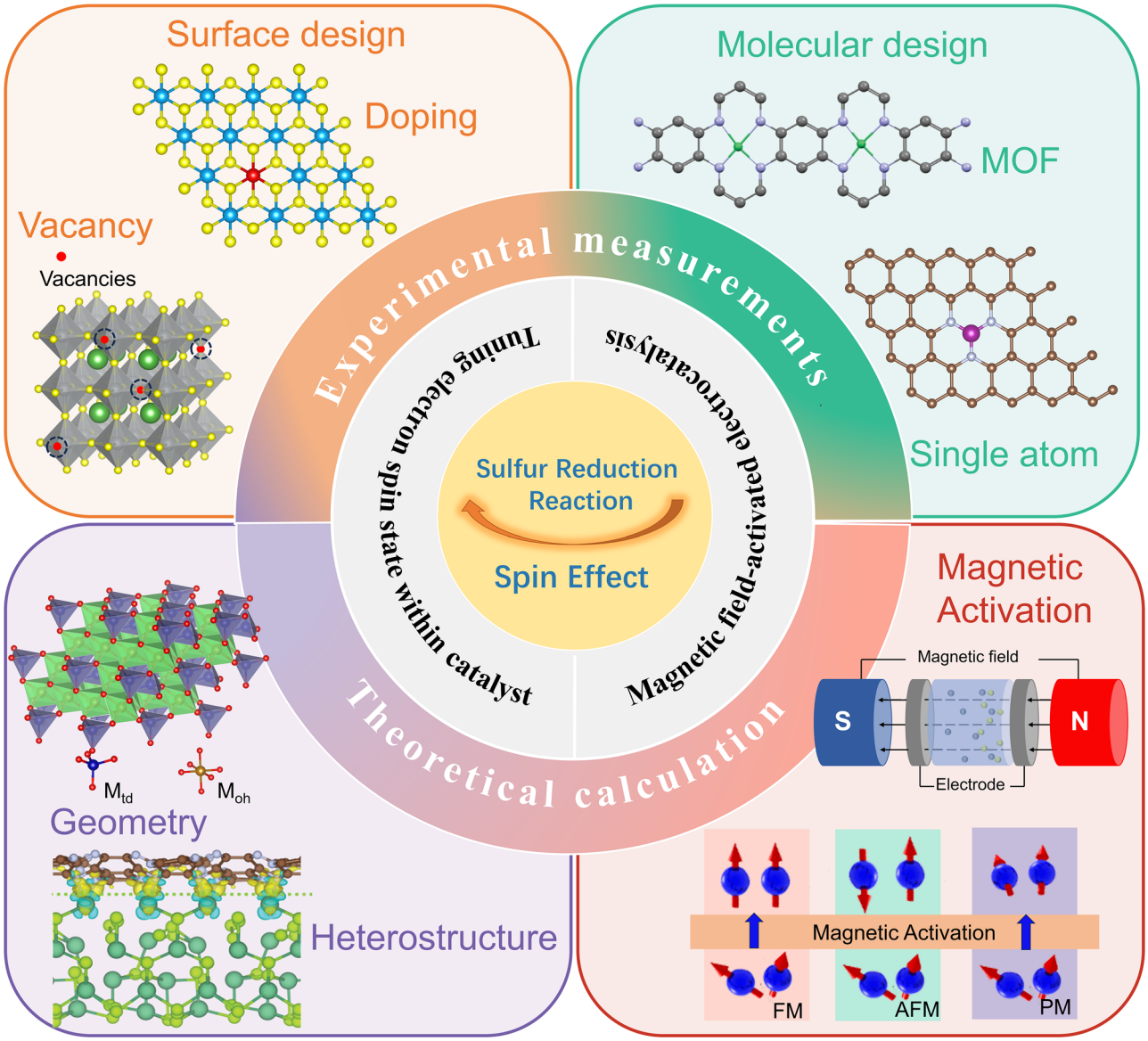

Fig. 2 | Schematic overview of spin effect on SRR. Schematic overview of spin effect on SRR, including electron spin engineering magnetohydrodynamics, surface spin filters, and spin alignment under a magnetic field. Heterostructure, reproduced with permission from ref. 218 (copyright Wiley-VCH, 2021).

In this review, we provide a comprehensive analysis of theoretical and experimental studies exploring the relationship between electronic spin effects and SRR performance (Fig. 2). Unlike previous reviews on electron spin catalysis, which largely emphasize external magnetic fields as a convenient yet impractical means of spin manipulation, our focus is on the rational design of electrocatalysts with intrinsically controlled spin states. These strategies are considered not only for metal–sulfur batteries but also for other conversion-type batteries (e.g., metal–air systems) and electrochemical energy devices, such as fuel cells and electrolyzers. We highlight approaches to enhance electrocatalytic performance by tailoring the coordination environment of active sites through defect engineering, molecular and geometric design, and heterostructure construction. The review also summarizes state-of-the-art techniques for probing electron spin states, together with theoretical frameworks and computational tools used to model spin-related catalytic behavior. Finally, we discuss key challenges, emerging opportunities, and future research directions, aiming to inspire rational catalyst design and support the development of high-performance electrocatalysts across diverse energy conversion technologies.

Fundamentals of electron spin electrocatalysis

Electrochemical reactions are governed by three fundamental electronic parameters: the relative position of the energy levels, their occupation, and the spin of the electrons involved[29]. Electron transfer, and thus chemical reactivity, occurs from occupied to unoccupied states only when the energy levels are properly aligned. Moreover, in accordance with the Pauli exclusion principle, such transfers are permitted only if the spin states of the reactants and products are conserved. In other words, a reaction is considered spin-allowed only when the total spin state remains unchanged[61].

Beyond microwave irradiation, three main practical strategies have been developed to modulate electron spin within catalytic systems (Fig. 3): (i) the application of an external magnetic field; (ii) the incorporation of chiral elements; and (iii) the modification of the coordination environment of catalytic sites[8,45,62]. In addition to influencing spin states, external or internal magnetic fields can affect charge transport within the electrode, as well as ion transport, mass transfer, and local ion concentrations within the electrolyte. Furthermore, alternating magnetic fields can induce localized heating, contributing to performance enhancement via increased reaction kinetics.

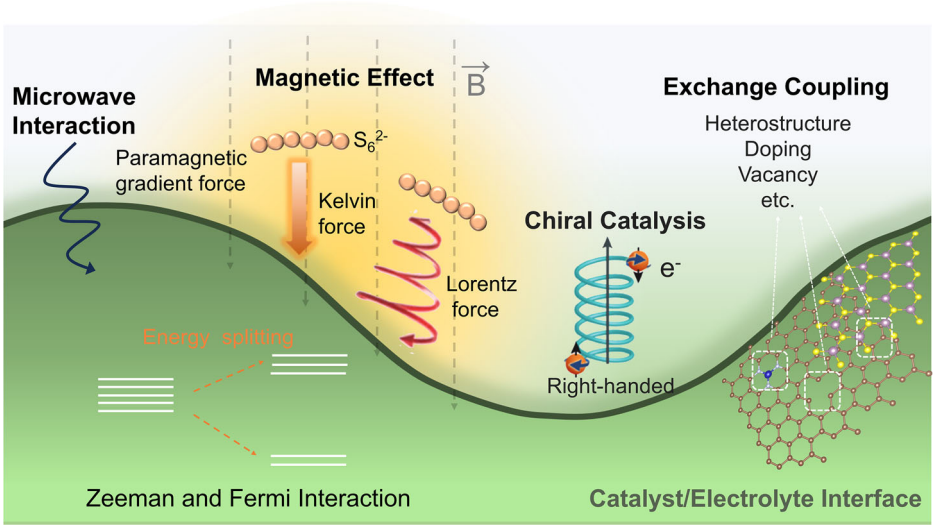

Fig. 3 | General scheme showing the influence of the magnetic field on catalysis and additional strategies to modify electronic spins within the system. The scheme includes microwave irradiation, magnetic field effects at the electrolyte and electrode level, chiral elements for spin-selective charge transfer at the interface, and coordination design and engineering to tune electronic spin within the catalyst through exchange coupling and spin pinning.

Based on these mechanisms, current strategies for optimizing the electrochemical performance of batteries can be broadly classified into three categories: (1) Application of external magnetic fields to influence the catalyst or electrolyte behavior; (2) Spin-engineering of the catalyst, achieved by modifying its structure and coordination environment; (3) Incorporation of spin filters, such as chiral molecules or ligands, at the catalyst surface to induce spin-selective electron transfer.

In this section, we briefly introduce the underlying principles of each approach. Sections 3 and 4 will further elaborate on specific examples directly related to SRRs.

Magnetic field-activated electrocatalysis

The application of an external magnetic field is the simplest and most direct approach to polarize electron spin at the solid–liquid interface, allowing the investigation of its influence on the electronic properties and catalytic performance of electrodes[63]. In electrocatalysis, magnetic fields can operate on multiple levels: (i) at the reaction interface, by modulating the electronic energy levels and spin states of active sites; (ii) at the level of the catalyst material, by influencing charge transport properties; and (iii) at the electrolyte level, by enhancing ionic transport and local ion concentrations.

The impact of an external magnetic field is highly dependent on the magnetic properties of the catalyst material. In FM electrocatalysts, strong exchange interactions align electron spins within localized magnetic domains, even in the absence of an applied field. However, due to the random orientation of these domains, the material may exhibit no net macroscopic magnetization[57,64]. Upon application of an external magnetic field, these domains reorient or shift in the direction of the field, resulting in a net magnetization and enhanced spin polarization at the active sites[65].

Importantly, even without an applied field, the intrinsic spin alignment in FM materials can significantly influence charge transport, reaction kinetics, and electrolyte behavior in their immediate vicinity. This intrinsic property explains why the majority of reported spin-related effects in electrocatalysis have been observed in FM systems.

Spin alignment and electronic energy level splitting. In the absence of an external magnetic field, electron spins are randomly oriented, and the spin-up and spin-down states remain degenerate. When a magnetic field is applied, this degeneracy is lifted, splitting the spin states into two energy levels depending on whether their orientation is parallel or antiparallel to the field vector. This electron Zeeman interaction produces an energy splitting proportional to the field strength. Although typically very small, comparable to thermal energies at ambient conditions, it introduces measurable spin asymmetry at the electronic level. An even subtler contribution arises from the Fermi interaction, caused by magnetic dipole coupling between the electron and the atomic nucleus in a magnetic field. However, since magnetic energies are far weaker than thermal or electrostatic energies, static magnetic fields contribute negligible chemical energy directly to reactions.

Nevertheless, magnetic fields influence the spin configuration at the reaction interface, establishing preferential spin orientations that can profoundly affect the course of chemical reactions. In particular, the relative spin alignment between reactants and products plays a key role in determining whether a reaction proceeds through a spin-allowed or spin-forbidden pathway[44,65,66].

To quantify this spin asymmetry, a commonly used figure of merit is spin polarization (P), defined as the difference in the number of spin-up and spin-down electrons, normalized to their total population:

$$P = (N\uparrow - N\downarrow)/(N\uparrow + N\downarrow) \quad (1)$$

where N↑ and N↓ represent the number of electrons with spin-up and spin-down orientations, respectively[67,68]. The spin polarization value ranges from −1 to 1, and its accurate determination depends on reliable measurements or calculations of the spin-resolved electronic structure.

Electrolyte effects: magnetohydrodynamics. Magnetohydrodynamic (MHD) effects arise from the interaction between an external magnetic field and both paramagnetic species, i.e., those containing one or more unpaired electrons, and moving charges, such as electrons and ions, within an electrochemical system. When subjected to a magnetic field, these paramagnetic or charged species experience multiple forces, including the paramagnetic gradient force (F_P), field gradient or Kelvin force (F_K), and Lorentz force (F_L)[69].

F_P arises from spatial variations in the paramagnetic susceptibility within the diffusion layer, which are caused by concentration gradients of charged or paramagnetic species. While F_P may become significant locally within the diffusion layer, its overall influence on the catalytic process is often considered negligible. This is because, at room temperature, the thermodynamic driving force for diffusion greatly outweighs the magnetic contribution exerted by F_P[69].

F_K is generated by the interaction between paramagnetic species and a non-uniform magnetic field, and it is directly proportional to the field gradient. This force drives paramagnetic species toward regions of higher magnetic field strength, while diamagnetic species are pushed in the opposite direction. As a result, F_K can induce local concentration gradients of electroactive species, particularly near the electrode surface. This magnetic separation effect enables the selective accumulation or depletion of species based on their unpaired electrons, thereby influencing electrode

coverage and potentially altering reaction pathways[70]. The effect of F_K is especially pronounced at the surfaces of FM electrodes, which inherently produce strong and spatially non-uniform magnetic fields in the adjacent electrolyte. These localized gradients can enhance electrocatalytic performance by promoting mass transport, reducing diffusion layer thickness, and increasing the effective concentration of reactants at the reaction interface.

F_L results from the interaction between moving charged species and an applied magnetic field, and it is proportional to the strength of the field. As F_L acts perpendicular to both the direction of charge movement and the magnetic field vector, it alters the linear motion of ions and electrons into a spiral or curved trajectory, inducing electrolyte convection. This magnetically induced stirring promotes enhanced mass transport, reduces the thickness of both the diffusion layer and the electrical double layer, and thereby increases the rate of electroactive species transport to the electrode surface. In addition to improving ion distribution and homogenizing nucleation processes, F_L contributes to the removal of gas bubbles that may form during gas-evolving reactions, further improving reaction efficiency.

Furthermore, within the diffuse layer of the electrical double layer, electrokinetic shear stress may act on charge carriers when a non-electrostatic force, such as a magnetic field, is applied parallel to the electrode surface[55]. This shear stress can influence local ion dynamics and surface charge distribution. Additionally, the Maxwell stress, arising from interactions between the magnetic field and magnetic dipole moments of species near the electrode, can further influence electrochemical behavior. Specifically, it can alter the wettability of the electrode surface for different species, impacting the coverage, capacitance of the electric double layer, and charge transfer resistance[70,71].

Magnetoresistance. External magnetic fields can also affect the charge transport properties of electrode materials, a phenomenon broadly known as magnetoresistance. This effect must be distinguished from spin-selective charge transfer at the electrode–electrolyte interface, which is governed by different mechanisms. Magnetoresistance is observed in diverse materials, including non-magnetic and magnetic metals, semiconductors, and composites, and can arise from multiple factors.

One contributing factor is the F_L acting on charge carriers in the electrode. Under a magnetic field, charge trajectories are altered, leading to increased scattering and reduced mobility, which typically manifests as positive magnetoresistance (i.e., increased electrical resistance). In electrochemical systems, this added resistance can diminish charge transport efficiency and impair device performance.

However, negative magnetoresistance, in which resistance decreases with an applied magnetic field, has also been reported under specific conditions. For example, in polycrystalline Fe_3O_4, it results from spin-dependent charge transport between adjacent grains, underscoring the role of spin alignment and domain structure in governing electrical conductivity[72–74].

Magnetothermal effect

The magnetothermal effect refers to the heating of a material via energy dissipation induced by the application of an alternating magnetic field, primarily mediated by spin fluctuations within magnetic domains. Also known as magnetic hyperthermia, this phenomenon is widely utilized in biomedical applications, particularly for the targeted destruction of cancerous tissues, where magnetic nanoparticles (NPs) generate localized heat to raise the temperature of tumor environments[75]. In recent years, magnetic hyperthermia has also found application in the field of magnetically induced catalysis[76,77]. In this context, the heat generated by magnetic NPs under alternating magnetic fields is harnessed to initiate or accelerate catalytic reactions. Depending on the system design, these NPs can serve directly as active catalysts, as catalyst supports, or as thermal agents that enhance the reactivity of nearby catalytic components by localized heating.

Spin state engineering within the catalyst: exchange coupling and spin pinning

The use of external magnetic fields offers a powerful strategy to fundamentally investigate the role of electron spin states in electrochemical performance. However, their application for performance enhancement during battery operation remains impractical, primarily due to the additional cost, weight, and volume of the equipment or materials required to generate and maintain such fields. One potential workaround is the integration of multifunctional or structural materials with hard FM properties directly into the electrode or battery casing, allowing for internal magnetic field generation without external systems.

A more practical and scalable alternative involves the intentional design and engineering of spin states within the electrode materials themselves. This can be achieved through exchange coupling and spin pinning strategies, which stabilize or manipulate spin configurations at active sites. Although the magnetic energy contributions from Zeeman and Fermi interactions are generally negligible compared to chemical and electrostatic potential energies, the exchange-correlation energy between two electrons of opposite spin occupying the same orbital region can reach values on the order of 1 eV[78]. This exchange interaction is central to spin catalysis and can be tuned by modifying the coordination geometry of reaction sites, thereby altering their preferred spin states[79]. Indeed, exchange coupling is widely considered the dominant driving force in spin-selective catalysis[29].

Another promising strategy is the use of spin pinning, particularly in pre-magnetized materials, to direct the reaction pathway toward products that would otherwise be spin-forbidden. This concept has been successfully demonstrated using core–shell heterostructured NPs, such as $Co_{3-x}Fe_xO_4$@$Co_{1-y}Fe_yOOH$ and Fe_3O_4@$Ni(OH)_2$[37,80–82]. In these systems, the FM core exerts a robust pinning effect on the electron spins within the (oxy) hydroxide shell, where the electrochemical reaction takes place. Notably, spin-selective electron transport has also been observed within the shell layer, suggesting additional opportunities for tuning reaction kinetics and selectivity through magnetic coupling effects.

Surface spin filters: chiral elements

The incorporation of chiral elements at the electrode surface represents a direct and effective strategy for activating electrochemical reactions through electron spin polarization. Chiral molecules enable the preferential transmission of electrons with a specific spin orientation—a phenomenon known as chiral-induced spin selectivity (CISS). This spin filtering effect was first described by Ray Krishanu in 1999, who demonstrated that chiral molecules can function as spin-selective conduits, effectively determining the spin orientation of transmitted electrons[83].

By exploiting the intrinsic relationship between molecular chirality and spin orientation, the CISS effect has emerged as a promising breakthrough for enabling spin-controlled electrocatalysis. This approach holds significant potential for tuning reaction kinetics and selectivity without relying on external magnetic fields or complex material architectures[78,84–86].

Probing spin states: experimental tools and theoretical frameworks

The development of spin-engineered materials with enhanced electrocatalytic performance fundamentally relies on the ability to experimentally control and accurately characterize spin states, along with the advancement of robust theoretical models that deepen our understanding of the mechanisms governing spin behavior and its influence on catalysis[21].

The spin state configuration of a material is governed by key factors, including orbital occupancy, electronic symmetry, coordination geometry, and energy level distribution. In TM compounds, understanding the role of spin in electronic transitions begins with the concept of crystal field splitting, particularly in metals with d^4 to d^7 electron configurations, where the distribution of electrons across split d orbitals dictates the spin state.

In an octahedral coordination environment, for example, the five d orbitals split into two distinct energy levels: (i) the lower-energy t_2g orbitals (dxy, dxz, dyz), oriented between the axes, where they experience less direct electrostatic repulsion from ligands, and (ii) the higher-energy eg orbitals (dz^2, dx^2-y^2), which point along the axes, directly facing ligand orbitals and thus subject to greater repulsion (Fig. 4a).

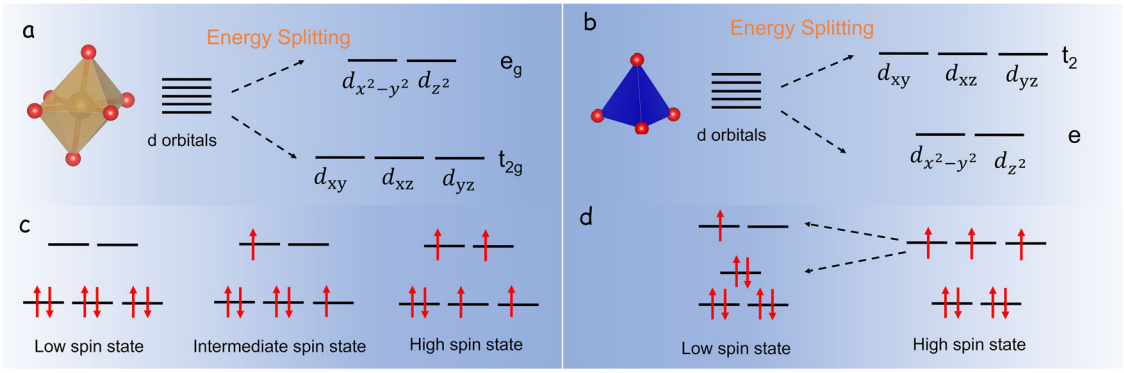

Fig. 4 | Geometry dependence of the spin effect. Crystal field splitting of d orbitals in octahedron (**a**) and tetrahedron (**b**) structures. **c** Electronic arrangement of Co^{3+} in different orbitals under LS, intermediate spin, and HS states, from left to right. **d** Electronic arrangement of Co^{2+} in different orbitals under LS and HS states, from left to right.

The occupancy of the antibonding eg orbitals determines the electronic spin state of the metal (Fig. 4c), whether high-spin (HS), intermediate-spin, or low-spin (LS), and plays a crucial role in governing electrocatalytic activity, particularly by influencing σ-bonding interactions and charge transfer processes between the catalyst and adsorbed reaction intermediates[87].

In other geometries, such as spinel structures containing Co^{2+} in tetrahedral coordination, the electronic configuration differs (Fig. 4b). In this case, Co^{2+} typically adopts a HS state. However, further orbital splitting and spin transitions can be induced by modifying the local chemical environment, potentially leading to an LS configuration (Fig. 4d)[88].

Effectively understanding and manipulating spin states thus requires both the rational design of structural frameworks that influence orbital splitting and access to experimental techniques capable of resolving the electronic and spin properties of metal centers. For example, HS states are typically more apparent under steady-state conditions, while HS and intermediate-spin states are more readily identified using ultrafast pump–probe spectroscopic techniques (Fig. 4b)[89].

This section provides a comprehensive overview of the experimental methods available for evaluating spin and oxidation states, as well as a summary of the theoretical modeling approaches used to study spin-state transitions in TM-based catalysts.

Experimental measurements

Characterizing the spin states of catalysts and their evolution during interactions with reactants is essential for understanding catalytic mechanisms and for regulating catalytic activity and stability. Probing the electronic structure and spin-related processes at the catalyst surface offers critical insights that guide the design and optimization of advanced catalysts. Several experimental techniques are available to monitor the energy levels, their occupancy, and the degree of spin polarization within catalytic materials. These include X-ray absorption spectroscopy (XAS), electron paramagnetic resonance (EPR), superconducting point contact (SPC)[90–94], X-ray magnetic circular dichroism (XMCD)[95–97], angle-resolved photoemission spectroscopy (ARPES)[98–100], polarized photoluminescence (PPL)[68,101–103], and polarized neutron diffraction (PND)[104–106], among others.

X-ray absorption spectroscopy. XAS allows for the direct determination of HS and LS states as a function of the relative intensity of TM centers to the split unoccupied orbitals, because of differences found in the spectra shape from different orbital occupations in HS and LS forms. XAS is also sensitive to the local crystal field environment of the ionic species under study, thus enabling the discrimination of ions at different crystallographic sites[95].

X-ray absorption near edge structure (XANES) and extended X-ray absorption fine structure (EXAFS) have been demonstrated to be especially useful for the determination of the unoccupied electron states and the local structure around the absorbing atom, respectively[89,107,108]. From the XAS-fitted spectra, parameters, such as HS fraction, temperature at which the transition takes place, and thickness of the film, can be inferred and further correlated to the degree of coalescence obtained from the analysis of topography images.

Taking the Co L-edge spectrum as an example, it is split into two due to spin-orbit coupling (Fig. 5a), denoted as the L_3 edge (780 eV) and the L_2 edge (796 eV)[109–111]. The shape of the spectrum strongly depends on the multiple structures given by the Co 3d-3d Coulomb interaction and hybridization with the 2p orbital of the ligand[108]. Therefore, the position and intensity of the L-edge peak of Co give information about the symmetry and spin state. For instance, the decrease in the intensity of Co L_2-edge indicates the spin state transition of Co^{3+} from a HS state to an LS state as demonstrated in the work of L. H. Tjeng et al.[108]. It was shown that Co^{3+} ions in the perovskite-structured $LaCoO_3$ at different temperatures have a diversity of spin states (Fig. 5b). The temperature dependence was fitted by taking the different LS and HS state ratios contributing to the spectra. The percentage of extracted HS as a function of temperature is displayed in Fig. 5b, showing that as the temperature increases, the proportion of HS in the material increases[108].

X-ray magnetic circular dichroism. Related to XAS, XMCD involves the use of circularly polarized X-rays to characterize the spin state of specific elements within a sample. The absorption of photons with a specific circular polarization (either left-handed or right-handed) depends on the polarization and the orientation of the magnetic moments (spins and orbital angular momentum) of the electrons in the material. The difference in X-ray absorption for left-circularly polarized versus right-circularly polarized light provides information on the alignment of electronic spins and orbitals[97,112,113]. A positive XMCD signal indicates an excess of one spin orientation, while a negative XMCD signal indicates an excess of the other spin orientation.

As an example, Fig. 5c shows the XAS and XMCD spectra of $BiFeO_4$-$CoFe_2O_4$ (BFO-CFO) nanopillar films at normal incidence[95]. The spectra show two sub-peaks, L_3 and L_2, which are due to the spin-orbit splitting of Co^{2+} ions. Comparing the ratio of X-ray absorption for left-circularly polarized versus right-circularly polarized light, the Co^{2+} XMCD spectra show a 50% spin polarization.

Electron paramagnetic resonance. EPR, also known as electron spin resonance (ESR), is a semiquantitative spectroscopic technique based on the interaction of electron spins with an applied magnetic field. From the changes in the frequency and intensity of microwave radiation absorbed or emitted by a sample when an external magnetic field is applied, information about the electron spin state and environment can be obtained. Unpaired electrons gaining or losing angular momentum can change the value of the g-factor of the EPR. Besides, the interaction of unpaired electrons with their environment can also affect the shape of the EPR spectrum[114].

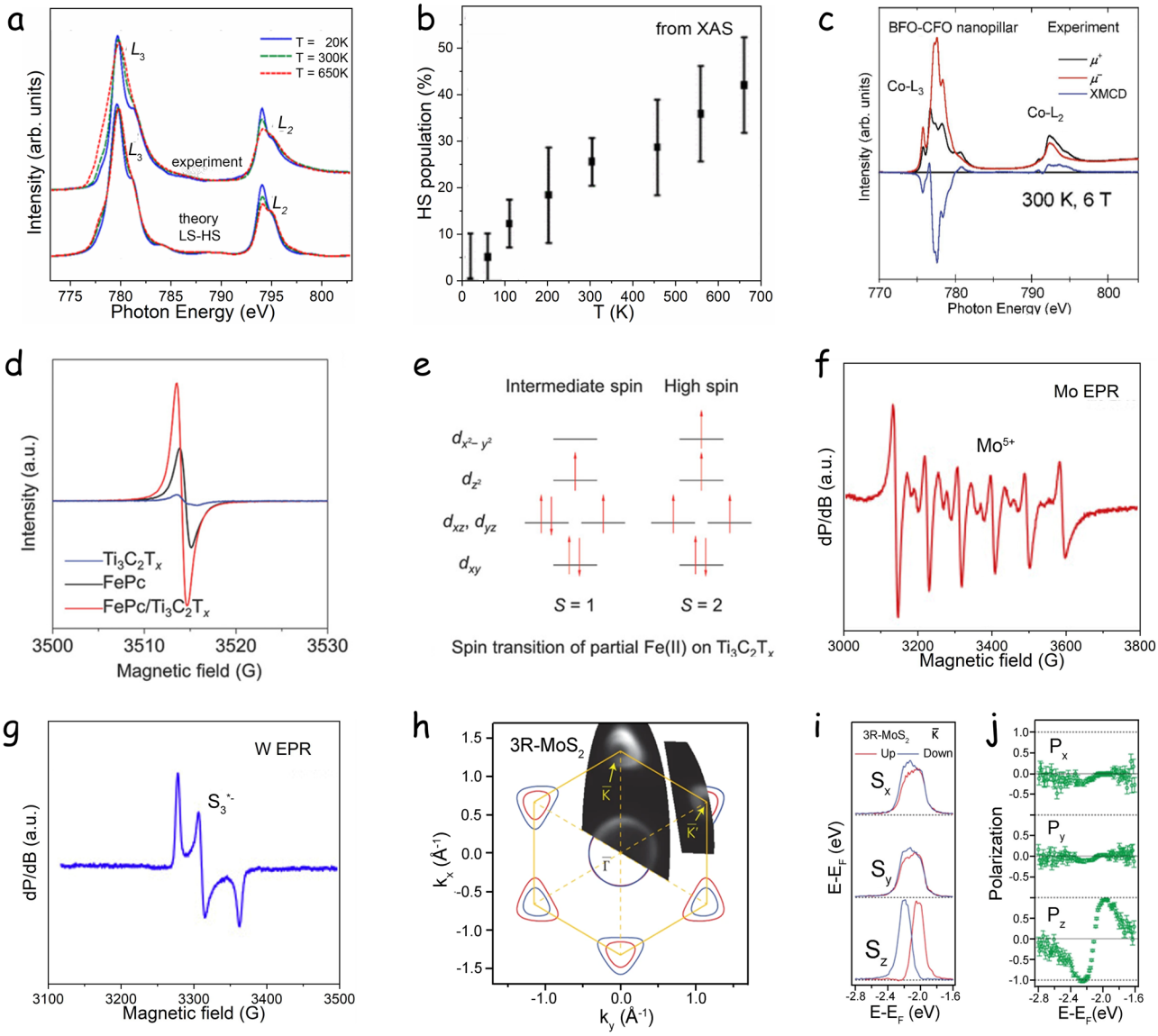

Fig. 5 | Spin state characterization. a Experimental Co-$L_{2,3}$ XAS spectra from $LaCoO_3$ at various temperatures, 20, 300, and 650 K, and corresponding theoretical spectra calculated in LS and HS. **b** HS population from XAS data. **a,b** Reproduced with permission from ref. 108 (copyright American Physical Society, 2006). **c** Experimental Co-$L_{2,3}$ XAS and XMCD spectra of BFO-CFO nanopillar films (300 K and 6 T). X-ray absorption for left-circularly polarized and right-circularly polarized light (μ^+ and μ^-) are shown as black and red lines, while XMCD difference spectrum is shown as a blue line. Reproduced with permission from ref. 95 (copyright Elsevier, 2020). **d** EPR spectra of pristine $Ti_3C_2T_x$, FePc and FePc/$Ti_3C_2T_x$. **e** Schematic diagram of the spin transition of Fe(II) on $Ti_3C_2T_x$. **d,e** Reproduced with permission from ref. 114 (copyright Wiley-VCH, 2022). Characterization of the $(NH_4)_2MS_4$–Li_2S_x reaction product in ether-based solvents. **f** X-band EPR spectrum of the solution-phase reaction product of $(NH_4)_2MoS_4$–Li_2S_8. **g** X-band EPR spectrum of the solution-phase reaction product of $(NH_4)_2WS_4$–Li_2S_8. **f,g** Reproduced with permission from ref. 115 (copyright Elsevier, 2022). **h** Intensity map obtained by ARPES ($h\nu$ = 21.2 eV) at 0.3 eV relative to the top of the valence band at point $\bar{K}$ ($E - E_{\bar{K}} = -0.3$eV) and the iso-energy surface c calculated at $k_z = \pi/c$ overlaid on 2D on the first Brillouin zone. Hereafter, red and blue represent the spin-up and spin-down electrons, respectively. **i** Spin-resolved energy distribution curves (EDCs) at the $\bar{K}$ point and **j** the corresponding spin polarization and statistical error of photoelectron counts for 3R-MoS_2, obtained by SARPES. **h-j** Reproduced with permission from ref. 68 (copyright Nature Publishing Group, 2014).

As an example, the EPR spectrum of iron phthalocyanine (FePc)/$Ti_3C_2Ti_x$ (Fig. 5d, e) shows changes in the three-dimensional (3D) electron spin configuration and chemical environment of the Fe(II) center with respect to that of FePc[114]. The strong interaction between Fe(II) and $Ti_3C_2Ti_x$ MXene induces electron density redistribution and spin state transition, with a spin configuration change from $d_{xy}^2 d_{xz}^2 d_{yz}^1 d_{z^2}^1 d_{x^2-y^2}^0$ to $d_{xy}^2 d_{xz}^1 d_{yz}^1 d_{z^2}^1 d_{x^2-y^2}^1$.

EPR has also been employed to detect soluble polysulfide intermediates[115,116]. Since ions in diamagnetic oxidation states are EPR-silent, the presence and transformation of paramagnetic species can be readily monitored as the reaction progresses. This allows for direct observation of spin transitions, providing valuable insight into the reaction mechanism (Fig. 5f, g)[115].

Angle-resolved photoemission spectroscopy. ARPES is a powerful tool based on the photoelectric effect to study the electronic structure of materials, providing information about the electronic spin state[98,100,117]. In an ARPES experiment, the surface of the material is irradiated with UV or X-ray photons to excite electrons to higher energy states, giving them enough energy to escape from the material's surface. By measuring the energy and emission angle of the scaped electrons, the electronic energy band structure of the material can be determined[99]. Information about

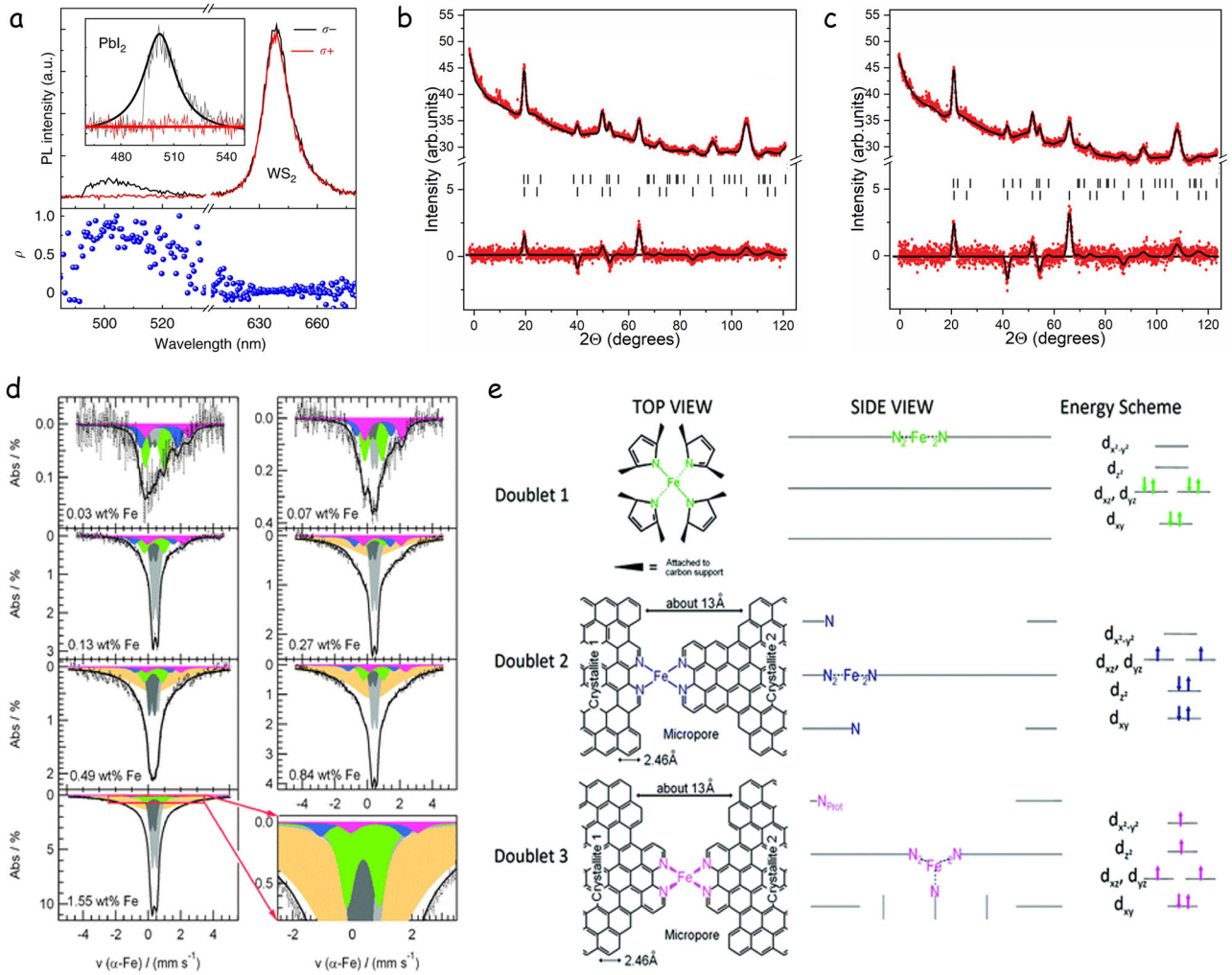

Fig. 6 | Spin state characterization. a Circularly polarized PPL spectrum of pure PbI_2 at room temperature (top) and the corresponding degree of polarization ρ of pure PbI_2 calculated from the PPL spectrum (bottom). Reproduced with permission from ref. 103 (copyright Nature Publishing Group, 2020). **b**,**c** Refinement of the sum (spin up + spin down; top curves) and difference (spin up − spin down; bottom curves) of the spin-up and spin-down pattern at **b**) 5 kOe and **c**) 50 kOe. **b**,**c** Reproduced with permission from ref. 124 (copyright Wiley-VCH, 2022). **d** Deconvoluted Mössbauer spectra of a Fe/N/C-catalysts. **e** Side views and top views of the proposed structures obtained from the correlation of the corresponding peak position of the doublets and the quadrupole splitting with the content of Fe, energy schemes of D1, D2, and D3, and filling of the molecular orbitals for the Fe^{II} ion in the structure for each site according to its proposed spin state. **d**,**e** Reproduced with permission from ref. 128 (copyright Royal Society of Chemistry, 2012).

electron spin state can be obtained by analyzing the distribution of electrons in energy-momentum space.

As an example, the equi-energy band surface of 3R-MoS_2 at $E - E_{\bar{K}} = -0.3$eV is shown in Fig. 5h, where $E - E_{\bar{K}}$ represents the energy level relative to the valence band maximum at K point[68]. The experimental images show the existence of hole-like equi-energy surfaces around the $\bar{\Gamma}$, $\bar{K}$, and $\bar{K}'$ points. In Fig. 5i, the red (blue) curves represent the intensity of the spin-up (spin-down) electrons obtained at the K point. The z-directed spin spectrum shows that the upper (lower) bands at the top of the K-dot are spin-up (spin-down) polarized, while the in-plane s_x and s_y components have nearly equal intensities. Figure 5j shows almost complete polarization along the z-direction ($P_z \approx \pm 1$) along the material, which could quantitatively describe the change of spin state of 3 R MoS_2 when compared with 2H MoS_2.

Polarized photoluminescence. PPL involves the excitation of electrons using polarized light and the analysis of the polarization properties of the light they emit upon returning to a lower energy state[102]. When a material is excited with circular or linear polarized light, it preferentially excites electrons into specific spin states. Thus, the polarization characteristics of the photoluminescence spectra carry information about the spin of the electrons in the excited state[101,118]. Using a polarization analyzer, the luminescent photons can be divided into left-handed (σ^-) and right-handed (σ^+) polarization directions.

As an example, when PbI_2 is excited with the σ− light, the dominant emission is σ^- polarized (Fig. 6a). On the other hand, in the PPL signal from a PbI_2/WS_2 heterostructure, PPL for both σ^+ and σ^- polarizations was detected (Fig. 6a top)[103]. Thus, it was inferred that the degree of polarization of PbI_2 in the heterostructure increased dramatically, reaching almost 100% (Fig. 6a bottom).

Polarized neutron diffraction. Based on the remarkable sensitivity of polarized neutrons to weak magnetic signals, PND, together with spherical neutron polarimetry (SNP), can be unequivocally considered the most sensitive methods for the study of magnetic structures using unpolarized beams[119–121]. PND can determine magnetization distributions in the unit cell and unambiguously reveal the spin delocalization and the polarization sign. PND also allows separating the spin and orbit contributions and is a powerful tool to investigate intra- and intermolecular interactions. Until very recently, PND has been limited to

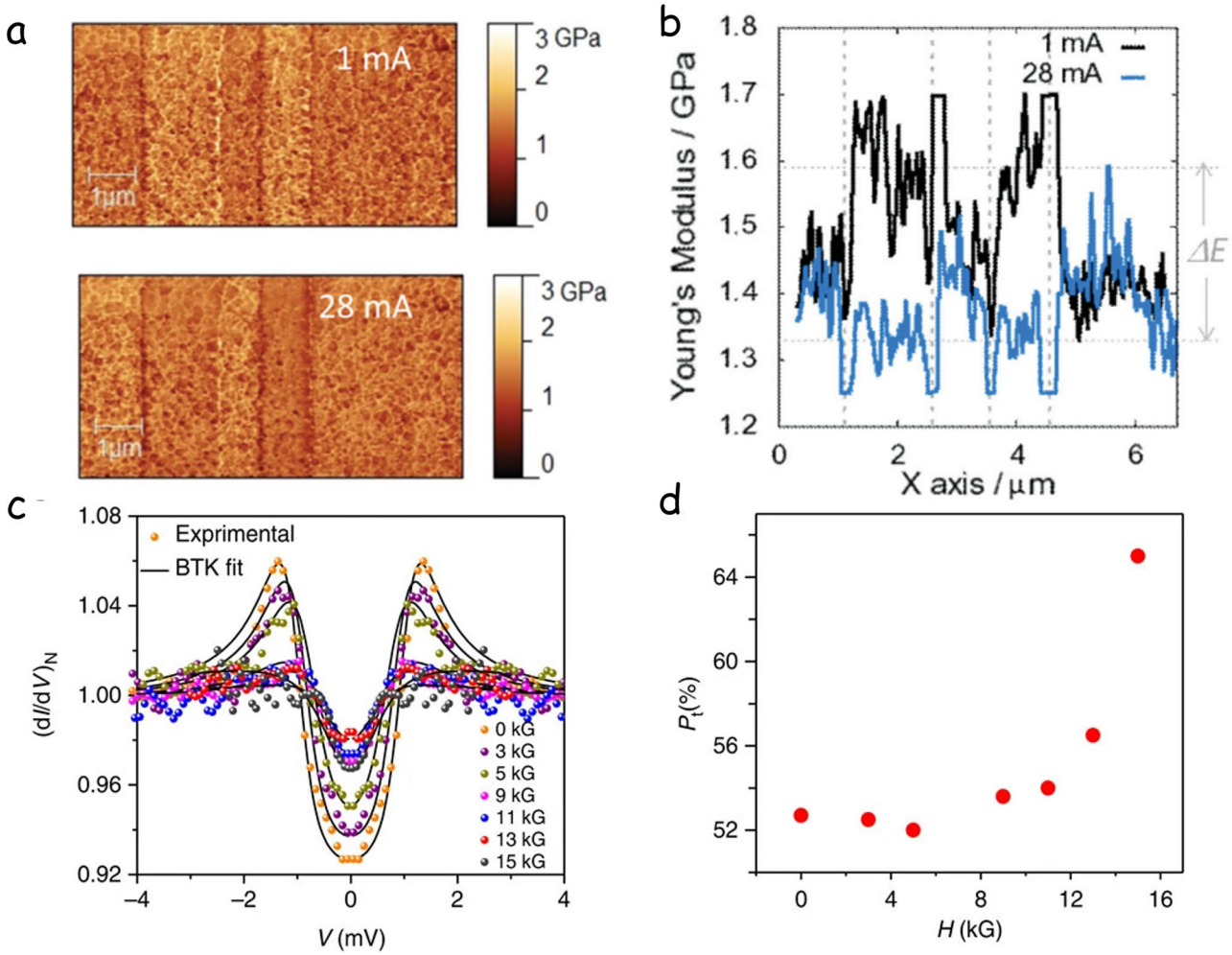

Fig. 7 | Spin state characterization. Young's modulus plots (**a**) and Young's modulus mean cross-sections. **b** for I = 1 mA and 28 mA. **a**,**b** Reproduced with permission from ref. 130 (copyright Wiley-VCH, 2014). **c** Magnetic field dependence of one of the ballistic point contact spectra showing HS polarization. **d** Magnetic field dependence of spectral spin polarization P in (**c**). **c, d**)Reproduced with permission from ref. 94 (copyright Nature Publishing Group, 2017).

single-crystal and some polycrystalline samples. Further developments in instrumentation, specifically ^{3}He neutron spin filters, have broadened their applicability to a wider variety of samples unsuited otherwise[122]. Besides, since 2019, it has been possible to study powder materials[123], even at the nanoscale[124], using a novel two-dimensional (2D) Rietveld data analysis[106].

As an example, Nogués et al.[124] determined, for Fe_3O_4@Mn_3O_4 core@shell NPs, not only the magnetic moment for each phase but also the orientation of the magnetic moment at each ion site within the crystal lattice (Fig. 6b, c). This novel analysis strategy allowed disentangling the origin of the change of the exchange coupling, from antiFM to FM, at the core@shell interface when applying high magnetic fields.

Mössbauer spectroscopy. Mössbauer spectroscopy, utilizing the resonant absorption and emission of γ−rays by atomic nuclei, involves a source and an absorber containing the same type of nucleus. The source, in an excited state, is moved variably to alter the γ-ray energy via the Doppler effect, matching the absorber's nuclear energy levels. Detected intensity changes in g-rays passing through the absorber indicate resonance, providing insights into the chemical environment of the absorbing nuclei, such as oxidation state, electronic environment, and chemical bonding. Mossbauer spectroscopy can also give insights into the spin state and magnetic properties of materials, including magnetic ordering and the strength of internal magnetic fields at the atomic level[42,125–127]. Specifically, ^{57}Fe Mössbauer allows for the detection of changes in the coordination environment of Fe and Co, i.e., sites of similar structure but in different oxidation and/or spin states, which can be correlated to the corresponding energy schemes and filling of the molecular orbitals (Fig. 6d, e)[128,129].

Other experimental techniques. A variety of experimental techniques have been employed to directly or indirectly probe spin configurations and their effects across a wide range of materials. As an example, As an example, Hernández et al.[130] employed atomic force microscopy (AFM) in peak force tapping (PFT) mode coupled with quantitative nanomechanical mapping (QNM) and a gold microwire microheater to achieve reversible, high-resolution measurement of the Young's modulus (E) in 40–70 nm spin-crossover (SCO) films across the LS to HS transition (Fig. 7a). By continuously calibrating the tip radius against an adjacent reference region, they observed a ~25–30% decrease in E (ΔE ≈ 400 MPa) upon heating, which was independently confirmed by correlated fluorescence imaging of a Rhodamine 110 dopant (Fig. 7b). Spatially resolved analyses over 70 nm-wide regions of interest, corroborated by finite–element thermal simulations, further revealed the nanoscale distribution of the spin transition and demonstrated AFM's unique capability to map phase boundaries and electron–lattice coupling effects in SCO nanostructures.

In SPC experiments, a spin-polarized interface is created between the superconductor and the material[90,93]. When a superconductor is in contact with a nonmagnetic material, the interface between the superconducting

material and the nonmagnetic material can lead to spin-selective electron scattering[94]. This scattering process changes the spin state of the electrons and creates spin polarization in the contact region. Thus, by measuring the electrical properties of SPC materials, the spin state of the material can be inferred (Fig. 7c, d)[91,92]. However, this technique has limited applications because of the complexity of data theoretical treatment[131,132].

High-resolution X-ray photoelectron spectroscopy (XPS) also provides valuable information on orbital occupancy and, consequently, the electronic spin state of TM complexes. Changes in the metal–ligand bonding character during spin-state crossover can be detected in the XPS spectra of both metal ions and, to a certain extent, ligand atoms. Notably, spectral line broadening and an increased presence of shake-up satellites, which are characteristic features of the HS state, result from enhanced time-of-flight coupling between emitted photoelectrons and partially filled paramagnetic d-orbitals.

This increased coupling, arising from uncompensated magnetic moments, reflects the higher ionicity of coordination bonds in HS species. As a result, transitions between HS and LS states influence both the binding energy and the charge distribution within chemical bonds. HS configurations are generally associated with a greater ionic character, providing a spectroscopic handle for probing spin-state changes and their effects on bonding interactions and electronic structure[21,133–135].

Hall devices have also been used to probe spin-selective charge transfer, which can be used to infer information about the spin state of materials[136]. Additional methods include electron energy-loss spectroscopy (EELS)[137–139], tomographic Kerr rotation[140], and scanning tunneling microscopy (STM), which can also be used to retrieve spin states[141]. In addition, the basic magnetic properties of a material can be determined through the measurement of magnetization under an externally applied magnetic field[142–146].

Most of the techniques discussed above offer a static snapshot of the electronic spin state of a material. However, extending spin state characterization to capture its dynamic evolution during a catalytic reaction remains highly challenging. To resolve the intermediate steps involved in spin transitions, ultrafast pump–probe techniques have emerged as powerful tools. Techniques capable of probing spin states on the femtosecond to nanosecond (fs–ns) timescale, such as X-ray emission spectroscopy (XES) and resonant inelastic X-ray scattering (RIXS), have been refined to overcome previous limitations in time-resolved X-ray spectroscopy. These methods have been successfully applied to investigate the photochemical behavior of Fe-based light-energy conversion systems[147].

Nevertheless, for low-Z elements like sulfur, the emission energy range lies outside the detection window of conventional hard X-ray emission spectrometers. To address this, in-vacuum tender XES spectrometers have been developed, enabling the extension of ultrafast spin-sensitive measurements to sulfur-containing systems[148–151].

Additionally, it is important to note that most of the aforementioned techniques are qualitative or semi-quantitative. They typically reveal relative changes in spin state, which may arise not only from actual spin transitions but also from other overlapping electronic effects. Consequently, accurate spin state characterization often relies on the correlation of experimental observations with complementary techniques and theoretical calculations. A notable example is the determination of electron occupancy in t_2g and e_g orbitals in $FeCoPS_3$, a 2D-layered TM chalcogenide used in LSBs, achieved by combining high-resolution XPS with density functional theory (DFT) simulations[21,133].

Theoretical calculation

Theoretical calculation methods are essential tools for investigating the spin states of materials. By solving equations related to the electronic structure, the spin Hamiltonian, or spin dynamics, these approaches provide valuable insights into the spin-dependent properties and behavior of materials at the atomic and electronic levels. They allow researchers to predict and analyze spin configurations, offering a deeper understanding of how spin states influence material performance. Moreover, theoretical calculations play a critical role in guiding the design and optimization of materials with tailored spin characteristics, thereby driving progress in electrocatalysis, particularly in the development of high-performance materials for conversion-type batteries.

Density functional theory. DFT is a powerful computational tool for investigating the electronic structure and intrinsic properties of materials, including their spin states. Through the analysis of band structures and density of states (DOS), DFT calculations provide critical insights into the distribution of electronic energy levels and their associated spin orientations. The band structure reveals how electronic states are dispersed across momentum space and can be used to identify spin-resolved energy bands, while DOS analysis offers a more detailed view of the number of available electronic states at each energy level for spin-up and spin-down orientations. Together, these analyses enable the quantification of spin polarization and support the characterization of magnetic and electronic behavior in a wide range of materials. Such insights are invaluable for the rational design of spin-active materials in fields, such as electrocatalysis, spintronics, and energy storage[67,141,152].

In spin-polarized materials, the spin-up and spin-down components of the DOS near the Fermi level represent the number of electrons in each respective spin orientation. The difference in electron occupancy between the spin-up and spin-down states at the Fermi level defines the degree of spin polarization, which can be quantitatively expressed as a ratio describing the extent of spin imbalance[67]:

$$P = \frac{\mathrm{DOS}\uparrow_{E_F} - \mathrm{DOS}\downarrow_{E_F}}{\mathrm{DOS}\uparrow_{E_F} + \mathrm{DOS}\downarrow_{E_F}} \quad (2)$$

When calculating the degree of spin polarization, it is crucial to select an appropriate approximation method and exchange–correlation functional, as these choices significantly influence the accuracy of the results[153]. For materials with complex spin configurations or strong electron correlation effects, more advanced approaches, such as the spin-polarized Hubbard model, may be necessary to capture the correct spin behavior and electronic structure[154].

As an example, the insets of Fig. 8a show the calculated spin polarization for Co and $FeGe_1/_2Ga_1/_2$ terminations, revealing important depth-dependent trends. In the case of $FeGe_1/_2Ga_1/_2$ as the terminating layer, the outermost atomic layer displays 100% spin polarization, which decreases to approximately 80% in the third atomic layer, as inferred from the DOS.

Spin density plots, derived from DFT calculations, also offer a visual and quantitative means of assessing spin state variations. For example, as illustrated in Fig. 8b, the spin density around Co atoms changes significantly upon considering spin alignment. Additionally, $CoFe_2O_4$ with parallel spin alignment exhibits a higher spin density on oxygen atoms compared to its antiparallel counterpart, providing a clear graphical representation of spin state modulation[65].

Beyond overall spin density visualization, it is also possible to represent spin-up and spin-down components separately. As demonstrated in Fig. 8c–e, this approach highlights the differential spin occupancy of Co^{2+} ions in $LiCoVO_4$, further elucidating spin asymmetry within the material[155].

In summary, DFT calculations serve as a powerful tool for evaluating the degree of spin polarization in materials. By analyzing both numerical results and graphical representations, such as DOS and spin density maps, researchers can obtain quantitative and qualitative insights into spin-dependent properties, which are essential for the design and understanding of spin-functional materials.

Diffusion quantum Monte Carlo. The diffusion quantum Monte Carlo (DQMC) method can be used to obtain information on electron spin and spin correlation[156,157]. An estimate of the spin polarization can be obtained by comparing the energy difference of systems with different spin configurations[158]. A low energy difference indicates a higher degree of spin polarization. By simulating spin configurations and energy differences, qualitative and quantitative information about electron spins can be obtained[159].

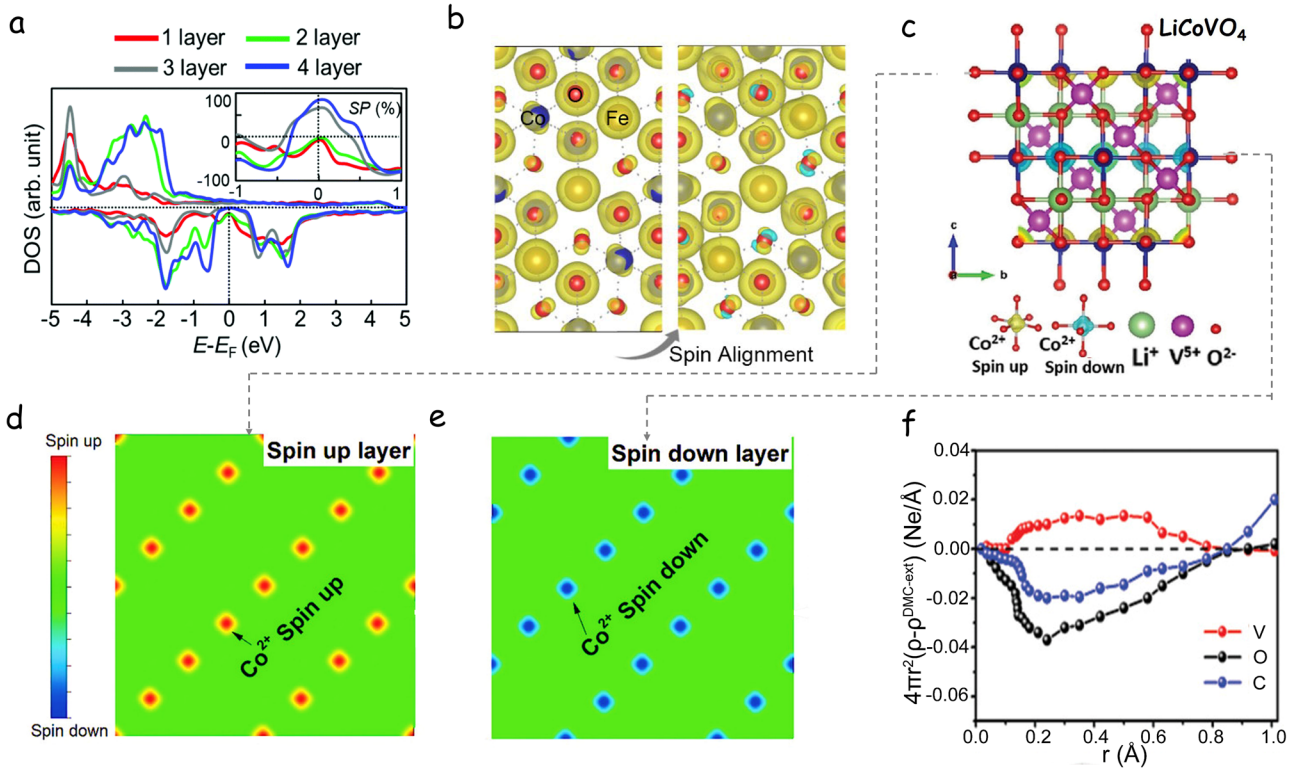

Fig. 8 | Spin state characterized by DFT. a Layer-resolved DOS of $FeGe_{1/2}Ga_{1/2}$-termination. The inset shows the layer-resolved spin polarization. Reproduced with permission from ref. 267 (copyright Royal Society of Chemistry, 2022). **b** Spin density for $CoFe_2O_4$ with and without spin alignment. Reproduced with permission from ref. 65 (copyright Nature Publishing Group, 2019). **c** $LiCoVO_4$ crystal structure with spin isosurfaces; yellow, blue, and none isosurfaces represent up-, down-, and zero net spin. **d,e** Spin distribution along the [001] direction for the spin-up (**d**) and spin-down (**e**) layers in $LiCoVO_4$. **c–e** Reproduced with permission from ref. 155 (copyright Wiley-VCH, 2020). **f** Simulated radial spin polarization density differences by the DQMC method. Reproduced with permission from ref. 160 (copyright Wiley-VCH, 2022).

As an example, Xiao et al.[160] observed that the V_2C-VO_2 heterointerface in the V-H mode exhibits the smallest polarization on the V-O and V-C layers using the spin-charge density distribution results obtained by DQMC, because all values of the calculated radial spin polarization density around the core region of vanadium atoms are smaller than those of other modes (Fig. 8f).

However, DQMC also has some limitations, such as computational complexity and statistical error[161,162]. Therefore, in practical applications, it is necessary to comprehensively consider different calculation methods and techniques to obtain more comprehensive and accurate electron spin information.

Influence of magnetic field on the performance of metal-sulfur batteries

External magnetic fields can significantly alter electrochemical reaction pathways, enabling transitions between spin-allowed and spin-forbidden channels[44,65,66]. In metal–sulfur batteries, such fields have been shown to enhance sulfur trapping, accelerate SRR kinetics, and improve overall performance, partly through MHD effects driven by the Lorentz force.

However, the influence of magnetic fields on electrochemical performance is highly complex, governed by factors, such as electrode composition, microstructure, reaction environment, and the field's intensity and orientation. Disentangling MHD effects from those arising from spin alignment and polarization is especially challenging, as both may occur simultaneously under magnetic influence. This complexity has often led to ambiguous interpretations of reported performance enhancements, with the origin, whether spin-state modulation, MHD-driven mass transport, or other magnetic effects, remaining unclear. Addressing this challenge requires a synergistic approach that integrates experimental studies with theoretical modeling and employs well-defined reference systems. Such strategies are essential to clarify the regulatory role of external magnetic fields in spin polarization dynamics during SRR and to guide the rational design of optimized catalysts for advanced energy storage applications.

MHD effect on sulfur cathodes

According to Lorentz's law, F_L acts perpendicular to both the velocity of negatively charged polysulfide anions and the applied magnetic field, imparting them with angular momentum as they move between the two electrodes. This rotational motion promotes a more homogeneous dispersion of the anions and uniform deposition on the catalyst surface. The nature of F_L and the resulting polysulfide diffusion can vary significantly depending on whether the magnetic field is applied externally in a homogeneous manner (Fig. 9a) or generated internally by magnetic domains (Fig. 9b). In all cases, however, the induced FL remains perpendicular to the direction of polysulfide motion, ensuring it cannot be misconstrued as an attractive or bonding interaction.

Several groups have reported a promoted polysulfide trapping using ferro/ferri/paramagnetic particles associated with an external or internal magnetic field. Pioneering work on the adsorption ability of LiPSs facilitated by superparamagnetic particles under an external magnetic field was carried out by Cui et al. on a semiliquid battery configuration[163]. They showed how in the presence of superparamagnetic Fe_3O_4 NPs, a concentrated polysulfide catholyte exhibited magnetofluidic behavior, enabling controlled localization in response to a magnetic field (Fig. 9c,d)[163]. Such ferrofluidic properties enabled a hybrid battery with enhanced electrochemical performance in the presence of a magnetic field that maintains the polysulfide catholyte in close contact with the cathode current collector (Fig. 9e).

Inspired by this and other previous works on the effect of magnetic fields on capacitors[164,165], Li et al. demonstrated promoted polysulfide trapping by introducing FM iron/iron carbide (Fe/Fe_3C) NPs into graphene

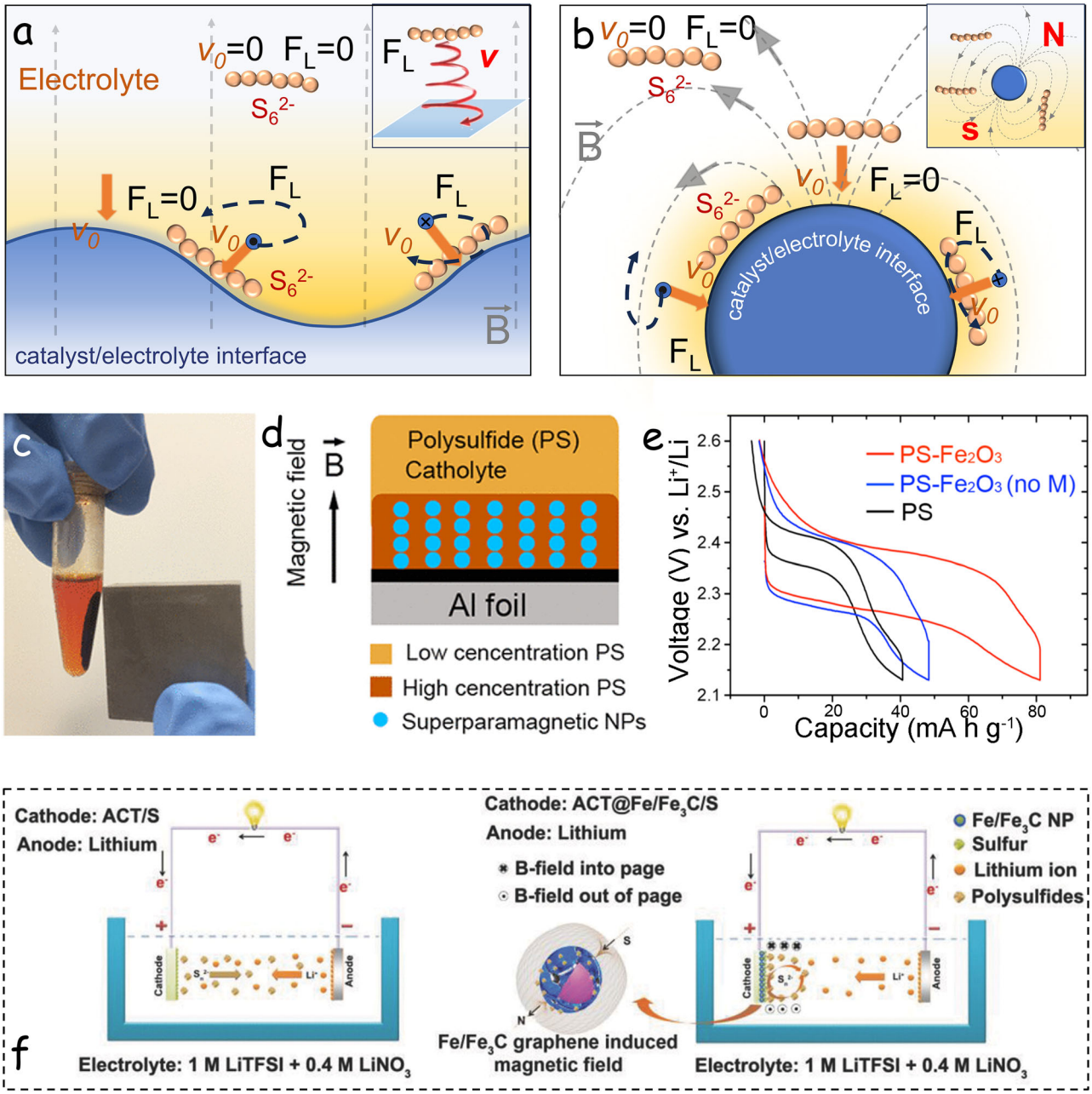

Fig. 9 | Influence of magnetic fields. a,b Schematic diagram of the movement direction and F_L of polysulfides on a catalyst surface with an external magnetic field (**a**) and on the surface of a magnetized nanoparticle (**b**). F_L: Lorenz force; V_0: initial polysulfide speed; S_6^{2-}: polysulfides and B: magnetic field. **c** Photograph showing the ferrofluid behavior of the condensed phase containing polysulfides and γ-Fe_2O_3 in the presence of a magnet. **d** Biphasic magnetic solution containing LiPS and magnetic γ-Fe_2O_3 at the catholyte. **e** Composed of biphasic magnetic polysulfide catholytes containing γ-Fe_2O_3 and without an external magnetic field, measured at a current density of 0.2 C. **c–e** Reproduced with permission from ref. 163 (copyright American Chemical Society, 2015). **f** Description of magnetic field inhibition of the shuttle effect and battery working mechanism. With Fe/Fe_3C NPs (right figure) and without Fe/Fe_3C NPs (right figure) in activated cotton textile (ACT)@Fe/Fe_3C/S cathode. The ACT cathode, infused with Fe/Fe_3C nanoparticles, generates a soft magnetic field that spirals dissolved polysulfides toward its surface, forming a protective, ion-rich boundary that enhances sulfur utilization and cycling stability (middle image). Reproduced with permission from ref. 24 (copyright Wiley-VCH, 2018).

shells (Fe/Fe_3C/graphene) and those within flexible active cotton textile (ACT) fibers to yield an ACT@Fe/Fe_3C/graphene sulfur host (Fig. 9f)[24]. The batteries assembled with ACT@Fe/Fe_3C/S cathodes exhibited excellent capacity retention (61%, after 600 cycles) associated with a promoted polysulfide adsorption in the presence of the magnetic field internally generated by the FM NPs. The authors associated the improved polysulfide trapping with the F_L generated by the intrinsic magnetic field in the cathode proximity related to the presence of the FM NPs. F_L alters the path of the dissolved negative polysulfide ions, attracting them toward the cathode, thus promoting their trapping. They named this mechanism a "shielding effect," and ruled out the trapping mechanism to be driven by chemical bonding between Fe and the polysulfide species based on X-ray diffraction patterns of the cycled battery showing the Fe/Fe_3C diffraction peaks.

Several other authors have afterward reported similar shielding effects aided by the use of magnetic particles to prevent polysulfide migration. As an example, Xia et al. reported on the effective use of FM porous Fe_3O_4@C nanorods as a sulfur host to reduce polysulfide migration[166]. The improved properties are related to the anchoring of polysulfides through F_L associated

with the presence of magnetic Fe_3O_4 NPs. Zhu et al. incorporated FM Fe_3O_4 NPs into the LSB separator to block LiPS diffusion, associating the blocking effect with the magnetic field generated by the magnetized Fe_3O_4 NPs, which produces a F_L that restrains the polysulfides movement[167]. F_L changes the movement direction of polysulfide ions and thus increases the polysulfide concentration around the cathode, accelerates the SRR, and increases the specific capacity. Yue et al. also reported on a separator containing FM Fe_3O_4 NPs as an improved LiPS barrier[168]. The Fe_3O_4 NPs act as mediators of the redox reaction to block the polysulfide migration and dynamically facilitate conversion by changing the molecular structure of PSs and reducing the reaction barrier.

Wang et al.[169] introduced magnetic carbonyl iron powder in the electrolyte to create a magnetic shield to trap polysulfides. By coupling the external magnetic field or using cathode materials with FM characteristics, the uniform distribution of carbonyl iron powder avoids the accumulation of polysulfides on the surface of the cathode. The induced magnetic field effectively traps the dissolved S_x^{2-} through magnetic attraction. Polysulfide adsorption and battery performance are promoted in the presence of an external magnetic field, which is associated with F_L.

Additionally, on the anode side of metal-sulfur batteries, the MHD effect can homogenize ion distribution and suppress localized metal deposition. This redistribution of metal ions effectively mitigates the formation of metal dendrites, which are a major cause of short-circuiting and capacity fading in all kinds of lithium metal batteries. As a result, the magnetic field contributes to a more stable anode/electrolyte interface, enabling longer cycling life and enhanced battery safety, as reported by several authors[58].

Magnetic field influence via spin effect

The mechanisms behind performance enhancement under a magnetic field can be various, and it is generally extremely challenging to discern among them, especially when the magnetic field is intrinsically generated by magnetic particles located within the electrode. The main mechanisms of enhancing the trapping of polysulfides rely on MHD effects or surface adsorption effects. Whether it is one or the other is an important issue worth clarifying to optimize the system.

While the effect of magnetic particles has been almost unanimously associated with the effect of F_L generated by the magnetic field on the moving polysulfide ions, several experimental results challenge this hypothesis: i) The Lorentz effect should increase with the particle magnetization, i.e., with the NP size, but the opposite trend was observed by Yue et al.[168], which points towards a surface driven effect. ii) When applying external magnetic fields on non-FM materials, negligible effects are observed even if the magnetic field is orders of magnitude larger than those generated by the randomly distributed magnetic NPs. iii) A random distribution of particles should result in a random distribution of F_L forming very weak and local microvortexes, thus having a minimal perturbation on the trajectory of an ion in solution. These very local magnetic fields have an associated gradient that could contribute to the polysulfide trapping through the F_K. However, the enhanced LiPS adsorption ability is more likely associated with the change of the spin state of the catalyst surface/site in the presence of the magnetic field.

Recently, we explored the effect of an external magnetic field in the SRR by evaluating the performance of CoS_x-based cathodes toward polysulfide adsorption and conversion[44]. When testing the CoS_x-based LSB within an external magnetic field, higher capacities and much lower capacity decay rates per cycle were measured. In subsequent work, we compared the effect of an external magnetic field on the Na-S reaction performance of three catalysts supported on carbon nanofibers (CNFs) and characterized by different magnetic properties: ferrimagnetic $CoFe_2O_4$, and paramagnetic Co_3O_4 and VO_2[46], the CV curves in a 5 mM sodium polysulfide electrolyte and the corresponding Tafel plots for the three catalysts in the presence and absence of a 900 mT magnetic field are shown in Fig. 10a–c. Under an external magnetic field, the position and area of the redox peak obtained from the $CoFe_2O_4$-based electrode showed a significant increase. In addition, the presence of the magnetic field reduced the Tafel slope from 15.2 to 9.6 mV dec^{-1}, indicating a significant improvement in the rate of conversion of sodium polysulfide to sodium sulfide (Fig. 10d–f). In contrast, no significant effect of the field was observed with the paramagnetic catalysts, which excluded the influence of an improved mass transport within the electrolyte. The performance of CNF/$CoFe_2O_4$ electrodes for the conversion of sodium polysulfide showed dependence on the magnitude of the external magnetic field, as observed in Fig. 10g. Besides, upon removal of the external magnetic field, its effect just gradually disappeared, which can be attributed to the magnetic remanence within the FM CNF/$CoFe_2O_4$. With the support of DFT calculations, we concluded that the eternal field contributes to the spin alignment within the catalysts, moving the bonding and antibonding states up, which influences both the adsorption of polysulfides and their reaction rate by lowering the energy barrier (Fig. 10h,i).

Sun et al. reported on different Ni-doped MoS_2 with FM and antiFM properties, as shown in Fig. 11a, b, respectively[170]. The FM Ni/MoS_2 sample displayed a significantly higher degree of unidirectional spin alignment compared to its antiFM counterpart. The excellent magnetic-field-enhanced catalytic performance on FM Ni/MoS_2 was clearly demonstrated in the hydrogen evolution reaction (HER), where application of a modest external magnetic field (≈0.2 T) boosted the exchange current density by over 25% and lowered the overpotential by ~30 mV at 10 mA cm^{-2}—evidence that spin polarization actively promotes H* adsorption and recombination kinetics. In Ni_1/MoS_2, a distorted tetragonal coordination drives robust, room-temperature ferromagnetism that—when combined with a mild external magnetic field—triggers spin alignment and spin-density redistribution at sulfur active sites via field-modulated S(p)–Ni(d) hybridization, thereby lowering adsorption energies of radical intermediates, which optimizes the adsorption energy of reaction intermediates to reduce the overall reaction barrier.

Similarly, our theoretical calculations reveal that the adsorption energy of polysulfides is significantly higher in the presence of a magnetic field than in its absence (Fig. 11c)[44]. The increase in adsorption energy is attributed to the spin-aligned component of the electron system under the magnetic field. Specifically, our spin-polarized DFT calculations indicate that the adsorption energy of long-chain polysulfides on the CoS_x(200) facet increases by roughly 0.1–0.2 eV when a modest external magnetic field (~0.3 T) is applied. This enhancement arises because the field induces a net spin alignment in the FM CoS_x lattice, shifting the spin-resolved DOS so that the S(p)–Co(d) hybrid orbitals lie closer to the Fermi level and bind anionic polysulfide radicals more strongly. Experimentally, as shown in the inset of Fig. 11c, static adsorption tests under a 0.3 T field demonstrate a 50–70% increase in CoS_x's polysulfide uptake compared to the zero-field case. When assembled into Li–S cells and cycled at 2 C (Fig. 11d), the magnetic-field-treated CoS_x/S cathode exhibits a capacity retention of 315 mAh g^{-1} after 8000 cycles, along with Coulombic efficiencies consistently above 99%. By contrast, a control experiment using paramagnetic carbon fiber under identical field conditions shows no appreciable change in either adsorption or cycling stability, confirming that the magnetic-enhancement effect requires both an external field and an intrinsically FM (or ferrimagnetic) host. In essence, the applied field "switches on" a spin-polarized adsorption channel that both anchors dissolved polysulfides more effectively, suppressing the shuttle and accelerating their conversion kinetics, thereby lowering the overall reaction barrier and dramatically improving battery performance.

Other effects

In addition to the MHD and spin effects induced by magnetic fields, other magnetic field-related phenomena can further enhance the electrochemical performance of batteries. For example, applying a magnetic field during material synthesis can promote favorable structural orientation, thereby improving catalytic activity. In this direction, annealing $FeCo_2O_4$ nanofibers under a magnetic field has been shown to enhance spin polarization[51]. Likewise, magnetic field-assisted alignment of CNF@Co_3O_4 provides an

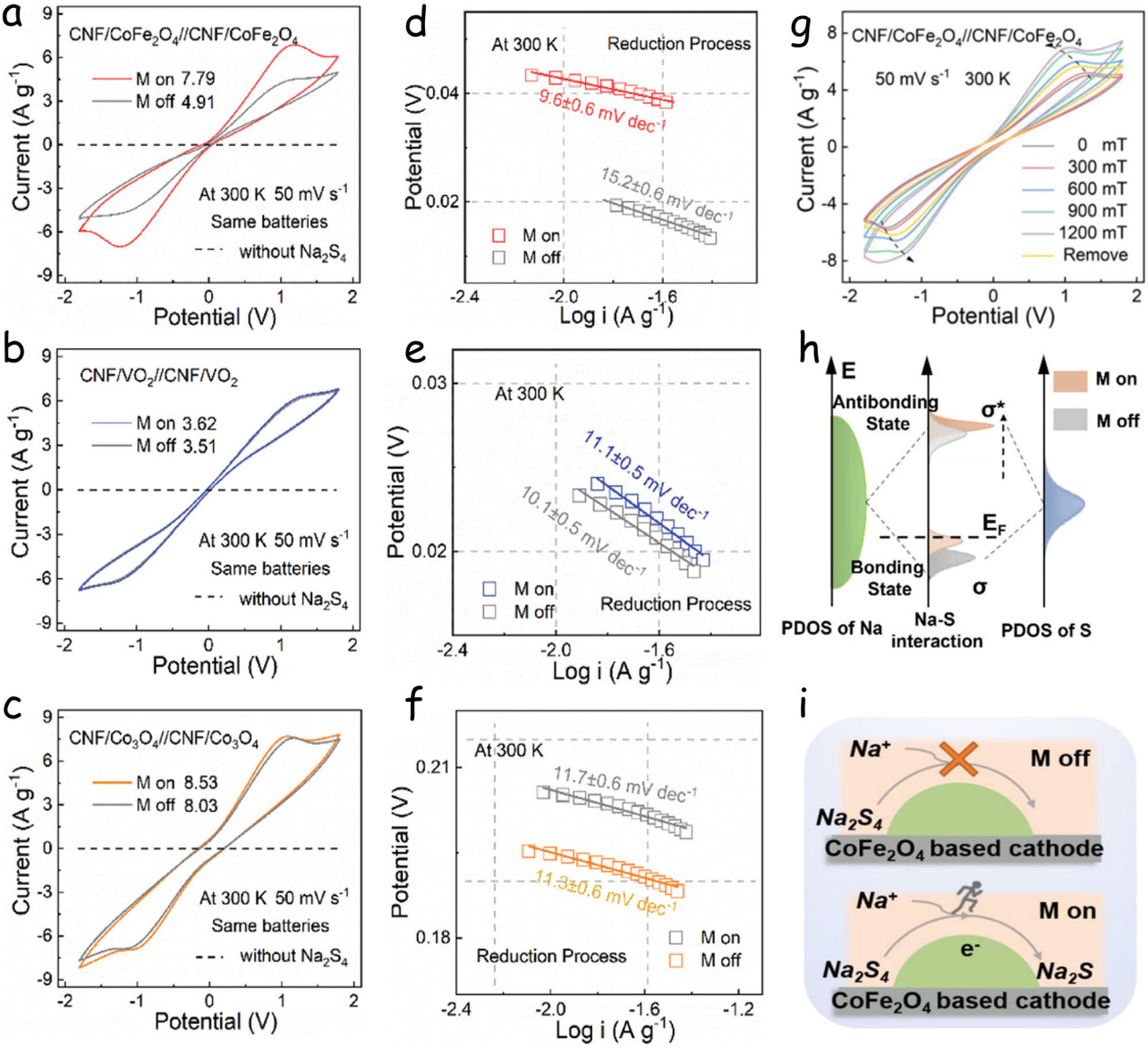

Fig. 10 | Spin effect in sodium sulfur batteries. a–c CV curves of $CNF/CoFe_2O_4$, CNF/VO_2, and CNF/Co_3O_4 electrode in 5 mM Na_2S_4 with and without magnetic field. **d–f** Corresponding Tafel plots. **g** CV curves of $CNF/CoFe_2O_4$ recorded before, during, and after the application of magnetic fields with varying intensities. **h** Energy level diagram showing orbital hybridization for Na_2S_4. **i** Schematic diagram of the catalytic $Na_2S_4 \rightarrow Na_2S$ process in the presence and absence of a magnetic field. Reproduced with permission from ref. 46 (copyright Wiley-VCH, 2023).

effective approach to improve mass transfer kinetics, especially in thick electrodes[171].

Spin engineering within the catalyst

For gene, protein, and other specialized names, taxonomic nomenclature, go to Formatting Guide – Readability. Exchange interaction and spin states are closely intertwined with the atomic chemical environment, which is determined by the crystal structure, atomic arrangement, and defects of the material. For instance, the spin state of a TM cation within a lattice depends on the d-orbital electron spin configuration of the metal and correlates with the occupancy of the d-orbital, which also determines the orbital interaction between the TM cation and the reactant. Depending on the arrangement and coordination of d-orbital electrons, the spin state of TM cations can vary between LS, intermediate-spin, and HS states. Cations with different spin states exhibit different thermodynamic reaction properties. Therefore, adjusting the spin state of metal cations within the crystal structure becomes an effective and feasible method to tune the reaction barrier and thus its rate. This section presents strategies to modify the spin state of the catalyst through tuning the atomic coordination environment. Several approaches have been proposed in this direction, including the introduction of defects and dopants, the atomic level design of the molecular/atomic coordination in metal-organic frameworks (MOFs) and single-atom catalysts (SACs), and the engineering of heterostructures, among others (Fig. 2). Spin-polarized active sites, such as those in doped carbon, SACs, or vacancy-rich TM compounds, create localized unpaired electrons. These sites enable strong orbital hybridization with the π* orbitals of Li_2S_4/Li_2S_6 species. This increases binding energy and reduces the chemical potential for LiPS desorption, thereby physically anchoring the species even during battery rest.

Defect engineering

Defects, particularly point defects, such as vacancies and doping atoms, play a key role in enhancing electrocatalytic activity through several different mechanisms, including the generation of additional free carriers, creating and exposing active catalytic sites[172,173], adjusting interatomic distances, and tuning the electronic structure, among others[14]. At the surface of the catalyst, variations in the atomic coordination can generate unsaturated orbitals and

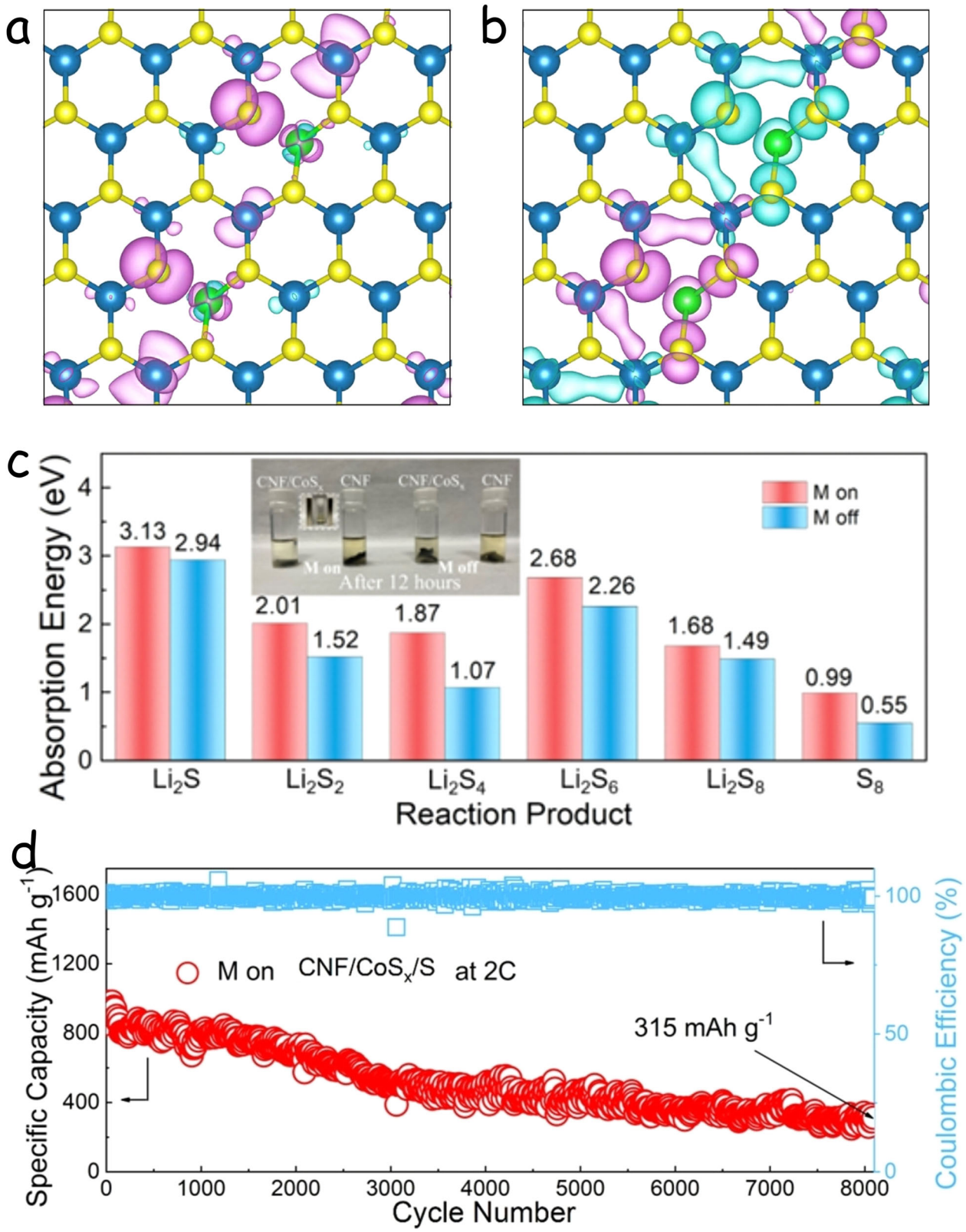

Fig. 11 | Field-driven spin polarization for enhanced catalytic stability. a,b Spin density in Ni-doped MoS_2 with FM (**a**) and antiferromagnetic (**b**) coupling. Yellow, blue, and green spheres denote S, Mo, and Ni atoms, respectively. The light blue and purple isosurfaces represent the spin-up and spin-down states, respectively. Reproduced with permission from ref. 170 (copyright Nature Publishing Group, 2022). **c** Adsorption energy of CoS_2 (200) surface to different sulfur species. The inset shows optical images of the polysulfide solutions after interaction with different adsorbents during 12 h. **d** Cycling performance of CNF/CoSx/S at the current density of 2 C. **c-d** Reproduced with permission from ref. 44 (copyright Wiley-VCH, 2022).

modify the spin state of surface electrons[174]. Besides, while in perfect lattices, electron spins are usually stable, in a defective material, defects can facilitate spin flipping[175]. While research on spin interaction in the SRR process is still in its infancy, there are already several examples of spin engineering through defect engineering toward optimizing the SRR activity. Still, it is urgent to decipher the intrinsic structure-activity relationship within catalysts containing defective electronic spin states[176,177].

Vacancies. Over the past decade, a wide range of sulfur host materials with engineered vacancies have been developed to maximize the exposure of active sites, increase electrical conductivity, and optimize their electronic structures. More recently, the regulation of electronic spin states through vacancy engineering within sulfur cathodes has also gained significant attention[174,176,178,179].

Carbon is the most extensively used and developed sulfur host material due to its low weight, natural abundance, and excellent electrical conductivity. However, pure carbon exhibits only moderate capability for the adsorption and catalysis of key reaction species. An effective strategy to boost the intrinsic catalytic activity of carbon materials is to introduce surface defects, particularly vacancies, showing various carbon vacancies on graphene, including single (SVG), double (DVG), and reconstructed double (RDVG) vacancies, Stone–Wales defects (SWG), and pristine graphene (PG)[180]. Combined with MoS_2, the defective graphene served as a sulfur host in LSBs. Defects enhance interactions with LiPSs by increasing active site density and adsorption strength, following the order: SVG/MoS_2 > DVG/MoS_2 > RDVG/MoS_2 > SWG/MoS_2 > PG/MoS_2. Defect introduction induces spin polarization in the C-2p orbital, with spin clouds mainly at SV defect sites, where unpaired electrons originate. These extra electrons alter the valence band structure, enhancing electron transport during redox reactions. Different defects generate varying numbers of unpaired electrons and spin states[181]. Overall, the study highlights that vacancy-induced spin polarization significantly improves LiPS adsorption and catalysis, accelerating SRR kinetics.

Although direct experimental evidence quantitatively linking defect-induced spin states to polysulfide conversion kinetics is still limited, the electronic structure of carbon materials can be rationally correlated with their catalytic behavior. Zigzag edge states and single-atom vacancies are known to generate localized spin densities, which can facilitate π^*–π interactions with polysulfide species. This spin polarization enhances electron transfer during S–S bond cleavage, thereby accelerating the transformation from long-chain Li_2S_6 to insoluble Li_2S. On the other hand, overly dense vacancy clusters or oxygen functional groups may disrupt the conjugated π-system, reducing both spin activity and conductivity. These insights suggest a non-linear relationship between defect density, spin polarization, and electrochemical performance, calling for future combined experimental and theoretical investigations.

Vacancies can also be generated on the surface or inside of the supported catalysts. Guo et al.[182] achieved a high-performance cathode structure for LSBs by incorporating carbon nanotubes (CNT) and defective $LaNiO_{3-x}$ (LNO–V) NPs into graphitized pinus (GP) sylvestris.The presence of oxygen vacancies in $LaNiO_{3-x}$ leads to a large dispersion of spin-down electrons. These electrons can easily combine with the spin-up electrons present in LiPSs chains, as compared to defect-free planes of $LaNiO_3$, indicating the spin-selective adsorption of LiPSs on $LaNiO_{3-x}$. The changes in spin density around the $LaNiO_{3-x}$ oxygen vacancies also provided strong chemical immobilization and catalytic conversion of LiPSs since the binding elongates the S-S and Li-S bonds, facilitating their cleavage. EPR spectroscopy was employed to characterize the oxygen vacancies on the $LaNiO_{3-x}$ interface in Fig. 12a. The typical signal ($g = 2.001$) confirms the spin polarization resulting from oxygen vacancies. Compared with the GP/CNT/LNO cathode, GP/CNT/LNO–V combined with sulfur showed a higher rate capacity (exceeding 900 mAh g^{-1} at 1 C), indicating that the vacancy resulting in spin polarization of the metal sites is beneficial to enhance the transformation ability of LiPSs.

Changes in spin states associated with vacancies, promoting the SRR process, have also been observed in other catalytic materials, such as TM chalcogenides. As shown by Dai et al., sulfur vacancies in $NiCo_2S_4$ enhance the chemisorption of LiPSs, and the reorganization of the spin state through these vacancies can further accelerate the transformation kinetics of LiPSs (Fig. 12b)[183]. The asymmetric spin-up and spin-down DOS indicate the spin-polarized nature of absorbed Li_2S_x, especially in Li_2S_2 and Li_2S. As a result, $NiCo_2S_{4-x}$ cathodes with sulfur vacancies exhibit outstanding rate performance, delivering a capacity of 967.2 mAh g^{-1} at 3 C (Fig. 12c), along with enhanced suppression of the shuttle effect and improved sulfur utilization. Other types of defect vacancies, such as Te vacancies in ZnTe/$CoTe_2$[21], S vacancies in Co_9S_{8-x}[184], S vacancies in TiS_{2-x}[185], Se vacancies in WSe_2[186], and Cu vacancies in copper selenide[14] have also been reported to generate unpaired electrons and facilitate the SRR process.

Vacancies can also modulate the spin–orbit coupling (SOC) effect, which arises from the interaction between the spin and orbital motion of electrons[187]. This interaction leads to the splitting and rearrangement of energy levels depending on the electron spin and can significantly influence chemical reactions[188]. For instance, Gao et al.[186] employed 2D WSe_2 containing anionic Se vacancies and edge dislocations as a sulfur host material. Among the samples tested, $WSe_{1.51}$ exhibited an optimized electronic structure and enhanced SOC, which facilitated electron transport, strengthened LiPS adsorption, and promoted SRR activity. These improvements translated into long-cycle stability and high-energy performance in rechargeable LSBs.

Notably, the relationship between vacancies, spin states, and SRR performance is highly complex, involving the interplay of multiple factors. Consequently, a deeper understanding and precise control of this effect requires further advanced experimental characterization and theoretical modeling.

Heteroatomic doping. Heteroatomic doping, i.e., the introduction of small amounts of a foreign element to alter the properties or behavior of a material, is an effective way to fine-tune the orbital occupancy and spin configuration of materials, thereby optimizing the catalytic performance[174]. Dopant atoms can interact with electrons in the material, changing their spin states. Doping can also generate unsaturated coordination and introduce additional localized electronic states and potentially free-charge carriers that can affect the orientation and properties of surrounding spins. Additionally, dopants can modify the electronic structure and adsorption capacity of the reactant, effectively improving electrochemical performance[189].

As noted by Hou et al., considering the favorable outcomes observed in oxygen reduction processes[190], it is reasonable to anticipate that S-doped catalysts would exhibit a strong affinity for Li_2S_x species through the spin effect[191]. Building on this idea, Duan et al. investigated the influence of sulfur and nitrogen doping on graphene as a cathode material for LSBs[192]. Their results demonstrated that the combined doping of S and N significantly reduces the activation energy and enhances the stability of LSBs. The interaction between the dopants and the graphene electrons alters the electrons' spin states, thereby improving SRR kinetics.

N/O co-doping is another effective strategy to enhance the cycle stability and specific capacity of LSBs. Liu et al. demonstrated that a unique N/O double-doped honeycomb carbon structure not only physically encapsulates LiPSs but also promotes their chemisorption and catalytic conversion. The strong chemisorption of LiPSs was attributed to the altered spin density and charge distribution around the neighboring nitrogen- and oxygen-doped carbon atoms[193].

Several other non-metal elements have been used as dopants to modify the electronic configuration in carbon-based hosts and metal compound catalysts, including oxygen[194], phosphorus[195], boron[196], iodine[15], and selenium[189]. As an example beyond the doping of the carbon host, Wang et al. showed that the introduction of N into the porous sheet of N-$CoSe_2$ (Fig. 12d) changes the original spin state and improves the catalytic performance of the originally inactive $CoSe_2$. The hybridization of N elements

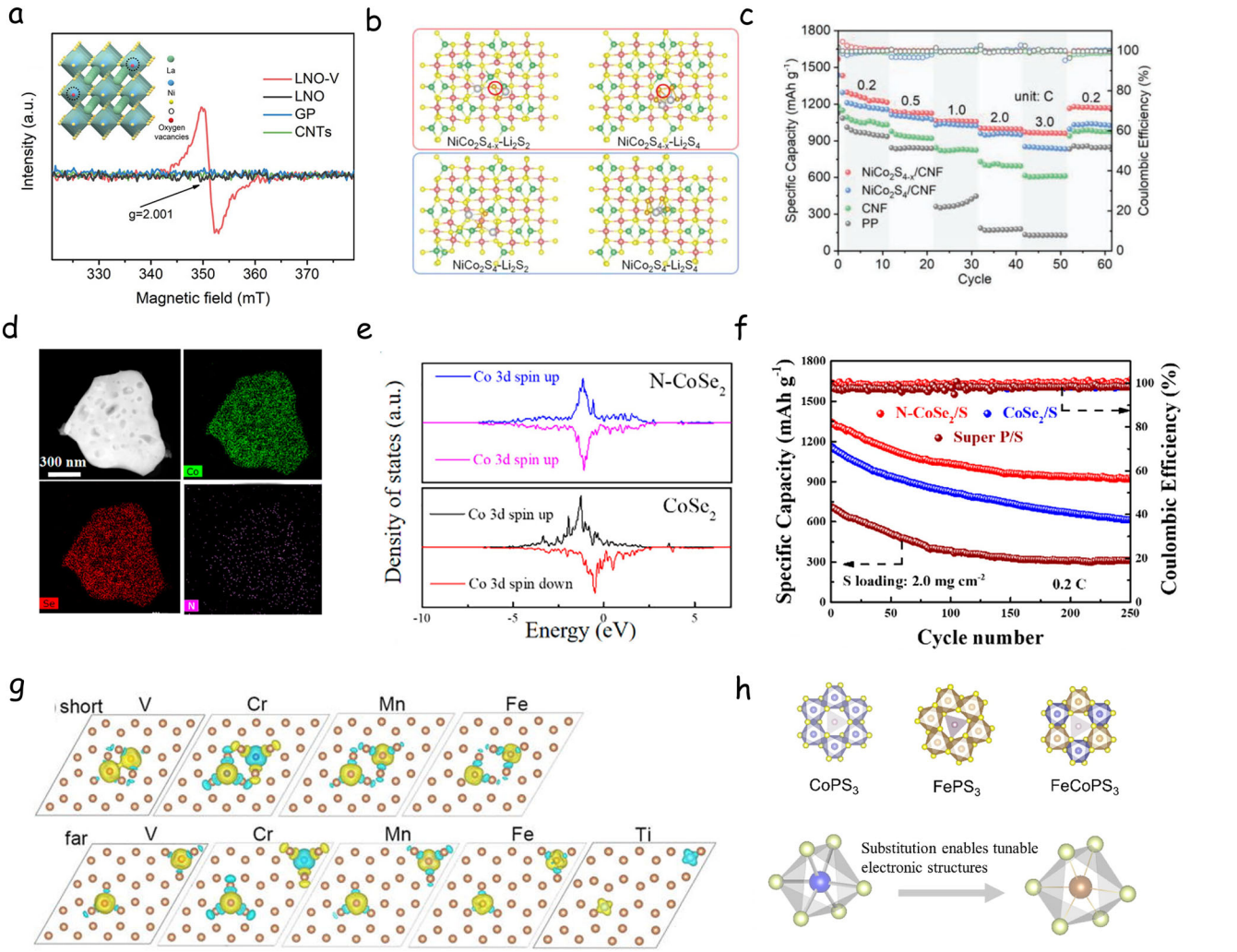

Fig. 12 | Spin state modification by defect engineering. a EPR spectra of $LaNiO_{3-x}$, $LaNiO_3$, CNT, and GP, with the inset representing the crystal structure of $LaNiO_{3-x}$. Reproduced with permission from ref. 182 (copyright Wiley-VCH, 2022). **b** Calculated geometries of Li_2S_2 and Li_2S_4 on the (101) plane of $NiCo_2S_4$ (top) and $NiCo_2S_{4-x}$ (down). **c** Rate performance of $NiCo_2S_{4-x}$/CNF, $NiCo_2S_4$/CNF, CNF, PP. **b, c** Reproduced with permission from ref. 183 (copyright Wiley-VCH, 2023). **d** EDX element mapping of N-$CoSe_2$. **e** PDOS of Co 3 d. **f** Cycle performance of N-$CoSe_2$. **d-f** Reproduced with permission from ref. 197 (copyright American Chemical Society, 2022). **g** Magnetization of two TM-doped antimonene when the distance between the two TM atoms is short (top) and long (down). Yellow and blue represent spin-up and spin-down densities with an isosurface value of 0.003 e/A^3. Reproduced with permission from ref. 198 (copyright American Institute of Physics Publishing, 2016). **h** Substitution metal cation enables tunable electronic structures for $CoPS_3$, $FePS_3$, and $FeCoPS_3$. Reproduced with permission from ref. 47 (copyright American Chemical Society, 2023).

into $CoSe_2$ can form shorter Co-N bonds, resulting in a higher Co central atom charge number (Fig. 12e)[197]. The projected DOS (PDOS) of Co 3 d orbital shows that N-doped $CoSe_2$ brings new defect levels and shifts the Co 3 d energy band closer to the Fermi level, which partially transforms Co into an LS state. Subsequently, the cycling stability of the cathode based on the N-$CoSe_2$ catalyst at 0.2 C showed a capacity fade rate per cycle of just 0.124%, significantly below that of $CoSe_2$, at 0.187%. (Fig. 12f). The authors also showed that the change in the spin state of the catalyst caused by doping can affect the migration rate of electrons in the catalyst, which is expected to maintain a high specific capacity at a large current density and achieve fast charge and discharge behavior.

Beyond doping sulfur hosts and catalysts with non-metallic elements, introducing metal atoms with different possible spin states offers additional opportunities to tune the overall spin state of the material. In this context, Yang et al. demonstrated that doping metal atoms into semiconductors can alter the original electron spin states, as shown by doping antimonene with various 3 d TMs (Fig. 12g)[170] Antimonene doped with Ti, V, Cr, Mn, and Fe exhibits magnetic properties, with Ti-, V-, and Mn-doped samples behaving as half-metals, characterized by nearly 100% spin polarization[198]. Another example is nickel doping in MoS_2, which induces a significant change in magnetic properties and spin orientation through metal ion incorporation. Recently, Li et al. synthesized V-doping-induced hexagonal nanosheets (V-Co_3O_4 NS) featuring intermediate spin states (IS, $t_2g^5e\_g^1$) based on ligand field theory and molecular orbital theory. These intermediate spin states enable strong bonding with LiS* species, thereby effectively accelerating sulfur conversion kinetics[199]. Benefiting from these properties, a battery employing a V-Co_3O_4 NS-modified separator achieved a high areal capacity of 15.37 mAh cm^{-2} at a high sulfur loading of 15.4 mg cm^{-2}.

Instead of introducing external metal atoms, Li et al. demonstrated that adjusting the Co/Fe ratio can effectively influence the overall catalytic performance of $FeCoPS_3$ catalysts without altering their crystal structure, as $CoPS_3$, $FePS_3$, and $FeCoPS_3$ all share the same monoclinic structure with space group C2/m (Fig. 12h)[47]. Due to the redistribution of 3 d electrons, the d-band center of $FeCoPS_3$ shifts upward compared to those of $FePS_3$ and $CoPS_3$. The coupling between Fe^{2+} and Co^{2+} ions leads to an increase in the net spin of the metal centers. This process breaks the degeneracy of the electronic states at the active catalytic centers, resulting in electron redistribution and a change in spin states. Additionally, the energy level of the

spin-up orbitals becomes higher than that of the spin-down orbitals, further shifting the d-band center upward. Incorporation of Fe or Co dopants into the octahedral sites enhances the d-band center position, strengthening the adsorption capacity of the active sites toward LiPSs. Moreover, the strong interaction between the active centers and polysulfides increases the filling rate of the polysulfide's lowest unoccupied molecular orbital (LUMO), thereby promoting the cleavage of S–S bonds.

In addition to the examples mentioned above, various other metal ions have been employed to enhance the performance of different catalysts, such as Ni- and Zn-doped $CoSe_2$[200], Mo-doped CoB[201], and Co-doped MoS_2[202]. These dopants can alter the metal coordination environment and, consequently, the electronic spin state, thereby improving the ability to facilitate LiPS conversion.

Molecular/atomic coordination design

Careful design and engineering of the molecular or atomic coordination environment offers another powerful strategy to tune not only the electronic band structure but also the spin states of catalytic materials. By precisely tailoring local coordination, charge distribution, spin polarization, and active-site reactivity can be modulated to enhance catalytic performance. Although this approach can, in principle, be applied to a wide range of materials, it has been most extensively explored in specific systems, such as MOFs and SACs, where the highly controlled coordination environment offers unique opportunities to fine-tune electronic and spin-related properties.

Metal-organic frameworks. MOFs are crystalline materials composed of periodically arranged metal ions or clusters coordinated by organic linkers[203]. Many TM ions possess unpaired d-electrons, which confer intrinsic spin properties. By selecting metal ions with different spin states, it is possible to tailor the magnetic and electronic characteristics of the MOF. In addition, the organic linkers, typically π-conjugated molecules, can significantly influence the spin states of the metal centers through their structural and electronic properties. Therefore, modifying the molecular structure and composition of the linkers provides a strategy to adjust the electron spin states of the metal ions[204]. Moreover, the spin interactions between metal ions and organic ligands, such as exchange interactions, spin states, and electron distribution, can also be finely tuned by engineering the metal–ligand bonding environment[11].

The electron spin state is particularly sensitive to the type of metal ions introduced, especially those with varying numbers of unpaired d-electrons. For instance, Liu et al.[40] leveraged spin-dependent charge transfer and orbital interactions in $Co_{0.8}Mn_{0.2}$-MOFs to accelerate the oxygen evolution reaction kinetics. The catalytic activity, enhanced by spin rearrangement, was over twentyfold higher compared to the pristine MOF, highlighting the role of improved charge transfer and orbital overlap between metal centers and reaction intermediates. The authors attributed this substantial performance boost to spin-dependent reaction kinetics.

Similarly, spin-state modulation plays a crucial role in governing the conversion kinetics of polysulfides. Wang et al. demonstrated that by carefully selecting different 3 d TM atoms to tune the electron spin states in MOFs, these materials could serve as highly efficient sulfur hosts in LSBs, achieving high performance and long cycle life[205]. In another study, Zhao et al.[206] investigated the influence of spin states on adsorption energy and catalytic activity by employing metal coordination compounds (M = Co, Fe, or CoFe) as catalytic additives to promote the sluggish heterogeneous reaction kinetics of polysulfides. By adjusting the spin density of free metal ions (Co, Fe, CoFe) and modulating the d-orbital distribution of Fe^{3+}, Co^{2+}, and Fe^{2+} with unpaired electrons, they achieved LSBs with significantly enhanced cycling stability.

On the other hand, adjusting the interaction of d electrons in metal center atoms with the π-electron in the ligand, the metal-ligand bond and the material's spin polarization can be optimized to enhance SRR kinetics[207,208]. In this direction, Yang et al. synthesized a 1D π–d conjugated MOF (Ni-MOF-1D) and demonstrated it to be an efficient sulfur host with fast SRR kinetics[11]. Besides, Zhao et al.[209] produced and studied 13 kinds of 2D MOFs composed of TM atoms (Co, Ni, Cu, and Zn) coordinated by nitrogen, sulfur, and oxygen to reveal their structure-activity relationship in terms of electrocatalytic performance. They showed the rapid reaction kinetics of LSBs can be realized by adjusting the coordination of MOF covalent bonds to change the electron spin interactions between metal ions and organic ligands.

The SOC plays an important role in the design of catalysts, especially MOFs. SOC can affect the energy level structure of the active site, regulate the rate and mechanism of electron transfer in the reaction, affect the transition path of electrons and distribution of electronic DOS, reduce the energy barrier of electron transfer, and promote the redox reaction. The structure of the MOF can be tuned to adjust the orientation of the SOC, thus maximizing the unpaired electrons on the catalyst and minimizing the reaction kinetic barrier of the polysulfide redox reactions. In this direction, Xu et al.[205] synthesized a spherical superstructured hafnium diboride derived from MOF NPs by a one-step boronation process. They demonstrated the strong SOC nature of the 5 d Hf electronic configuration shifts the p-orbitals of nonmetallic atoms closer to the Fermi level, endowing anionic redox activity and unconventional superconductivity. Benefiting from its unique superstructure, the obtained HfB_2 exhibits excellent catalytic activity for the conversion of polysulfides. Han et al. showed that adjusting the pyrolysis process of UiO-66-NH_2@rGO (U@rGO) is it possible to regulate the generated abundant low-oxidative free spin electrons at the Zr ion sites that serve as polysulfide anchors and transfer mediator active sites[210].

Single-atom catalysts. Single-atom coordination inherently introduces spin polarization effects, which contribute to enhanced adsorption and catalytic capabilities. This partially explains the exceptional catalytic performance of SACs supported on conductive carbon materials for LiPS conversion[211]. Numerous studies have demonstrated that manipulating the electron spin in atomically dispersed materials can effectively modify their electronic states and energy level distributions, thereby optimizing both the activity and selectivity of catalytic reactions[212–214].

The electron spin state of the catalytic atoms can be tuned by manipulating their electronic filling. This can be realized through manipulation of the electronic distribution within the compound, i.e., the charge transfer of electrons between metal atoms and coordination environments, which is determined by both the single-atom element and its surroundings.

Cai et al. evaluated the performance as cathode hosts for LSBs of four SACs within a nitrogen-doped graphene lattice (M-N_4-C, M = Co, Fe, V, and W) using spin-polarized DFT calculations[215]. Figure 13a shows the obtained energy distribution maps based on the Gibbs free energy. The V- and W-based SACs provided highly efficient LiPSs conversion and fast SRR process, up to 6.0 times that of PG greatly improving the reaction kinetics by reducing the S dissociation barrier for Li_2S_2 decomposition by about 2.5 times.

TMs coordinated with N are widely used in LiPSs conversion process[10,42,126,214]. A comparative study of the $Li_2S_2 - Li_2S$ catalytic reduction process on single-atom Fe, Ni, and Co with different metal-N_4 sites was reported by Li et al.[48]. As shown in Fig. 13b, Fe−N_4 has the largest spin density and a magnetic moment of ~1.91 μB, with a larger spin polarization degree than Co−N_4 and Ni−N_4. Through a series of theoretical studies, the authors demonstrated that the spin polarization can provide spin electrons to reduce the antibonding orbital occupation in $Li_2S_2 - TM - N_4$ and enhance the $TM - S$ interaction, thereby weakening the strength of the $S - S$ bond in Li_2S_2 and thus accelerating the reduction of $Li_2S_2 - Li_2S$ (Fig. 13c). Fe-N_4-based cathode exhibited the fastest Li_2S_2-Li_2S reduction kinetics, which resulted in batteries with a capacity of 226 mA h g^{-1} that far exceeded that of hierarchical porous single atomic Co (177 mA h g^{-1}) and single atom Ni (208 mA h g^{-1}) (Fig. 13d). This study showed a positive correlation between the magnetic moment generated by single-atom doping, the spin polarization degree of the induced electrode, the catalytic

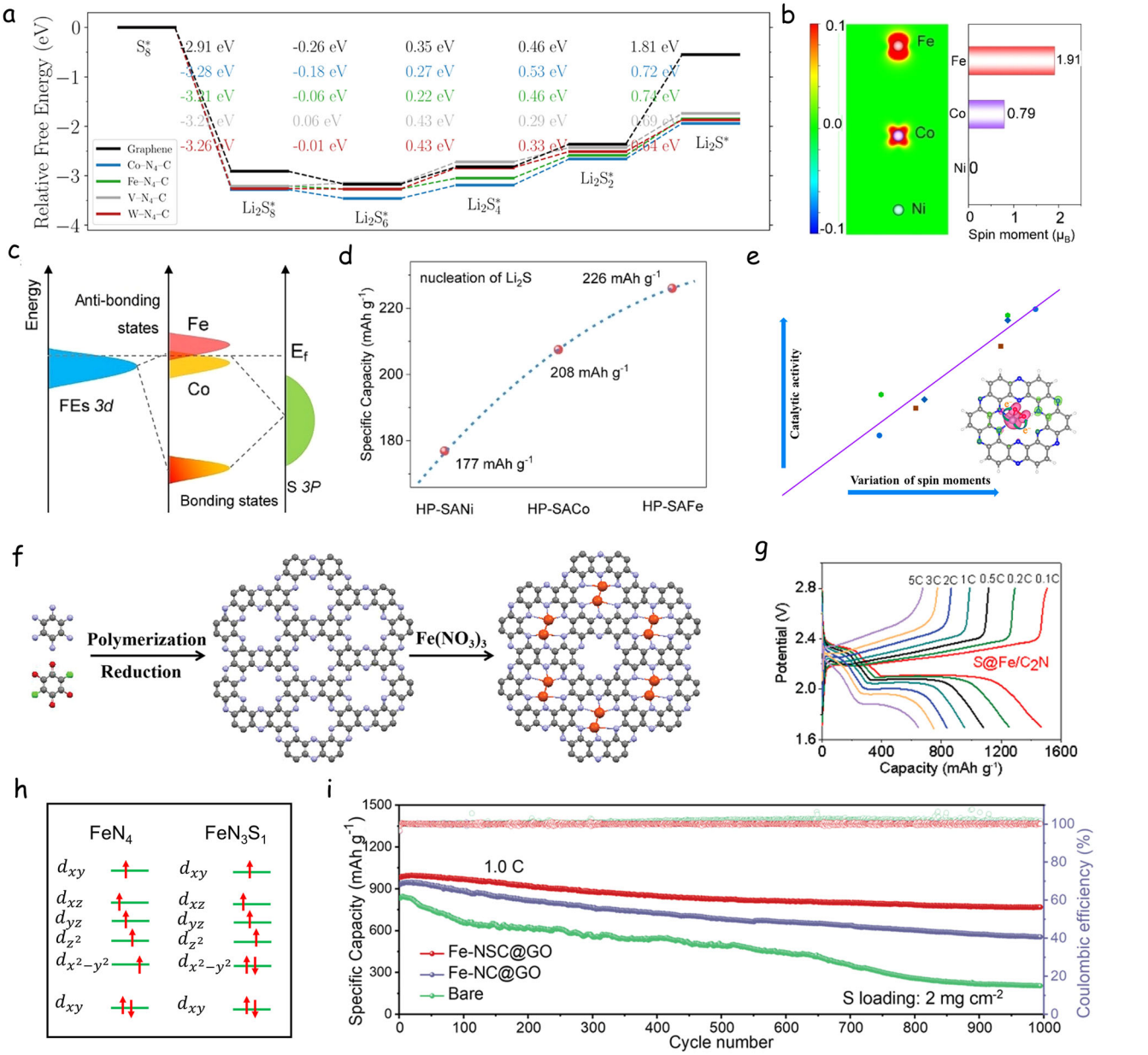

Fig. 13 | Spin effect by single atomic engineering. a Relative Gibbs free energy for the examined disproportionation reactions for graphene and TM − N_4 − C (TM = Co, Fe, V, and W) materials. The numerical values show the stepwise relative free-energy change of each reaction. Reproduced with permission from ref. 215 (copyright American Chemical Society, 2021). **b** Calculated spin density and magnetic moment of Fe, Co, and Ni-N_4. **c** Schematic illustration of the local electronic structure of Fe/Co 3d-orbitals in Li_2S_2 Fes N_4, E_f is the Fermi level. **d** Specific capacities for the step of Li_2S deposition on the HP-SAFes. **b–d** Reproduced with permission from ref. 48 (copyright Wiley-VCH, 2021). **e** Relationship between the variation of spin moments and the catalytic ability of Fe in C_2N. Reproduced with permission from ref. 214 (copyright American Chemical Society, 2021). **f** Schematic illustration of the synthetic route of Fe/C_2N 2D layered materials (blue is nitrogen, gray is carbon, red is oxygen, green is chlorine, orange is iron). **g** Galvanostatic charge-discharge profiles of S@Fe/C_2N and S@C_2N electrodes at various rates. **f,g** Reproduced with permission from ref. 10 (copyright Wiley-VCH, 2021). **h** Scheme of the orbital interaction of FN_4 and FN_3S_1. Reproduced with permission from ref. 79 (copyright Wiley-VCH, 2022). **i** Long-term cycling performance at 1 C of LSB cells using different separators. Reproduced with permission from ref. 225 (copyright Wiley-VCH, 2023).

ability, the Li_2S_2/Li_2S deposition capacity, and the specific capacity of the batteries.

Zhang et al. proposed a molecular spin engineering to break the symmetry of Fe-N-C and achieve spin modulation of triplet to singlet conversion through ligand field theory[133]. Fe-N-C displays the 3 d electronic structure of $(d_{xy})^2(d_{xz})^2(d_{yz})^2$ and significantly accelerates LiPS switching kinetics. According to DFT, the energy level of LiPSs increases after being adsorbed on the Fe center. As a result, the optimized catalyst has a capacity decay rate of 0.026% per cycle at a current density of 2 C.

Adjusting the coordination environment, thereby modifying coordination sites, numbers, and bonds, allows further optimization of the spin effect of SACs and hence their catalytic performance[42]. The change in the coordination environment may affect the spin orientation of metal atoms by adjusting the SOC for instance[216]. As an example, the coordination of C and N within graphene affects the spin polarization of Fe and the occupation and location of its 3 d orbital around the Fermi level, which has an impact on the exchange interaction energy between atoms and hence on its catalytic ability[217].

Beyond graphene, C_2N has been regarded as an excellent sulfur host and single-atom support due to its large density of N-coordination environment that offers abundant sites for single-atom immobilization[218]. Using DFT calculations, Jiang et al.[214] investigated the oxygen evolution reaction catalyzed by Fe single atoms supported on C_2N (C_2N-Fe). They obtained a nearly linear relationship between the electronic spin moment of Fe and O_2, which correlates with the amount of electron transfer from Fe to O_2, and the catalytic activity (Fig. 13e). The strong metal-ligand exchange interactions between Fe centers and coordinating ligands lead to strong electron delocalization, making the spin density of ionic centers closer to that of HS iron states. These results further confirm the strong influence of the electronic spin state on the electrocatalytic activity of catalysts based on TMs. From theory to practice, we used a 2D layered C_2N material hosting iron single-atoms (Fe/C_2N) as a cathode additive in LSBs (Fig. 13f)[10]. The Fe/C_2N-based cathode exhibited excellent rate capability and long-term cycling stability, with an initial capacity of 1540 mA h g^{-1} at 0.1 C and 678.7 mA h g^{-1} at 5 C (as shown in Fig. 13g).

Beyond SACs, dual-atom catalysts (DACs) offer additional versatility. Graphitic carbon nitride (g-C_3N_3), with its high pyridinic nitrogen content and distinctive 2D porous structure, serves as an ideal host material for anchoring diatomic catalytic sites. The growth of different diatomic species on g-C_3N_3 allows for precise tuning of spin effects, leading to high-performance LSB systems. In heteronuclear DACs, the coupling between two different metal atoms enables mutual adjustment of their d-electron spin states, enhancing the anchoring strength and catalytic activity toward polysulfides more effectively than homonuclear DACs[219]. For example, when Co–Mn@g-C_3N_3 is used as a cathode material for LSBs, it exhibits outstanding performance due to the hybridization between Mn^{2+} HS d-electrons and the half-filled Co^{2+} dz^2 orbitals. This unique electronic interaction not only reduces the Gibbs free energy of polysulfide conversion but also lowers the reaction energy barrier for the transformation of Li_2S_2 to Li_2S to just 0.26 eV, significantly accelerating the sulfur reduction reactions.

The utilization of single or dual atoms as host catalysts for LSBs has gained significant attention in recent years. Various types of single atoms, including Co[220], Ni[221], V[222], and Zn[223] have been investigated as sulfur hosts for LSBs. While excellent performances have been reported, a full understanding of the underlying mechanisms should take into account the outer electron spin state of the single atoms.

Another feasible strategy to manipulate the local spin state of isolated Fe sites is via S-coordination doping (FeSA-NSC)[79,224]. As an example, Hou et al. gradually changed the single Fe coordinate environment from N to S coordinate forming FeN_4 to FeN_1S_3, FeN_2S_2, and FeN_3S_1[79]. As shown in Fig. 13h, the incorporation of S in the coordination of FeSA-NSC affects the spin-polarized configuration and particularly the middle-spin state of Fe ($t_{2g}^6e_g^1$), which facilitates the penetration of electrons into antibonding π orbitals.

Within the LSB framework, Sun et al. demonstrated that, compared to the bare Fe–N_4 configuration, the introduction of sulfur leads to greater charge density accumulation around the Fe–NSC structure, altering the original electron spin state[225]. This modification enhances LiPS adsorption and accelerates sulfur conversion. As a result, LSBs incorporating a Fe–NSC@GO-modified separator exhibit significantly improved performance, achieving a discharge capacity of 1156 mA h g^{-1} at 1 C and excellent cycling stability, with a minimal capacity decay rate of just 0.022% over 1000 cycles (Fig. 13i).

Instead of using S, Huang et al.[226] changed the N coordinate environment of Fe single atoms with P, also demonstrating a decrease in the energy barrier of polysulfide conversion and LSBs with improved stability. Additional examples of the change of the coordination environment surrounding SACs to change the spin state and improve the polysulfide conversion can be found for $conn_3S$[227], CoB_2N_2[228], FeN_2[229], and MnN_1O_3[193].

Heterostructures and geometry

Another effective strategy for spin manipulation is the construction of heterostructured materials, where the electronic properties at the interface can be tuned and spin alignment can be achieved. Additionally, adjusting the atomic geometric configuration of the material offers further control over spin states, providing a versatile approach to optimizing catalytic performance.

Heterostructure engineering. At the interface of heterostructured materials, unique electronic structures, chemical environment, coupling effects, and charge redistribution play a crucial role in regulating the electronic spin states[103,230,231]. As an example of a heterostructure formation resulting in an evident change of spin state, Li et al. showed a PbI_2/WS_2 Van der Waals heterostructure with a high degree of spin polarization (Fig. 14a)[103], as detected through PPL (Fig. 14b).

Within the framework of LSBs, Zhang et al. showed Mn_3O_4-MnP_4 heterostructured materials as excellent SRR catalysts[232]. The interface between Mn_3O_4-MnP_4 shows a lattice mismatch that influences the interface electronic spin. The DOS curves for Mn_3O_4, MnP_4, and Mn_3O_4-MnP_4 are presented in Fig. 14c. Mn_3O_4 exhibits pronounced magnetism, characterized by a small band gap for the spin-up state and a large band gap for the spin-down state. In contrast, MnP_4 possesses a small band gap without significant spin polarization. Upon the formation of the heterostructure, the spin-up and spin-down electrons of Mn_3O_4-MnP_4 aggregate at the Fermi level, thereby enhancing the conductivity of the heterostructure. The electron accumulation on MnP_4 improves the Li_2S_x adsorption energy and consequently enhances the catalytic activity. Simultaneously, the large band gap in the spin-down state of Mn_3O_4 contributes to a high adsorption energy for polysulfides. Overall, the modification of the electronic spin states within Mn_3O_4-MnP_4 heterostructures inhibits the LiPS migration and improves the SRR efficiency.

Recently, we reported the development of NiS_2/$NiSe_2$ heterostructures encapsulated within a nitrogen-doped carbon matrix (NiS_2/$NiSe_2$@NC) as catalytic additives for sulfur cathodes[233]. The heterostructure promotes spin splitting of the Ni 3 d orbitals and induces a transition of Ni^{3+} from a LS to a HS state. This HS configuration elevates the electron energy levels and activates the electronic states, thereby accelerating charge transfer and optimizing the adsorption energy for polysulfides. As a result, the reaction energy barrier for polysulfide conversion is significantly lowered. Benefiting from these advantages, lithium–sulfur batteries employing the NiS_2/$NiSe_2$@NC/S cathode exhibit a high initial capacity of 1458 mAh·g^{-1} at 0.1 C and excellent rate performance, maintaining 572 mAh·g^{-1} at 5 C.

Due to the difference in the unpaired electrons of different cations, heterostructure interfaces can result in stronger or weaker charge transfer and coupling effects, increasing the degree of spin polarization to some degree and causing orbital splitting. For example, some TM cations form octahedral complexes with dimers, such as S_2^{2-}, Se_2^{2-} or Te_2^{2-} in LS energy states, while the 3 d orbitals of the TM ion are split into two subordinate orbitals t_{2g} and e_g[234]. This is the case of Co within $CoTe_2$, whose 3 d electron configuration takes the LS of $t_{2g}^6e_g^1$ providing the compound with a metallic character. In the same direction, vanadium ditelluride (VTe_2) demonstrates favorable metal conductivity due to the LS state of $t_{2g}^6e_g^1$ in its 3 d electronic configuration. This characteristic facilitates rapid charge transfer at the electrode, thereby promoting efficient catalytic conversion of polysulfides. By constructing a VTe_2@MgO heterostructure (Fig. 14d), Sun et al. demonstrated the possibility to effectively regulate the electronic properties and spin state, enabling high LiPSs capture/conversion efficiency and efficient decomposition of Li_2S[28].

A similar reasoning applies in vanadium diselenide-based heterostructure materials. Y. Li et al. evaluate the heterostructure formed between 1T-VSe_2 and MXene ($Ti_3C_2T_x$), as shown in Fig. 14e[235]. They found out the surface charge density of Ti atoms in $Ti_3C_2T_x$ decreases, while the charge density of Se atoms at the bottom of 1T-VSe_2 increases, effectively illustrating the changes in electronic structure. Moreover, PDOS reveals that V atoms primarily contribute to the electron density near the Fermi level. It is noteworthy that the PDOS intensity for spin-up electrons in 1T-VTe_2 is significantly higher than that for spin-down electrons without a heterostructure. However, upon introducing MXene, the intensity of both spin-up

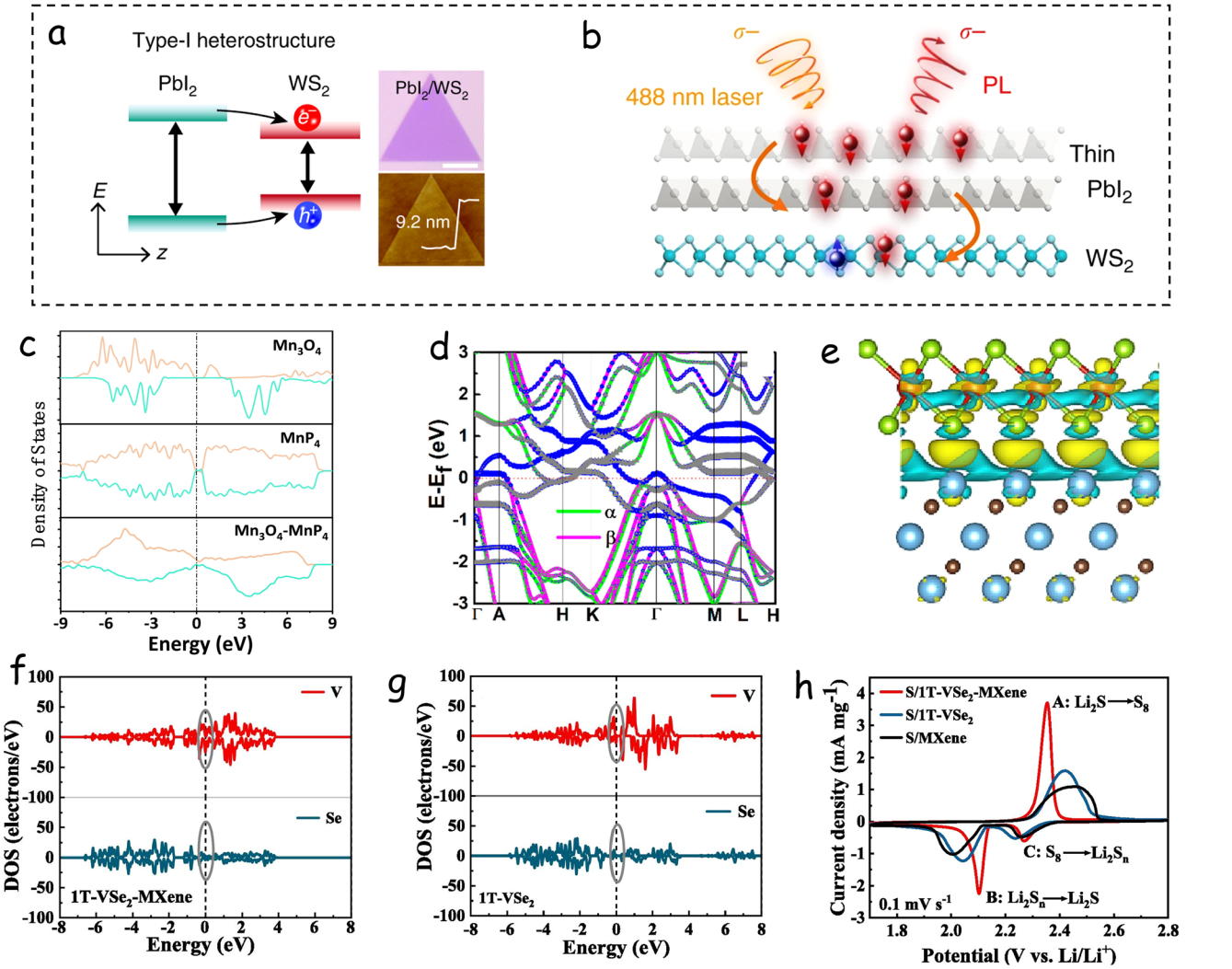

Fig. 14 | Spin effect by heterostructure engineering. a Schematic of the type-I heterostructure for the study of the carrier interlayer transportation. **b** Schematic illustrations of the resulting spin polarization in the thin and thick PbI_2/WS_2 heterostructures. **a**,**b** Reproduced with permission from ref. 103 (copyright Nature Publishing Group, 2020). **c** DOS analysis of Mn_3O_4, MnP_4 and Mn_3O_4-MnP_4. **c** Reproduced with permission from ref. 232 (copyright Elsevier, 2021). The atomic orbital projected band structure (**d**) of VTe_2 has a symmetry of $P\bar{3}m1$, and the red dashed line indicates the Fermi level. **d** Reproduced with permission from ref. 28 (copyright American Chemical Society, 2019). **e** Charge density difference redistribution between 1T-VSe_2 and MXene. **f**,**g** PDOS for V and Se elements of 1T-VSe_2-MXene heterostructure and 1T-VSe_2. **h** Electrochemical performance CV of 1T-VSe_2-MXene heterostructure and 1T-VSe_2. **e**–**h** Reproduced with permission from ref. 235 (copyright Elsevier, 2023).

and spin-down V atom PDOS at the Fermi level becomes nearly equal, providing strong evidence for MXene's influence on vanadium atom spin polarization degree. (Fig. 14f, g) Importantly, this results in excellent electrical conductivity and electron transfer ability as indicated by PDOS crossing over the Fermi level. As a consequence, the S/1T-VSe_2-MXene electrode exhibits lower oxidation peaks and higher reduction peak potential values, denoting promoted SRRs associated with the spin effect in vanadium atoms (Fig. 14h).

Because selenium shares periodic table group and main properties with sulfur, Li-Se batteries face similar challenges as LSBs[236]. Zhang et al. proposed a Li-Se battery based on $NiSe_2/Ni_2Co/CoSe_2$ heterostructures as a catalyst of the Li-Se reaction[146]. Within $NiSe_2$, the electronic configuration of Ni^{2+} is $t_{2g}^6e_g^2$, while that of Co^{2+} in $CoSe_2$ is $t_{2g}^6e_g^1$. In comparison to the $NiSe_2/CoSe_2$ heterostructure, the $NiSe_2/Ni_2Co/CoSe_2$ heterostructure exhibits a higher degree of magnetization and a larger coercive field at ambient temperature. The $NiSe_2/Ni_2Co/CoSe$@S-electrode also demonstrates a significantly improved reversible specific capacity of 224 mA h g^{-1} at 5 C, indicating that the presence of unpaired electrons facilitates selenide conversion under high current densities.

Several other heterostructures have been developed to accelerate polysulfide conversion in LSBs, e.g., WS_2–WO_3[237], MoN–VN[238], and TiN–VN[239]. By carefully designing and engineering these structures, it becomes possible to harness interface effects, thereby enabling precise manipulation of the electronic spin state and influencing its catalytic performance. However, the research on the effect of spin state on polysulfide adsorption and conversion at the complex heterostructure interfaces of 3D catalysts is still in its nascent stage, with most mechanisms remaining poorly understood.

Geometric configuration. The electron spin state, as well as the charge and orbital topology, can be modified by adjusting the geometric configuration of catalysts with perovskite (ABX_3)[240–242] or spinel (AB_2X_4)[65,155,243] structures for instance (where A and B are metals and X is a non-metal element), through changing the cation position within the structure[244]. Taking the spinel structure as an example, the trivalent cobalt cations at the octahedral center are usually in a HS state, while the divalent cobalt cations at the tetrahedral center are usually in an LS state. This modification changes the arrangement and coordination mode of

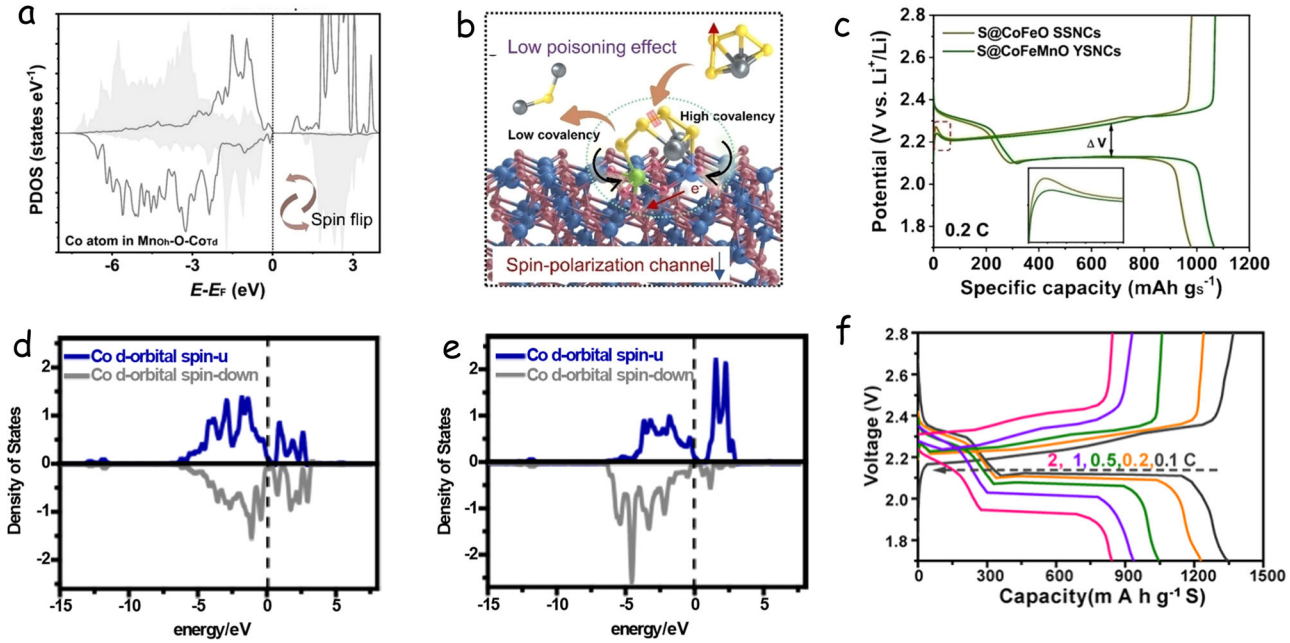

Fig. 15 | Spin effect by geometry engineering. a PDOS of the 3 d orbital of Co_{Td} in the Mn_{Oh}-O-Co_{Td} framework before and after Li_2S_4 adsorption. **b** Schematic diagram of the synergistic catalysis of LiPSs on the Mn_{Oh}-O-Co_{Td} backbone. **c** Galvanostatic charge-discharge curves at 0.2 C for the first cycle. **a**-**c** Reproduced with permission from ref. 243 (copyright Wiley-VCH, 2023). Field emission scanning electron microscopy image of the knot-like $NiCo_2S_4$. **d** LS and (**e**) HS states of Co d orbitals in LS to HS transitions. **f** discharge-charge curves of Chinese knot-like S@$NiCo_2S_4$ electrodes. **d**-**f** Reproduced with permission from ref. 252 (copyright Elsevier, 2021).

electron filling in the 3 d orbital, which affects the SRR catalytic activity, as we reported recently for sodium-sulfur batteries[244]. To determine the effect of geometric configuration, we selectively replaced Co_{td}^{2+} and Co_{oh}^{3+} in Co_3O_4 catalysts for sodium polysulfide conversion by Fe_{td}^{2+} and Fe_{oh}^{3+}, respectively, generating $FeCo_2O_4$ and $CoFe_2O_4$. Using both experimental results and theoretical calculations, it was concluded that Co_{oh}^{3+} is the main active site for S–S cleavage, while Co_{td}^{2+} is the main active site for S–Na bond formation.

There are several other reported cases of how changing the position of ions in the spinel structure can change the spin state of the material[245–247]. As an example, Zhang et al.[243] investigated the geometric site-dependent catalytic activity for sulfur redox within the $MnCo_2O_4$ spinel[243]. As observed in the PDOS of the 3 d orbitals of the cobalt tetrahedral site (Co_{Td}) in the manganese octahedral site $Mn_{Oh}-O-Co_{Td}$ before and after Li_2S_4 adsorption (Fig. 15a), a clear spin flip from the spin-up state to the spin-down state occurs upon Li_2S_4 adsorption. HS Co_{td}^{3+} sites with stronger Co-S covalency permanently anchor LiPSs, while electron-delocalized Mn_{oh}^{3+} with adsorption orbitals (d_{z^2}) play a better role in catalyzing specific LiPSs transformations (Fig. 15b). Regardless of where the Mn cation is in the spinel structure and what the valence state is, the manganese cation is always in a state of HS[248,249]. The optimized cathode (S@CoFeMnO) exhibited high specific capacity (Fig. 15c).

In the spinel structure, the spin state of the central atom can be adjusted by changing the distance between the tetrahedral or octahedral central atom and the surrounding coordination atoms, which offers a strategy to optimize the catalytic performance[155,250,251]. As an example, Xu et al. reported on $NiCo_2S_4$ nanotubes tightly interwoven to form a Chinese knot-like electrode as a sulfur host in LSBs[252]. Within this structure, the transition of Co ions between LS and HS caused by the extra sulfur atoms in LiPSs provides an electronic way to stabilize the adsorption system and lower the system energy, thereby suppressing the polysulfide migration (Fig. 15d, e) and enabling S@$NiCo_2S_4$ cathodes with a high specific capacity of 1348 mA h g^{-1} at 0.1 C (Fig. 15f).

As noted above, $CoTe_2$ has a metallic character associated with Co taking the LS of $t_{2g}^6e_g^1$. To further promote this compound towards the efficient conversion of LiPS within LSBs, Xu et al. added Zn ions with a similar ionic radius and electronic configuration yet different spin states to produce a slight distortion in the crystal structure of $CoTe_2$ based on the Jahn–Teller effect[234]. This distortion has the potential to enhance the exposure of active sites in $CoTe_2$, thereby improving its electrocatalytic capability and facilitating efficient conversion of polysulfides in LSBs[234].

Additional intriguing methods have been developed for altering the spin state of electrons within the perovskite structure[224,253–256], which hold promise for enhancing the metal-sulfur redox reaction in future sulfur cathodes. Overall, by manipulating the atomic geometric configuration, it is possible to achieve control of spintronics in the investigation of spin structures, which opens up new avenues and possibilities for the use of spin effects to optimize electrochemical and particular sulfur reactions.

Mechanistic insights: from spin to electrochemical performance

Understanding how electron spin modulates SRRs at different stages of LSB operation is critical to justifying the use of spin-polarized catalysts. In this section, we dissect the mechanistic roles of spin at various reaction stages and link them directly to measurable electrochemical performance (Fig. 16).

Spin effects on SRRs

Spin modulation plays a significant role in promoting the multi-step redox reactions of sulfur species, particularly during the S_8 activation, polysulfide conversion, and Li_2S precipitation/decomposition stages.

S_8 ring activation. The opening of the S_8 ring is the first step in the sulfur reduction pathway. Spin-polarized catalytic sites facilitate electron transfer to the antibonding orbitals of S_8, lowering the activation energy for ring cleavage. For instance, Du et al. demonstrated that MgPc anchored on fluorinated CNT exhibits unpaired electron-rich phthalocyanine centers, which promote S_8 activation via π–π stacking and electron delocalization. This system achieved a high areal capacity of 6.5 mAh·cm^{-2} under lean electrolyte conditions (~6.5 μL mg^{-1})[257]. After induced spin polarization in $NiSe_2/NiS_2$ heterostructure, the batteries

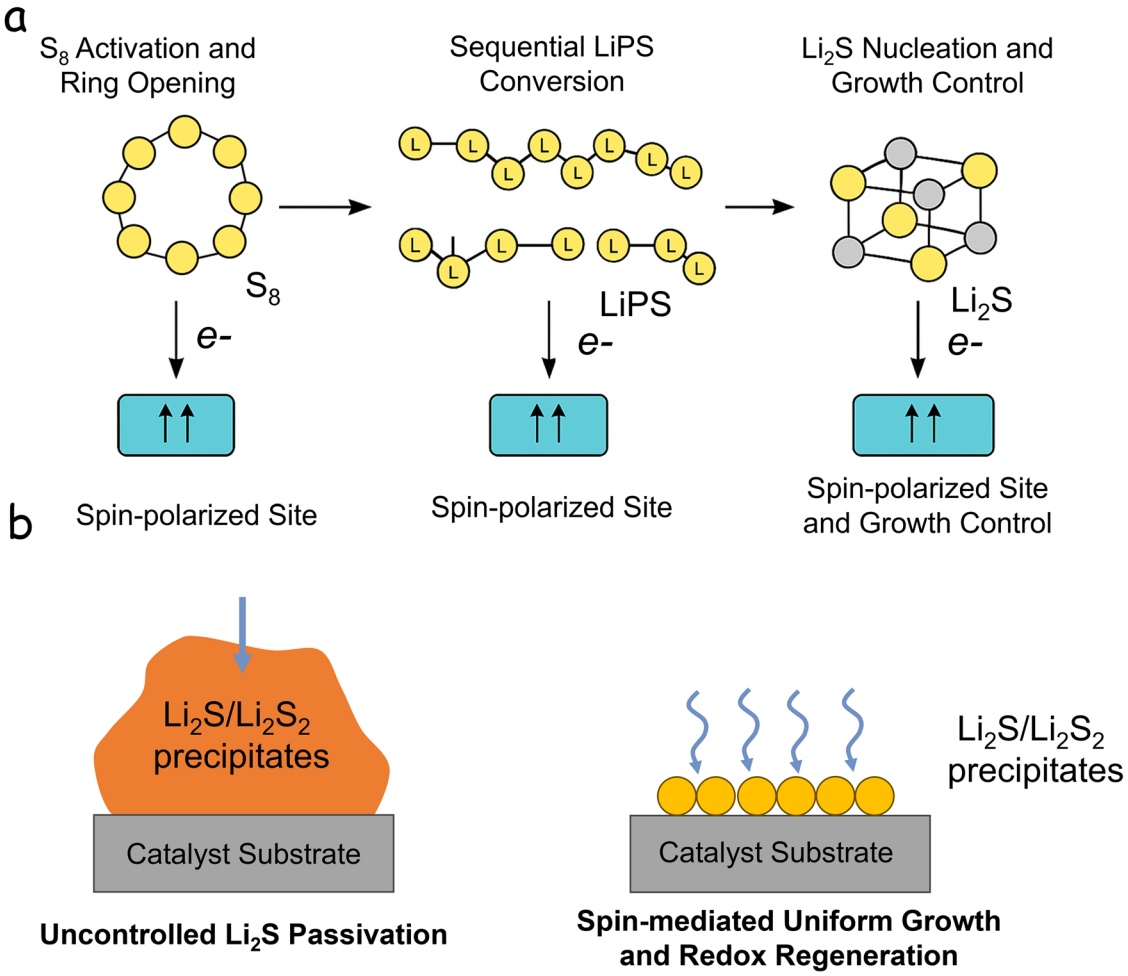

Fig. 16 | Spin effect on sulfur reduction reaction. a Spin-regulated sulfur redox pathways in LSBs: from S_8 activation to Li_2S formation. **b** Schematic comparison of (left) uncontrolled Li_2S passivation, where insulating Li_2S/Li_2S_2 precipitates form randomly and block electron pathways, and (right) spin-mediated uniform growth and redox regeneration, where controlled spin polarization promotes homogeneous deposition and facilitates reversible decomposition during cycling.

under lean electrolyte show excellent performance even under high sulfur loading (6.2 mg cm^{-2}) and lean electrolyte conditions (7.5 ml mg^{-1})[233]. Similarly, the results from our group showed that a cobalt-based magnetic catalyst under external magnetic alignment induced stronger spin polarization, facilitating rapid ring-opening reactions of S_8 and enabling fast activation even at high sulfur loadings[44].

Polysulfide conversion (Li_2S_8 to Li_2S_4, Li_2S_2). Spin-polarized surfaces accelerate intermediate polysulfide conversions by modulating the adsorption energy and enabling more effective electron transfer to S–S bonds. For example, Yu et al. reported that Co-vacancy-rich cobalt selenide, featuring high spin density near the Fermi level, improved the conversion kinetics of long-chain LiPS by stabilizing their adsorption and reducing energy barriers for S–S bond cleavage, which achieved 1089 mAh·g^{-1} at 1 C with only 0.017% capacity loss per cycle over 1500 cycles[258]. In another case, defect-engineered N-doped carbon generated pyridinic nitrogen sites with localized spin, which selectively interacted with Li_2S_6 species and enhanced intermediate reduction to Li_2S_2[259].

Li_2S nucleation and decomposition. The formation and decomposition of Li_2S are critical to capacity retention and cycle stability. Spin-active sites guide uniform Li_2S nucleation and assist decomposition during charging. Zhang et al. showed that magnetic spin-aligned catalysts promoted uniform Li_2S deposition, avoiding thick passivation layers and supporting continuous redox cycling over 8000+ cycles[44]. Another study demonstrated that Fe–N_4 centers in a spin-polarized carbon matrix accelerated the decomposition of Li_2S through enhanced charge delocalization, improving charge efficiency and cycle life[260].

Stage-specific impacts in Li–S cell operation

To establish a mechanistic framework, we categorize spin influences according to battery operation stages: initial activation, intermediate cycling, and long-term cycling.

Initial activation. During the first few cycles, sluggish S_8 activation and poor conductivity hinder sulfur utilization. Spin-active catalysts lower the energy barrier of S_8 cleavage. As an example, Zhang et al. synthesized spin-polarized 10 wt.% Co-doped MoS_2 nanosheets that exhibited enhanced electronic conductivity and facilitated S_8 ring activation, leading to initial capacities over 1550 mAh g^{-1}[119]. In the same direction, Kim et al. reported on single-atom Fe sites embedded in a graphene matrix that exhibited localized magnetic moments, enabling fast S_8 activation and high initial Coulombic efficiency (~98%)[261].

Intermediate cycling (LiPS shuttling and conversion). In this stage, spin modulation aids in reducing LiPS solubility and accelerating redox reactions. As the battery undergoes repeated charge–discharge, spin-active surfaces (e.g., doped phthalocyanines or metal–organic frameworks with magnetic ions) maintain catalytic activity by sustaining dynamic LiPS adsorption/desorption. Spin-altered states reduce surface

Table 1 | Mechanisms for inducing spin effects to enhance catalyst activity and boost electrochemical performance

Mechanism	Catalyst name	Current density/ cycle number	Decay rate (per cycle)	Active material loading (mg cm^{-2})	Reference
Vacanices	GP/CNT/LNO-V-S	0.05 C/100 cycles	0.045%	4.4	182
	$NiCo_2S_{4-x}$/CNF	3 C/3000 cycles	0.021%	1.65	183
	$S/WSe_{1.51}$/CNT	0.1 C/1000	0.032%	1.5	186
Single atom	FePc@WS_2	2 C/1000 cycles	0.026%	~ 1.0	133
	S@Fe/C_2N	3 C/2600 cycles	0.013%	1.0	10
	S@HP-SAFe	2 C/400 cycles	0.087 %	1.0	48
Doping	$FeCoPS_3$/NC	1 C/1000 cycles	0.037%	6.5	47
	V-Co3O4 NS	3 C/1900 cycles	0.015%	1.0-2.0	199
Heterostructure	$NiS_2/NiSe_2$	3 C/1000 cycles	0.058%	1.8	233
	1T-VSe_2-MXene	0.5 C/550 cycles	0.058 %	1.5	235
	Mn_3O_4-MnPx	2 C/1000 cycles	0.043%	1.5	232
	VTe_2@MgO	1 C/1000 cycles	0.055%	1.6	28
	$NiSe_2/Ni_2Co/CoSe_2$	12 C/2200 cycles	0.018%	0.95	146
Geometric configuration	S@CoFeMnO/Se YSNCs	1 C/600 cycles	0.06%	1.0-1.3	243
	S@$NiCo_2S_4$	1 C/1000 cycles	0.02%	~ 2	252

passivation, thereby delaying the onset of intermediate-phase degradation and improving Coulombic efficiency. This is particularly relevant to the 100–500 cycle range, where catalytic consistency determines rate capability. In this direction, Yu et al. showed that Mn-based catalysts with high spin configuration accelerated LiPS conversion and reduced shuttle current density, extending stable operation for over 100 cycles[262]. Besides, a study by Li et al. used CoF_2 hosts exhibiting localized unpaired electrons, which immobilized Li_2S_4 and suppressed the shuttle effect, leading to improved cycling stablity[263].

Long-term cycling and stability. Over-extended cycles, surface passivation, and catalyst deactivation often occur. Spin-polarized catalysts maintain their reactivity via dynamic spin centers. As an example, Li et al. demonstrated that DACs with dynamic spin-polarized Co–Fe sites retained over 90% capacity after 2000 cycles at 1 A g^{-1}, owing to their high stability and resistance to polysulfides passivation[264]. A recent study by Yang et al. employed TiO_2 catalysts to make S_8 spin polarized that maintained catalytic activity over long-term cycling, with <0.01% capacity decay per cycle across 1000 cycles.

Suppression of polysulfide shuttle and self-discharge

Beyond reaction kinetics, spin-active catalysts help mitigate polysulfide shuttle and self-discharge by two mechanisms: thermodynamic trapping via spin–orbital coupling and magnetic confinement of LiPS migration.

Spin-polarized active sites form strong orbital hybridizations with LiPS π^* orbitals. For instance, Tian et al. investigated a spin-polarized $NiCo_2S_4$ catalyst that demonstrated strong orbital overlap with Li_2S_6, effectively anchoring LiPS and reducing self-discharge during extended rest periods[265]. In the same context, Song et al. reported a VO_x–carbon hybrid structure with oxygen vacancies that introduced spin-polarized sites. These centers showed a high binding affinity to Li_2S_4, stabilizing LiPS species and minimizing voltage loss[266]. Spin-aligned or FM materials can reduce LiPS diffusion. As an example, Li et al. demonstrated that a spin-polarized Fe_3O_4/graphene composite suppressed the diffusion of LiPS through localized magnetic confinement, verified via symmetric cell and shuttle current tests[163].

Together, these mechanisms illustrate how spin regulation is not merely a theoretical concept but a practical lever to tune key stages of sulfur redox and improve measurable battery metrics in real systems.

Summary, challenges, and opportunities

The unique role of spin effects in catalysis has recently gained widespread attention as a promising avenue to enhance catalytic performance. This review highlights the emerging concept of spin-state tuning at catalytic active centers, with a particular emphasis on its application to conversion-type cathodes, most notably sulfur cathodes in metal–sulfur batteries. Early studies revealed that external magnetic fields could accelerate polysulfide conversion and enable high-performance LSBs, sparking growing recognition of the critical role of spin in governing LiPS deposition, adsorption, and ion diffusion. Building on these insights, spin engineering is now being explored as a powerful strategy to manipulate reaction pathways, optimize catalytic efficiency, and ultimately advance next-generation energy storage technologies.

In this review, we systematically examined theoretical and experimental advances in spin catalysis, concluding that catalytic performance can be significantly enhanced by tuning the spin state of catalysts. We also provided an overview of current experimental and computational methods for probing spin states and transitions, underscoring their importance in advancing understanding of spin effects in metal–sulfur systems. Furthermore, we analyzed and discussed a range of spin-tuning strategies and their effects: i) External magnetic fields modulate spin states by adjusting Zeeman energy, aligning spin arrangements at active centers, and forming spin channels, thereby enhancing catalytic performance; ii) Intrinsic spin channels, governed by local spin moments, are critical for charge transfer. Spin states can be engineered via composition and doping, defect creation, tailored synthesis of MOFs and SACs, SOC, and spin-flip coordination. Table 1 summarizes electrochemical performance gains from surface engineering strategies that trigger spin effects in LSBs; iii) Surface engineering regulates electron spin distribution, influencing energy-level structures, electron transport, and ion diffusion at the catalyst surface; iv) Spin-dependent charge transport allows tuning of electron–ion interactions and charge transfer rates, directly impacting adsorption, dissociation, and recombination processes. By accelerating conversion and depleting soluble intermediates, spin manipulation helps mitigate shuttling, particularly during open-circuit rest; and v) Reactivity and adsorption strength are strongly spin-dependent. HS catalysts, with unpaired electrons, generally stabilize intermediates more strongly, whereas LS catalysts favor faster desorption and lower barriers. Following the Sabatier principle, optimal adsorption strength depends on the reaction system: HS states are preferable when stabilizing high-energy intermediates, while LS states are advantageous for systems requiring rapid desorption. Mismatched spin states can hinder polysulfide redox processes.

Despite substantial progress, spin catalysis remains in its early stages and faces critical challenges. The precise mechanisms by which spin states influence catalytic activity remain unclear, and direct characterization of spin phenomena during reactions remains limited. The impact of spin-state

transitions on polysulfide adsorption and reaction pathways, as well as the interplay between spin polarization, polysulfide kinetics, and magnetic fields within complex sulfur cathodes, is poorly understood.

While spin clearly plays a pivotal role in catalysis, achieving controlled spin manipulation to reliably improve catalytic performance remains a formidable experimental challenge. The fundamental mechanisms are still debated, and direct observation of spin effects during catalysis has yet to be fully realized.

While this review has focused on the role of electron spin modulation in LSBs, many of the mechanistic principles discussed, such as spin-induced catalytic enhancement, defect-mediated spin polarization, and magnetic field-assisted electron transfer, are not unique to sulfur cathodes alone. Rather, they represent a broader class of emerging strategies for tailoring electrochemical interfaces via spin-state engineering.

For LSBs specifically, the redox complexity of sulfur species and the sensitivity of LiPS intermediates to surface electronic structure make them an ideal platform to probe spin–catalysis relationships. The dynamic S–S bond-breaking/forming reactions, soluble–insoluble conversion steps, and surface-passivation challenges (e.g., Li_2S deposition) all present spin-relevant catalytic opportunities that are less dominant in other battery chemistries. Thus, the Li–S system is a particularly fertile ground for establishing design principles based on unpaired electron behavior and spin density control.

That said, the design strategies highlighted here, such as vacancy and dopant engineering, magnetic catalyst integration, spin-polarized active centers, have clear potential beyond LSBs. For instance, in oxygen reduction and oxygen evolution reactions relevant to metal–air batteries, fuel cells, and electrolyzers, spin selection rules and orbital symmetry also play critical roles. Similarly, in CO_2 or N_2 electroreduction systems, unpaired d-electrons at catalyst centers are directly implicated in intermediate stabilization and multi-electron transfer. Therefore, the conceptual framework proposed in this review can inform the rational design of spin-active catalysts in a range of electrochemical technologies.

Moving forward, several promising research directions and challenges can be identified:

1. *Strategies for spin engineering and the need for deeper understanding.* Current efforts to engineer catalyst spin states primarily rely on two approaches: external magnetic field induction and internal modification of the local coordination environment through doping, defect generation, and heterostructure formation. While external magnetic fields have proven useful for fundamental investigations, they are impractical for commercial devices due to cost and integration complexity. More critically, the correlation between spin modulation strategies and improved polysulfide catalysis remains partially understood. A deeper mechanistic understanding of how spin polarization influences Li–S redox kinetics and thermodynamics is urgently needed.
2. *Understanding and optimizing spin-dependent catalysis.* Although HS states are often associated with enhanced catalytic activity, the benefit of specific spin states should be carefully examined. Many spin modulation strategies, such as heteroatom doping or defect engineering, inevitably introduce multiple electronic and geometric effects. Therefore, rigorous studies combining in operando experiments and spin-polarized theoretical simulations are required to disentangle the role of spin states from other variables. Future research should seek to build quantitative spin–performance relationships.
3. *The critical role of operando spin-state characterization*. One of the key challenges in advancing spin-regulated catalysis is the lack of operando diagnostic tools to monitor spin dynamics under working battery conditions. Conventional spectroscopic techniques such as EPR, XAS, Mössbauer, and XMCD provide valuable spin information in static or ex situ modes. However, their operando adaptations are still underdeveloped. Developing time-resolved or in situ spin probes will be essential for tracking real-time spin transitions, spin flips, and coupling behaviors throughout the battery operation.
4. *Theoretical modeling: A key tool for mechanism exploration*. Theoretical simulations offer a powerful route to examine spin-related processes in depth, but challenges remain. Spin-polarized DFT is sensitive to structural models, boundary conditions, and applied fields. Capturing realistic spin evolution, spin–orbital coupling, and reaction pathway energetics requires advanced tools, such as real-time time-dependent DFT or ab initio molecular dynamics (AIMD) incorporating solvent and field effects. Developing benchmark spin models aligned with experimental systems will be crucial.
5. *Stimuli-responsive spin control*. Beyond static modifications, external stimuli, such as strain, light, thermal gradients, and electromagnetic fields offer dynamic control over spin states. These approaches enable tunable catalysis without altering catalyst composition. Although some work has demonstrated light-induced spin flipping or strain-tuned magnetism in 2D materials, these methods remain underexplored in sulfur cathode systems and present exciting future directions.
6. *CISS: A promising yet untapped approach*. CISS refers to the phenomenon where chiral molecules or surfaces preferentially transmit electrons with a specific spin orientation. This strategy has been shown to enhance electrocatalytic reactions by minimizing spin scattering and promoting directional charge flow. While CISS has received attention in ORR and HER contexts, it remains largely unexplored in Li–S chemistry. Incorporating CISS into cathode design could offer a field-free pathway to spin-selective catalysis and enhanced cycle life.
7. *How spin effects affect lithium-sulfur processes*. Spin-dependent mechanisms are emerging as an emerging research direction for modulating redox dynamics and improving the stability of rechargeable batteries. However, the specific stages of lithium-sulfur battery operation at which these mechanisms exert their greatest influence remain unclear. For example, spin polarization may accelerate the initial activation process by enhancing charge transfer; whereas, during mid-cycle, it helps stabilize reaction intermediates and suppress undesirable side reactions. During long-term cycling, spin-dependent effects may help maintain structural integrity and catalytic activity. Currently, direct experimental verification remains scarce, and systematic studies exploring stage-dependent effects have not yet been conducted. Defining this issue as an open question presents a significant opportunity for future research: developing advanced characterization methods and theoretical models to disentangle the dynamic role of spin at different electrochemical stages. Addressing this challenge will not only deepen our fundamental understanding of spin-electrochemical coupling but also guide the rational design of spin-engineered materials for high-performance energy storage.
8. *Expanding beyond Li–S systems*. The concepts and principles outlined here have implications beyond lithium–sulfur batteries. Similar spin-regulated strategies could be deployed in sodium–sulfur, magnesium–sulfur, lithium–selenium, or lithium–iodine systems, as well as in broader electrochemical transformations. Future efforts should investigate how spin control intersects with different charge carriers, solvation structures, and solid-state or aqueous environments.

In conclusion, the emerging field of spin catalysis offers transformative opportunities to enhance the kinetics, efficiency, and durability of metal–sulfur batteries. While exciting strides have been made, many fundamental challenges remain, including the precise control, characterization, and understanding of spin-related phenomena during catalytic processes. Continued exploration, driven by advanced operando characterization techniques, realistic computational modeling, and innovative material design strategies, such as external stimuli modulation and chiral engineering, promises to unlock major breakthroughs. By systematically integrating spin control into catalyst design and deepening our fundamental understanding, future research can usher in a new era of high-performance, sustainable energy storage technologies.

Received: 28 April 2025; Accepted: 25 September 2025;
Published online: 18 November 2025

References

1. Han, Z. et al. Machine-learning-assisted design of a binary descriptor to decipher electronic and structural effects on sulfur reduction kinetics. *Nat. Catal.* **6**, 1073–1086 (2023).
2. Zhao, M. et al. Lithium–sulfur batteries under lean electrolyte conditions: challenges and opportunities. *Angew. Chem. Int. Ed.* **59**, 12636–12652 (2020).
3. Jeoun, Y. et al. Lean-electrolyte lithium-sulfur batteries: recent advances in the design of cell components. *Chem. Eng. J.* **450**, 138209 (2022).
4. Chen, H. et al. Catalytic materials for lithium-sulfur batteries: mechanisms, design strategies and future perspective. *Mater. Today* **52**, 364–388 (2022).
5. Do, V.-H. & Lee, J.-M. Orbital occupancy and spin polarization: from mechanistic study to rational design of transition metal-based electrocatalysts toward energy applications. *ACS Nano* **16**, 17847–17890 (2022).
6. Fei, B. et al. Hierarchical nanoreactor with multiple adsorption and catalytic sites for robust lithium–sulfur batteries. *ACS Nano* **15**, 6849–6860 (2021).
7. Zhang, C. et al. Tubular CoFeP@CN as a Mott–Schottky catalyst with multiple adsorption sites for robust lithium−sulfur batteries. *Adv. Energy Mater.* **11**, 2100432 (2021).
8. Lu, Z. W. et al. One-pot sulfur-containing ion assisted microwave synthesis of reduced graphene oxide@nano-sulfur fibrous hybrids for high-performance lithium-sulfur batteries. *Electrochim. Acta* **325**, 134920 (2019).
9. Sun, G. W. et al. Construction of all-carbon micro/nanoscale interconnected sulfur host for high-rate and ultra-stable lithium-sulfur batteries: role of oxygen-containing functional groups. *J. Colloid Interface Sci.* **608**, 459–469 (2022).
10. Liang, Z. et al. Atomically dispersed Fe in a C_2N based catalyst as a sulfur host for efficient lithium–sulfur batteries. *Adv. Energy Mater.* **11**, 2003507 (2021).
11. Yang, D. et al. A high conductivity 1D π–d conjugated metal–organic framework with efficient polysulfide trapping-diffusion-catalysis in lithium–sulfur batteries. *Adv. Mater.* **34**, 2108835 (2022).
12. Zhang, C. Y. et al. Surface strain-enhanced MoS2 as a high-performance cathode catalyst for lithium–sulfur batteries. *eScience* **2**, 405–415 (2022).
13. Wang, X. et al. Strain engineering of a MXene/CNT hierarchical porous hollow microsphere electrocatalyst for a high-efficiency lithium polysulfide conversion process. *Angew. Chem. Int. Ed.* **60**, 2371–2378 (2021).
14. Yang, D. et al. Phase engineering of defective copper selenide toward robust lithium–sulfur batteries. *ACS Nano* **16**, 11102–11114 (2022).
15. Li, M. et al. Enhanced polysulfide conversion with highly conductive and electrocatalytic iodine-doped bismuth selenide nanosheets in lithium–sulfur batteries. *Adv. Funct. Mater.* **32**, 2200529 (2022).
16. Zhang, C. Y. et al. Cooperative chemisorption of polysulfides via 2D hexagonal WS2-rimmed Co9S8 heterostructures for lithium–sulfur batteries. *Chem. Eng. J.* **392**, 123734 (2020).
17. Sabatier, P. *La catalyse en chimie organique*. Vol. 3 (C. Béranger, 1920).
18. Zhou, J. et al. Deciphering the modulation essence of p bands in co-based compounds on li-s chemistry. *Joule* **2**, 2681–2693 (2018).
19. Zhang, C. Y. et al. Metal doping activation of anion-mediated electron transfer in catalytic reactions. *J. Am. Chem. Soc.* **147**, 7070–7082 (2025).
20. Santos, E. & Schmickler, W. d-band catalysis in electrochemistry. *ChemPhysChem* **7**, 2282–2285 (2006).
21. Huang, C. et al. Combined defect and heterojunction engineering in ZnTe/$CoTe_2$@NC sulfur hosts toward robust lithium–sulfur batteries. *Adv. Funct. Mater.* **33**, 2305624 (2023).
22. Han, Z. et al. Engineering d-p orbital hybridization in single-atom metal-embedded three-dimensional electrodes for li–s batteries. *Adv. Mater.* **33**, 2105947 (2021).
23. Liu, D. et al. Catalytic effects in lithium–sulfur batteries: promoted sulfur transformation and reduced shuttle effect. *Adv. Sci.* **5**, 1700270 (2018).
24. Gao, Z., Schwab, Y., Zhang, Y., Song, N. & Li, X. Ferromagnetic nanoparticle–assisted polysulfide trapping for enhanced lithium–sulfur batteries. *Adv. Funct. Mater.* **28**, 1800563 (2018).
25. Zhang, C. Y. et al. Deciphering the catalysis essence of vanadium self-intercalated two-dimensional vanadium sulfides (V_5S_8) on lithium polysulfide towards high-rate and ultra-stable Li-S batteries. *Energy Storage Mater.* **43**, 471–481 (2021).
26. Zhang, C. et al. Robust lithium–sulfur batteries enabled by highly conductive wse2-based superlattices with tunable interlayer space. *Adv. Funct. Mater.* **32**, 2201322 (2022).
27. Zhang, C. et al. Combined high catalytic activity and efficient polar tubular nanostructure in urchin-like metallic $NiCo_2Se_4$ for high-performance lithium–sulfur batteries. *Adv. Funct. Mater.* **29**, 1903842 (2019).
28. Wang, M. et al. Conductive and catalytic VTe_2@MgO heterostructure as effective polysulfide promotor for lithium–sulfur batteries. *ACS Nano* **13**, 13235–13243 (2019).
29. Buchachenko, A. L. & Berdinsky, V. L. Electron spin catalysis. *Chem. Rev.* **102**, 603–612 (2002).
30. Lao, Z. et al. Band structure engineering and orbital orientation control constructing dual active sites for efficient sulfur redox reaction. *Adv. Mater.* **36**, 2309024 (2024).
31. Vaz, D. C. et al. Mapping spin–charge conversion to the band structure in a topological oxide two-dimensional electron gas. *Nat. Mater.* **18**, 1187–1193 (2019).
32. Disa, A. S. et al. Orbital engineering in symmetry-breaking polar heterostructures. *Phys. Rev. Lett.* **114**, 026801 (2015).
33. Kent, A. D. & Worledge, D. C. A new spin on magnetic memories. *Nat. Nanotechnol.* **10**, 187–191 (2015).
34. Häkkinen, H. et al. Symmetry and electronic structure of noble-metal nanoparticles and the role of relativity. *Phys. Rev. Lett.* **93**, 093401 (2004).
35. Graham, M. J. et al. Influence of electronic spin and spin–orbit coupling on decoherence in mononuclear transition metal complexes. *J. Am. Chem. Soc.* **136**, 7623–7626 (2014).
36. Chen, X., Lv, H. & Wu, X. Synergistic promotion of electrocatalytic activities and multilevel descriptors in nitrogen-doped graphene supported dual-atom catalysts for lithium-sulfur batteries. *Energy Storage Mater.* **65**, 103187 (2024).
37. Wu, T. et al. Spin pinning effect to reconstructed oxyhydroxide layer on ferromagnetic oxides for enhanced water oxidation. *Nat. Commun.* **12**, 3634 (2021).
38. Zhang, Z. et al. Regulating spin states in oxygen electrocatalysis. *Angew. Chem. Int. Ed.* **62**, e202216837 (2023).
39. Fang, Z. et al. Spin-modulated oxygen electrocatalysis. *Precis. Chem.* **1**, 395–417 (2023).
40. Zhou, G. et al. Spin-state reconfiguration induced by alternating magnetic field for efficient oxygen evolution reaction. *Nat. Commun.* **12**, 4827 (2021).
41. Yang, G. et al. Regulating Fe-spin state by atomically dispersed Mn-N in Fe-N-C catalysts with high oxygen reduction activity. *Nat. Commun.* **12**, 1734 (2021).
42. Wei, X. et al. Tuning the spin state of Fe single atoms by Pd nanoclusters enables robust oxygen reduction with dissociative pathway. *Chem* **9**, 181–197 (2023).

43. Atodiresei, N. et al. Design of the local spin polarization at the organic-ferromagnetic interface. *Phys. Rev. Lett.* **105**, 066601 (2010).
44. Zhang, C. Y. et al. Spin effect to promote reaction kinetics and overall performance of lithium-sulfur batteries under external magnetic field. *Angew. Chem. Int. Ed.* **61**, e202211570 (2022).
45. Bai, H. et al. Advances in spin catalysts for oxygen evolution and reduction reactions. *Small* **19**, 2205638 (2023).
46. Zhang, C. Y. et al. Sodium-sulfur batteries with unprecedented capacity, cycling stability and operation temperature range enabled by a $CoFe_2O_4$ catalytic additive under an external magnetic field. *Adv. Funct. Mater.* **33**, 2305908 (2023).
47. Li, H. et al. Regulating the spin state configuration in bimetallic phosphorus trisulfides for promoting sulfur redox kinetics. *J. Am. Chem. Soc.* **145**, 22516–22526 (2023).
48. Yan, R. et al. Origin and acceleration of insoluble $Li_2S_2 - Li_2S$ reduction catalysis in ferromagnetic atoms-based lithium-sulfur battery cathodes. *Angew. Chem. Int. Ed.* **62**, e202215414 (2023).
49. Zhang, Q., Ao, R., Gao, R. & Yang, H. Manipulating the spin state of fe sites via Fe–O–Si bridge bonds for enhanced polysulfide redox kinetics in the Li–S battery. *Inorg. Chem.* **61**, 19780–19789 (2022).
50. Liu, G. et al. Strengthened d–p orbital hybridization through asymmetric coordination engineering of single-atom catalysts for durable lithium–sulfur batteries. *Nano Lett.* **22**, 6366–6374 (2022).
51. Zhang, Z. et al. Significant change of metal cations in geometric sites by magnetic-field annealing $FeCo_2O_4$ for enhanced oxygen catalytic activity. *Small* **18**, 2104248 (2022).
52. Cao, A. & Nørskov, J. K. Spin effects in chemisorption and catalysis. *ACS Catal.* **13**, 3456–3462 (2023).
53. Xie, C. et al. Insight into the design of defect electrocatalysts: from electronic structure to adsorption energy. *Mater. Today* **31**, 47–68 (2019).
54. Ye, C. et al. A Mo_5N_6 electrocatalyst for efficient Na_2S electrodeposition in room-temperature sodium-sulfur batteries. *Nat. Commun.* **12**, 7195 (2021).
55. Zou, K. et al. A highly efficient sulfur host enabled by nitrogen/oxygen dual-doped honeycomb-like carbon for advanced lithium–sulfur batteries. *Small* **18**, 2107380 (2022).
56. Pan, Y. et al. Boosting the performance of single-atom catalysts via external electric field polarization. *Nat. Commun.* **13**, 3063 (2022).
57. Ren, X. et al. The origin of magnetization-caused increment in water oxidation. *Nat. Commun.* **14**, 2482 (2023).
58. Shen, K. et al. Magnetic field–suppressed lithium dendrite growth for stable lithium-metal batteries. *Adv. Energy Mater.* **9**, 1900260 (2019).
59. Costa, C. M., Merazzo, K. J., Gonçalves, R., Amos, C. & Lanceros-Méndez, S. Magnetically active lithium-ion batteries towards battery performance improvement. *iScience* **24**, 102691 (2021).
60. Fang, C. M., de Wijs, G. A. & de Groot, R. A. Spin-polarization in half-metals (invited). *J. Appl. Phys.* **91**, 8340–8344 (2002).
61. Buchachenko, A. L. MIE versus CIE: comparative analysis of magnetic and classical isotope effects. *Chem. Rev.* **95**, 2507–2528 (1995).
62. Jackson, C. E., Moseley, I. P., Martinez, R., Sung, S. & Zadrozny, J. M. A reaction-coordinate perspective of magnetic relaxation. *Chem. Soc. Rev.* **50**, 6684–6699 (2021).
63. Duan, L. M., Demler, E. & Lukin, M. D. Controlling spin exchange interactions of ultracold atoms in optical lattices. *Phys. Rev. Lett.* **91**, 090402 (2003).
64. Luo, S., Elouarzaki, K. & Xu, Z. J. Electrochemistry in magnetic fields. *Angew. Chem. Int. Ed.* **61**, e202203564 (2022).
65. Ren, X. et al. Spin-polarized oxygen evolution reaction under magnetic field. *Nat. Commun.* **12**, 2608 (2021).
66. Buchachenko, A. L. & Frankevich, E. L. *Chemical Generation and Reception of Radio-and Microwaves*. (Wiley, 1996).
67. Mazin, I. I. How to Define and calculate the degree of spin polarization in ferromagnets. *Phys. Rev. Lett.* **83**, 1427–1430 (1999).
68. Suzuki, R. et al. Valley-dependent spin polarization in bulk MoS2 with broken inversion symmetry. *Nat. Nanotechnol.* **9**, 611–617 (2014).
69. Hinds, G., Coey, J. M. D. & Lyons, M. E. G. Influence of magnetic forces on electrochemical mass transport. *Electrochem. Commun.* **3**, 215–218 (2001).
70. Wang, H. et al. Magnetoelectric coupling for metal–air batteries. *Adv. Funct. Mater.* **33**, 2210127 (2023).
71. Dunne, P. & Coey, J. M. D. Influence of a magnetic field on the electrochemical double layer. *J. Phys. Chem. C.* **123**, 24181–24192 (2019).
72. Park, C., Peng, Y., Zhu, J.-G., Laughlin, D. E. & White, R. M. Magnetoresistance of polycrystalline Fe3O4 films prepared by reactive sputtering at room temperature. *J. Appl. Phys.* **97**, 10C303 (2005).
73. Coey, J. M. D., Berkowitz, A. E., Balcells, L., Putris, F. F. & Parker, F. T. Magnetoresistance of magnetite. *Appl. Phys. Lett.* **72**, 734–736 (1998).
74. Ziese, M. et al. Mechanism of grain-boundary magnetoresistance in Fe O films. *Eur. Phys. J. B - Condens. Matter Complex Syst.* **28**, 415–422 (2002).
75. Martinez-Boubeta, C. et al. Learning from nature to improve the heat generation of iron-oxide nanoparticles for magnetic hyperthermia applications. *Sci. Rep.* **3**, 1652 (2013).
76. Estrader, M., Soulantica, K. & Chaudret, B. Organometallic synthesis of magnetic metal nanoparticles. *Angew. Chem. Int. Ed.* **61**, e202207301 (2022).
77. Meffre, A. et al. Complex nano-objects displaying both magnetic and catalytic properties: a proof of concept for magnetically induced heterogeneous catalysis. *Nano Lett.* **15**, 3241–3248 (2015).
78. Naaman, R., Paltiel, Y. & Waldeck, D. H. Chiral molecules and the electron spin. *Nat. Rev. Chem.* **3**, 250–260 (2019).
79. Li, Y. et al. Local spin-state tuning of iron single-atom electrocatalyst by S-coordinated doping for kinetics-boosted ammonia synthesis. *Adv. Mater.* **34**, 2202240 (2022).
80. Ge, M. et al. Preparation of organic-modified magadiite–magnetic nanocomposite particles as an effective nanohybrid drug carrier material for cancer treatment and its properties of sustained release mechanism by Korsmeyer–Peppas kinetic model. *J. Mater. Sci.* **56**, 14270–14286 (2021).
81. Garcés-Pineda, F. A., Blasco-Ahicart, M., Nieto-Castro, D., López, N. & Galán-Mascarós, J. R. Direct magnetic enhancement of electrocatalytic water oxidation in alkaline media. *Nat. Energy* **4**, 519–525 (2019).
82. Garcés-Pineda, F. A., González-Cobos, J., Torrens, M. & Galán-Mascarós, J. R. Fluorine-doped tin oxide/alumina as long-term robust conducting support for earth-abundant water oxidation electrocatalysts. *ChemElectroChem* **6**, 2282–2289 (2019).
83. Ray, K., Ananthavel, S. P., Waldeck, D. H. & Naaman, R. Asymmetric scattering of polarized electrons by organized organic films of chiral molecules. *Science* **283**, 814–816 (1999).
84. Liu, T. & Weiss, P. S. Spin polarization in transport studies of chirality-induced spin selectivity. *ACS Nano* **17**, 19502–19507 (2023).
85. Liang, Y., Lihter, M. & Lingenfelder, M. Spin-control in electrocatalysis for clean energy. *Isr. J. Chem.* **62**, e202200052 (2022).
86. Möllers, P. V. et al. Spin-polarized photoemission from chiral CuO catalyst thin films. *ACS Nano* **16**, 12145–12155 (2022).
87. Suntivich, J., May, K. J., Gasteiger, H. A., Goodenough, J. B. & Shao-Horn, Y. A perovskite oxide optimized for oxygen evolution catalysis from molecular orbital principles. *Science* **334**, 1383–1385 (2011).

88. Jenkins, D. M., Di Bilio, A. J., Allen, M. J., Betley, T. A. & Peters, J. C. Elucidation of a low spin cobalt(II) system in a distorted tetrahedral geometry. *J. Am. Chem. Soc.* **124**, 15336–15350 (2002).
89. Wolny, J. A., Schünemann, V., Németh, Z. & Vankó, G. Spectroscopic techniques to characterize the spin state: vibrational, optical, Mössbauer, NMR, and X-ray spectroscopy. *Comptes Rendus Chim.* **21**, 1152–1169 (2018).
90. Parker, J. S., Watts, S. M., Ivanov, P. G. & Xiong, P. Spin polarization of CrO_2 at and across an artificial barrier. *Phys. Rev. Lett.* **88**, 196601 (2002).
91. Soulen, R. J. et al. Measuring the spin polarization of a metal with a superconducting point contact. *Science* **282**, 85–88 (1998).
92. Kant, C. H. et al. Origin of spin-polarization decay in point-contact Andreev reflection. *Phys. Rev. B* **66**, 212403 (2002).
93. Grein, R., Löfwander, T., Metalidis, G. & Eschrig, M. Theory of superconductor-ferromagnet point-contact spectra: the case of strong spin polarization. *Phys. Rev. B* **81**, 094508 (2010).
94. Aggarwal, L. et al. Mesoscopic superconductivity and high spin polarization coexisting at metallic point contacts on Weyl semimetal TaAs. *Nat. Commun.* **8**, 13974 (2017).
95. Wang, X. et al. Evidence for largest room temperature magnetic signal from Co^{2+} in antiphase-free & fully inverted $CoFe_2O_4$ in multiferroic-ferrimagnetic $BiFeO_3$-$CoFe_2O_4$ nanopillar thin films. *J. Magn. Magn. Mater.* **530**, 167940 (2021).
96. Stöhr, J., Padmore, H. A., Anders, S., Stammler, T. & Scheinfein, M. R. Principles of X-ray magnetic dichroism spectromicroscopy. *Surf. Rev. Lett.* **05**, 1297–1308 (1998).
97. De Luca, G. et al. Top-layer engineering reshapes charge transfer at polar oxide interfaces. *Adv. Mater.* **34**, 2203071 (2022).
98. Yaji, K. et al. Large Rashba spin splitting of a metallic surface-state band on a semiconductor surface. *Nat. Commun.* **1**, 17 (2010).
99. Lv, B., Qian, T. & Ding, H. Angle-resolved photoemission spectroscopy and its application to topological materials. *Nat. Rev. Phys.* **1**, 609–626 (2019).
100. Luo, Q. et al. Neutron and ARPES constraints on the couplings of the multiorbital Hubbard model for the iron pnictides. *Phys. Rev. B* **82**, 104508 (2010).
101. Lai, C. W., Maletinsky, P., Badolato, A. & Imamoglu, A. Knight-field-enabled nuclear spin polarization in single quantum dots. *Phys. Rev. Lett.* **96**, 167403 (2006).
102. Huang, Y. et al. Room-temperature electron spin polarization exceeding 90% in an opto-spintronic semiconductor nanostructure via remote spin filtering. *Nat. Photonics* **15**, 475–482 (2021).
103. Zhang, D. et al. Room temperature near unity spin polarization in 2D Van der Waals heterostructures. *Nat. Commun.* **11**, 4442 (2020).
104. Ressouche, E. Polarized neutron diffraction. *École thématique de. la Soci.été Française de. la Neutron.* **13**, 02002 (2014).
105. Schweizer, J. in *Collection de la Société Française de la Neutronique*. 87-110 (EDP Sciences).
106. Kibalin, I. A. & Gukasov, A. Local magnetic anisotropy by polarized neutron powder diffraction: application of magnetically induced preferred crystallite orientation. *Phys. Rev. Res.* **1**, 033100 (2019).
107. Zhang, J.-Y. et al. Local spin-state tuning of cobalt–iron selenide nanoframes for the boosted oxygen evolution. *Energy Environ. Sci.* **14**, 365–373 (2021).
108. Haverkort, M. W. et al. Spin state transition in $LaCoO_3$ studied using soft x-ray absorption spectroscopy and magnetic circular dichroism. *Phys. Rev. Lett.* **97**, 176405 (2006).
109. Merz, M. et al. X-ray absorption and magnetic circular dichroism of $LaCoO_3$, $La_{0.7}Ce_{0.3}CoO_3$, and $La_{0.7}Sr_{0.3}CoO_3$ films: Evidence for cobalt-valence-dependent magnetism. *Phys. Rev. B* **82**, 174416 (2010).
110. Abbate, M. et al. Electronic structure and spin-state transition of $LaCoO_3$. *Phys. Rev. B* **47**, 16124–16130 (1993).
111. Tong, Y. et al. Spin-state regulation of perovskite cobaltite to realize enhanced oxygen evolution activity. *Chem* **3**, 812–821 (2017).
112. Han, H. et al. Reversal of anomalous hall effect and octahedral tilting in $SrRuO_3$ thin films via hydrogen spillover. *Adv. Mater.* **35**, 2207246 (2023).
113. van der Laan, G. & Figueroa, A. I. X-ray magnetic circular dichroism—a versatile tool to study magnetism. *Coord. Chem. Rev.* **277-278**, 95–129 (2014).
114. Li, Z. et al. The marriage of the FeN_4 moiety and mxene boosts oxygen reduction catalysis: Fe 3 d electron delocalization matters. *Adv. Mater.* **30**, 1803220 (2018).
115. Nanda, S., Asl, H. Y., Bhargav, A. & Manthiram, A. Thiometallate-mediated polysulfide chemistry and lithium stabilization for stable anode-free lithium-sulfur batteries. *Cell Rep. Phys. Sci.* **3**, 100808 (2022).
116. Wild, M. et al. Lithium sulfur batteries, a mechanistic review. *Energy Environ. Sci.* **8**, 3477–3494 (2015).
117. Fujii, J. et al. Mitrofanovite Pt_3Te_4: a topological metal with termination-dependent surface band structure and strong spin polarization. *ACS Nano* **15**, 14786–14793 (2021).
118. Huang, H.-L., Tung, J.-C. & Guo, G.-Y. Anomalous Hall effect and current spin polarization in Co_2FeX Heusler compounds (X=Al, Ga, In, Si, Ge, and Sn): A systematic ab initio study. *Phys. Rev. B* **91**, 134409 (2015).
119. Shull, C. G. & Smart, J. S. Detection of antiferromagnetism by neutron diffraction. *Phys. Rev.* **76**, 1256–1257 (1949).
120. Nathans, R., Shull, C. G., Shirane, G. & Andresen, A. The use of polarized neutrons in determining the magnetic scattering by iron and nickel. *J. Phys. Chem. Solids* **10**, 138–146 (1959).
121. Brown, P. J., Forsyth, J. B. & Tasset, F. Neutron polarimetry. *Proc. R. Soc. Lond. Ser. A: Math. Phys. Sci.* **442**, 147–160 (1993).
122. Lelièvre-Berna, E. et al. Powder diffraction with spin polarized neutrons. *Meas. Sci. Technol.* **21**, 055106 (2010).
123. Kibalin, I. A., Damay, F., Fabrèges, X., Gukassov, A. & Petit, S. Competing interactions in dysprosium garnets and generalized magnetic phase diagram of S = 1/2 spins on a hyperkagome network. *Phys. Rev. Res.* **2**, 033509 (2020).
124. Golosovsky, I. V. et al. Elucidating individual magnetic contributions in bi-magnetic Fe_3O_4/Mn_3O_4 core/shell nanoparticles by polarized powder neutron diffraction. *Small Methods* **7**, 2201725 (2023).
125. Yu, Y. et al. Electron spin modulation engineering in oxygen-involved electrocatalysis. *J. Phys.: Condens. Matter* **34**, 364002 (2022).
126. Chen, Z. et al. Unraveling the origin of sulfur-doped Fe-N-C single-atom catalyst for enhanced oxygen reduction activity: effect of iron spin-state tuning. *Angew. Chem. Int. Ed.* **60**, 25404–25410 (2021).
127. Koshy, D. M. et al. Investigation of the structure of atomically dispersed NiNx Sites in Ni and N-Doped Carbon Electrocatalysts by 61Ni Mössbauer spectroscopy and simulations. *J. Am. Chem. Soc.* **144**, 21741–21750 (2022).
128. Kramm, U. I. et al. Structure of the catalytic sites in Fe/N/C-catalysts for O_2-reduction in PEM fuel cells. *Phys. Chem. Chem. Phys.* **14**, 11673–11688 (2012).
129. Kramm, U. I. et al. Influence of the electron-density of FeN4-centers towards the catalytic activity of pyrolyzed FeTMPPCl-based ORR-electrocatalysts. *J. Electrochem. Soc.* **158**, B69 (2011).
130. Hernández, E. M. et al. AFM imaging of molecular spin-state changes through quantitative thermomechanical measurements. *Adv. Mater.* **26**, 2889–2893 (2014).
131. Yates, K. A. et al. Andreev bound states in superconductor/ferromagnet point contact Andreev reflection spectra. *Phys. Rev. B* **95**, 094516 (2017).
132. Sauls, J. A. Andreev bound states and their signatures. *Philos. Trans. R. Soc. A Math. Phys. Eng. Sci.* **376**, 20180140 (2018).

133. Qu, G. et al. Tuning Fe-spin state of FeN_4 structure by axial bonds as efficient catalyst in Li-S batteries. *Energy Storage Mater.* **55**, 490–497 (2023).
134. Mazalov, L. N., Asanov, I. P. & Varnek, V. A. Study of electronic structure of spin-transition complexes by XPS and Mössbauer spectroscopy. *J. Electron Spectrosc. Relat. Phenom.* **96**, 209–214 (1998).
135. Burger, K., Furlani, C. & Mattogno, G. XPS Structural characterization of spin-state crossover in $FeII(NCS)_2$ $(ophen)_2$. *J. Electron Spectrosc. Relat. Phenom.* **21**, 249–256 (1980).
136. Fontanesi, C., Capua, E., Paltiel, Y., Waldeck, D. H. & Naaman, R. Spin-dependent processes measured without a permanent magnet. *Adv. Mater.* **30**, 1707390 (2018).
137. Lan, Q. Q. et al. Tuning the magnetism of epitaxial cobalt oxide thin films by electron beam irradiation. *Phys. Rev. Mater.* **1**, 024403 (2017).
138. Klie, R. F. et al. Direct measurement of the low-temperature spin-state transition in $LaCoO_3$. *Phys. Rev. Lett.* **99**, 047203 (2007).
139. Ma, C. et al. Origin of spin-state crossover and electronic reconstruction at the surface of a $LaCoO_3$ nanoparticle. *Phys. Rev. B* **99**, 115401 (2019).
140. Kosaka, H. et al. Spin state tomography of optically injected electrons in a semiconductor. *Nature* **457**, 702–705 (2009).
141. Coelho, P. M. et al. Charge density wave state suppresses ferromagnetic ordering in VSe_2 monolayers. *J. Phys. Chem. C.* **123**, 14089–14096 (2019).
142. Steinert, M., Schneider, B., Dechert, S., Demeshko, S. & Meyer, F. A trinuclear defect-grid iron(II) spin crossover complex with a large hysteresis loop that is readily silenced by solvent vapor. *Angew. Chem. Int. Ed.* **53**, 6135–6139 (2014).
143. Romero-Morcillo, T., Seredyuk, M., Muñoz, M. C. & Real, J. A. Meltable spin transition molecular materials with tunable TC and hysteresis loop width. *Angew. Chem. Int. Ed.* **54**, 14777–14781 (2015).
144. Freysz, E., Montant, S., Létard, S. & Létard, J. F. Single laser pulse induces spin state transition within the hysteresis loop of an Iron compound. *Chem. Phys. Lett.* **394**, 318–323 (2004).
145. Brooker, S. Spin crossover with thermal hysteresis: practicalities and lessons learnt. *Chem. Soc. Rev.* **44**, 2880–2892 (2015).
146. Cao, Y. et al. Interface engineering in $NiSe_2$/Ni_2Co/$CoSe_2$ heterostructures encapsulated in hollow carbon shells for high-rate Li–Se batteries. *Nanoscale* **14**, 13227–13235 (2022).
147. Vankó, G. et al. Spin-state studies with XES and RIXS: FROM static to ultrafast. *J. Electron Spectrosc. Relat. Phenom.* **188**, 166–171 (2013).
148. Abraham, B. et al. A high-throughput energy-dispersive tender X-ray spectrometer for shot-to-shot sulfur measurements. *J. Synchrotron Radiat.* **26**, 629–634 (2019).
149. Kuzmenko, D. et al. A von Hamos spectrometer for in situ sulfur speciation by non-resonant sulfur Kα emission spectroscopy. *J. Anal. At. Spectrom.* **34**, 2105–2111 (2019).
150. Rovezzi, M. et al. TEXS: in-vacuum tender X-ray emission spectrometer with 11 Johansson crystal analyzers. *J. Synchrotron Radiat.* **27**, 813–826 (2020).
151. Kavčič, M. et al. Characterization of Li–S Batteries Using Laboratory Sulfur X-ray Emission Spectroscopy. *ACS Appl. Energy Mater.* **4**, 2357–2364 (2021).
152. Du, J. L. et al. Density functional thermodynamic description of spin, phonon and displacement degrees of freedom in antiferromagnetic-to-paramagnetic phase transition in $YNiO_3$. *Mater. Today Phys.* **27**, 100805 (2022).
153. Gunnarsson, O. & Lundqvist, B. I. Exchange and correlation in atoms, molecules, and solids by the spin-density-functional formalism. *Phys. Rev. B* **13**, 4274–4298 (1976).
154. Kvashnin, Y. O. et al. Exchange parameters of strongly correlated materials: extraction from spin-polarized density functional theory plus dynamical mean-field theory. *Phys. Rev. B* **91**, 125133 (2015).
155. Chen, R. R. et al. Antiferromagnetic inverse spinel oxide $LiCoVO_4$ with spin-polarized channels for water oxidation. *Adv. Mater.* **32**, 1907976 (2020).
156. Thomas, D. M., Asiri, Y. & Drummond, N. D. Point defect formation energies in graphene from diffusion quantum Monte Carlo and density functional theory. *Phys. Rev. B* **105**, 184114 (2022).
157. Bertaina, G., Tarallo, M. G. & Pilati, S. Quantum Monte Carlo study of the role of p-wave interactions in ultracold repulsive Fermi gases. *Phys. Rev. A* **107**, 053305 (2023).
158. Hart, R. A. et al. Observation of antiferromagnetic correlations in the Hubbard model with ultracold atoms. *Nature* **519**, 211–214 (2015).
159. Falson, J. et al. Competing correlated states around the zero-field Wigner crystallization transition of electrons in two dimensions. *Nat. Mater.* **21**, 311–316 (2022).
160. Xu, M. et al. Self-regulation of spin polarization density propelling the ion diffusion kinetics for flexible potassium-ion batteries. *Adv. Funct. Mater.* **32**, 2203263 (2022).
161. Kim, H.-W. & Anderson, J. B. Quantum Monte Carlo: reduction of time-step error with the wave function correction method. *Int. J. Quantum Chem.* **123**, e27041 (2023).
162. Kang, B. & Yoon, J. Sign-problem-free variant of the complex Sachdev-Ye-Kitaev model. *Phys. Rev. B* **105**, 045117 (2022).
163. Li, W. et al. Magnetic field-controlled lithium polysulfide semiliquid battery with ferrofluidic properties. *Nano Lett.* **15**, 7394–7399 (2015).
164. Zhu, J. et al. Magnetic field induced capacitance enhancement in graphene and magnetic graphene nanocomposites. *Energy Environ. Sci.* **6**, 194–204 (2013).
165. Wei, H. et al. Significantly enhanced energy density of magnetite/polypyrrole nanocomposite capacitors at high rates by low magnetic fields. *Adv. Compos. Hybrid. Mater.* **1**, 127–134 (2018).
166. Huang, Y. et al. Ferromagnetic 1D-Fe_3O_4@C microrods boost polysulfide anchoring for lithium–sulfur batteries. *ACS Appl. Energy Mater.* **4**, 3921–3927 (2021).
167. Zhu, R. et al. Magnetic and mesoporous Fe_3O_4-modified glass fiber separator for high-performance lithium-sulfur battery. *Ionics* **26**, 2325–2334 (2020).
168. Yue, W. et al. Ultra-small ferromagnetic Fe_3O_4 nanoparticles modified separator for high-rate and long cycling lithium-sulfur batteries. *Batteries Supercaps* **5**, e202200020 (2022).
169. Cao, Y. et al. Magnetic control of electrolyte trapping polysulfide for enhanced lithium-sulfur batteries. *J. Electrochem. Soc.* **168**, 070510 (2021).
170. Sun, T. et al. Ferromagnetic single-atom spin catalyst for boosting water splitting. *Nat. Nanotechnol.* **18**, 763–771 (2023).
171. Ma, J. et al. Low tortuosity thick cathode design in high loading lithium sulfur batteries enabled by magnetic hollow carbon fibers. *Appl. Surf. Sci.* **542**, 148664 (2021).
172. Li, X. et al. Unidirectional spin–orbit interaction induced by the line defect in monolayer transition metal dichalcogenides for high-performance devices. *Nano Lett.* **19**, 6005–6012 (2019).
173. Li, Z., Xiao, C., Zhu, H. & Xie, Y. Defect chemistry for thermoelectric materials. *J. Am. Chem. Soc.* **138**, 14810–14819 (2016).
174. Koehl, W. F., Buckley, B. B., Heremans, F. J., Calusine, G. & Awschalom, D. D. Room temperature coherent control of defect spin qubits in silicon carbide. *Nature* **479**, 84–87 (2011).
175. Jozwiak, C. et al. Photoelectron spin-flipping and texture manipulation in a topological insulator. *Nat. Phys.* **9**, 293–298 (2013).
176. Shi, Z., Li, M., Sun, J. & Chen, Z. Defect engineering for expediting Li–S chemistry: strategies, mechanisms, and perspectives. *Adv. Energy Mater.* **11**, 2100332 (2021).
177. Hu, Y. et al. Strategies toward high-loading lithium–sulfur battery. *Adv. Energy Mater.* **10**, 2000082 (2020).

178. Liu, H. et al. Probing the atomic interaction between zinc clusters and defective carbon in promoting the wide temperature applications of lithium-sulfur battery. *Energy Storage Mater.* **41**, 703–714 (2021).
179. Yi, Z. et al. New insights into Li_2S_2/Li_2S adsorption on the graphene bearing single vacancy: a DFT study. *Appl. Surf. Sci.* **503**, 144446 (2020).
180. Li, Y. et al. Decoration of defective graphene with MoS_2 enabling enhanced anchoring and catalytic conversion of polysulfides for lithium–sulfur batteries: a first-principles study. *Phys. Chem. Chem. Phys.* **24**, 29214–29222 (2022).
181. Bourgeois, E., Gulka, M. & Nesladek, M. Photoelectric detection and quantum readout of nitrogen-vacancy center spin states in diamond. *Adv. Optical Mater.* **8**, 1902132 (2020).
182. Zou, K. et al. Defect engineering in a multiple confined geometry for robust lithium–sulfur batteries. *Adv. Energy Mater.* **12**, 2103981 (2022).
183. Dai, X. et al. Defect-engineered sulfur vacancy modified $NiCo_2S_{4-x}$ nanosheet anchoring polysulfide for improved lithium sulfur batteries. *Small* **19**, 2302267 (2023).
184. Li, H.-J. et al. Sulfur vacancies in Co_9S_{8-x}/N-doped graphene enhancing the electrochemical kinetics for high-performance lithium–sulfur batteries. *J. Mater. Chem. A* **9**, 10704–10713 (2021).
185. Zhao, Y. et al. Sulfur-deficient TiS_{2-x} for promoted polysulfide redox conversion in lithium-sulfur batteries. *ChemElectroChem* **6**, 2231–2237 (2019).
186. Li, H.-J. et al. Quantitatively regulating defects of 2D tungsten selenide to enhance catalytic ability for polysulfide conversion in a lithium sulfur battery. *Energy Storage Mater.* **45**, 1229–1237 (2022).
187. Kuemmeth, F., Ilani, S., Ralph, D. C. & McEuen, P. L. Coupling of spin and orbital motion of electrons in carbon nanotubes. *Nature* **452**, 448–452 (2008).
188. Wang, X. et al. Rare-Earth single-atom catalysts: a new frontier in photo/electrocatalysis. *Small Methods* **6**, 2200413 (2022).
189. Chen, X. et al. Ether-compatible sulfurized polyacrylonitrile cathode with excellent performance enabled by fast kinetics via selenium doping. *Nat. Commun.* **10**, 1021 (2019).
190. Yang, Z. et al. Sulfur-doped graphene as an efficient metal-free cathode catalyst for oxygen reduction. *ACS Nano* **6**, 205–211 (2012).
191. Hou, T.-Z. et al. Design principles for heteroatom-doped nanocarbon to achieve strong anchoring of polysulfides for lithium–sulfur batteries. *Small* **12**, 3283–3291 (2016).
192. Peng, L. et al. A fundamental look at electrocatalytic sulfur reduction reaction. *Nat. Catal.* **3**, 762–770 (2020).
193. Liu, Y. et al. O-, N-Coordinated single Mn atoms accelerating polysulfides transformation in lithium-sulfur batteries. *Energy Storage Mater.* **35**, 12–18 (2021).
194. Li, Y. et al. High-density oxygen doping of conductive metal sulfides for better polysulfide trapping and Li_2S-S_8 redox kinetics in high areal capacity lithium–sulfur batteries. *Adv. Sci.* **9**, 2200840 (2022).
195. Yao, W. et al. P-Doped $NiTe_2$ with Te-vacancies in lithium–sulfur batteries prevents shuttling and promotes polysulfide conversion. *Adv. Mater.* **34**, 2106370 (2022).
196. Wang, Y. et al. Binary Sulfiphilic nickel boride on boron-doped graphene with beneficial interfacial charge for accelerated Li–S dynamics. *Small* **19**, 2208281 (2023).
197. Wang, M. et al. Nitrogen-Doped $CoSe_2$ as a bifunctional catalyst for high areal capacity and lean electrolyte of Li–S Battery. *ACS Energy Lett.* **5**, 3041–3050 (2020).
198. Yang, L. F., Song, Y., Mi, W. B. & Wang, X. C. Prediction of spin-dependent electronic structure in 3d-transition-metal doped antimonene. *Appl. Phys. Lett.* **109**, 022103 (2016).
199. Zhou, W. et al. Engineering spin state in spinel Co_3O_4 nanosheets by V-doping for bidirectional catalysis of polysulfides in lithium–sulfur batteries. *Adv. Funct. Mater.* **n/a**, 2402114 (2024).
200. Chen, L. et al. Bifunctional catalytic effect of $CoSe_2$ for lithium–sulfur batteries: single doping versus dual doping. *Adv. Funct. Mater.* **32**, 2107838 (2022).
201. Feng, T. et al. 2D amorphous mo-doped CoB for bidirectional sulfur catalysis in lithium sulfur batteries. *Adv. Funct. Mater.* **32**, 2202766 (2022).
202. Liu, W. et al. Cobalt-doping of molybdenum disulfide for enhanced catalytic polysulfide conversion in lithium–sulfur batteries. *ACS Nano* **15**, 7491–7499 (2021).
203. Li, B. et al. Emerging multifunctional metal–organic framework materials. *Adv. Mater.* **28**, 8819–8860 (2016).
204. Kumar, A. et al. Chirality-induced spin polarization places symmetry constraints on biomolecular interactions. *Proc. Natl. Acad. Sci.* **114**, 2474–2478 (2017).
205. Wang, B. et al. Hafnium diboride spherical superstructure born of 5d-metal Hf-MOF-Induced p orbital activity of B atom and enhanced kinetics of sulfur cathode reaction. *Adv. Energy Mater.* **13**, 2300590 (2023).
206. Chen, Y. et al. Contribution of different metal nodes on stepwise electrocatalysis in lithium-sulfur batteries. *Energy Storage Mater.* **54**, 488–497 (2023).
207. Sun, Q. et al. Magnetic interplay between π-Electrons of open-shell porphyrins and d-electrons of their central transition metal ions. *Adv. Sci.* **9**, 2105906 (2022).
208. Dong, R. et al. A coronene-based semiconducting two-dimensional metal-organic framework with ferromagnetic behavior. *Nat. Commun.* **9**, 2637 (2018).
209. Wang, J. et al. Two-dimensional conductive metal–organic frameworks as highly efficient electrocatalysts for lithium–sulfur batteries. *ACS Appl. Mater. Interfaces* **13**, 61205–61214 (2021).
210. Han, J. et al. Thermal modulation of MOF and its application in lithium–sulfur batteries. *ACS Appl. Mater. Interfaces* **11**, 46792–46799 (2019).
211. Zhu, C. et al. Unveiling spin state-dependent micropollutant removal using single-atom covalent triazine framework. *Adv. Funct. Mater.* **33**, 2210905 (2023).
212. Gao, Y., Liu, B. & Wang, D. Microenvironment engineering of single/dual-atom catalysts for electrocatalytic application. *Adv. Mater.* **35**, 2209654 (2023).
213. Wan, W. et al. Mechanistic insight into the active centers of single/dual-atom Ni/Fe-based oxygen electrocatalysts. *Nat. Commun.* **12**, 5589 (2021).
214. Zhong, W. et al. Electronic spin moment as a catalytic descriptor for fe single-atom catalysts supported on C2N. *J. Am. Chem. Soc.* **143**, 4405–4413 (2021).
215. Andritsos, E. I., Lekakou, C. & Cai, Q. Single-Atom catalysts as promising cathode materials for lithium–sulfur batteries. *J. Phys. Chem. C.* **125**, 18108–18118 (2021).
216. Griffith, J. S. & Orgel, L. E. Ligand-field theory. *Q. Rev., Chem. Soc.* **11**, 381–393 (1957).
217. Han, M., Huang, Y. & Zhang, H. A coordination environment effect of single-atom catalysts on their nitrogen reduction reaction performance. *Phys. Chem. Chem. Phys.* **24**, 18854–18859 (2022).
218. Yang, D. et al. $NbSe_2$ Meets C_2N: a 2D-2D heterostructure catalysts as multifunctional polysulfide mediator in ultra-long-life lithium–sulfur batteries. *Adv. Energy Mater.* **11**, 2101250 (2021).
219. Dong, W. et al. Heterokaryotic transition-metal dimers embedded monolayer g-C_3N_3 as promising anchoring and electrocatalytic materials for lithium-sulfur battery: first-principles calculations. *J. Catal.* **433**, 115449 (2024).
220. Du, Z. et al. Cobalt in nitrogen-doped graphene as single-atom catalyst for high-sulfur content lithium–sulfur batteries. *J. Am. Chem. Soc.* **141**, 3977–3985 (2019).

221. Ma, Y. et al. Single nickel atom catalysts enable fast polysulfide redox for safe and long-cycle lithium–sulfur batteries. *Small* **18**, 2205470 (2022).
222. Zhou, G. et al. Theoretical calculation guided design of single-atom catalysts toward fast kinetic and long-life li–s batteries. *Nano Lett.* **20**, 1252–1261 (2020).
223. Zhang, D. et al. Catalytic conversion of polysulfides on single atom zinc implanted mxene toward high-rate lithium–Sulfur Batteries. *Adv. Funct. Mater.* **30**, 2002471 (2020).
224. Ran, J., Wang, L., Si, M., Liang, X. & Gao, D. Tailoring spin state of perovskite oxides by fluorine atom doping for efficient oxygen electrocatalysis. *Small* **19**, 2206367 (2023).
225. Ren, L. et al. Regulating electronic structure of Fe–N_4 single atomic catalyst via neighboring sulfur doping for high performance lithium–sulfur batteries. *Adv. Funct. Mater.* **33**, 2210509 (2023).
226. Huang, T. et al. Altering local chemistry of single-atom coordination boosts bidirectional polysulfide conversion of Li–S batteries. *Adv. Funct. Mater.* **32**, 2203902 (2022).
227. Liu, K. et al. N, S-coordinated co single atomic catalyst boosting adsorption and conversion of lithium polysulfides for lithium-sulfur batteries. *Small* **18**, 2204707 (2022).
228. Wang, Z. et al. Single-atomic Co-B_2N_2 sites anchored on carbon nanotube arrays promote lithium polysulfide conversion in lithium–sulfur batteries. *Carbon Energy* **5**, e306 (2023).
229. Ding, Y. et al. Enhanced dual-directional sulfur redox via a biotemplated single-Atomic Fe–N_2 mediator promises durable Li–S Batteries. *Adv. Mater.* **34**, 2202256 (2022).
230. Ohno, Y. et al. Electrical spin injection in a ferromagnetic semiconductor heterostructure. *Nature* **402**, 790–792 (1999).
231. Gong, C. & Zhang, X. Two-dimensional magnetic crystals and emergent heterostructure devices. *Science* **363**, eaav4450 (2019).
232. Guo, K. et al. Polysulfides shuttling remedies by interface-catalytic effect of Mn3O4-MnPx heterostructure. *Energy Storage Mater.* **36**, 496–503 (2021).
233. Huang, C. et al. Electronic Spin Alignment within Homologous NiS_2/$NiSe_2$ heterostructures to promote sulfur redox kinetics in lithium-sulfur batteries. *Adv. Mater.* **n/a**, 2400810 (2024).
234. Wang, B. et al. Zinc-assisted cobalt ditelluride polyhedra inducing lattice strain to endow efficient adsorption-catalysis for high-energy lithium–sulfur batteries. *Adv. Mater.* **34**, 2204403 (2022).
235. Wang, W. et al. Conductive metal–metal phase and built-in electric field of 1T-VSe_2-MXene hetero-structure to accelerate dual-directional sulfur conversion for high-performance Li-S batteries. *Chem. Eng. J.* **461**, 142100 (2023).
236. Deng, N. et al. Rational structure designs of 2D materials and their applications toward advanced lithium-sulfur battery and lithium-selenium battery. *Chem. Eng. J.* **401**, 125976 (2020).
237. Zhang, B. et al. Optimized Catalytic WS_2–WO_3 heterostructure design for accelerated polysulfide conversion in lithium–sulfur batteries. *Adv. Energy Mater.* **10**, 2000091 (2020).
238. Ye, C. et al. 2D MoN-VN heterostructure to regulate polysulfides for highly efficient lithium-sulfur batteries. *Angew. Chem. Int. Ed.* **57**, 16703–16707 (2018).
239. Yao, Y. et al. A Dual-Functional Conductive Framework Embedded with TiN-VN heterostructures for highly efficient polysulfide and lithium regulation toward stable li–s full batteries. *Adv. Mater.* **32**, 1905658 (2020).
240. Lu, H. et al. Highly distorted chiral two-dimensional tin iodide perovskites for spin polarized charge transport. *J. Am. Chem. Soc.* **142**, 13030–13040 (2020).
241. Hou, W. et al. Catalytic mechanism of oxygen vacancies in perovskite oxides for lithium–sulfur batteries. *Adv. Mater.* **34**, 2202222 (2022).
242. Tang, H. et al. Spin unlocking oxygen evolution reaction on antiperovskite nitrides. *J. Mater. Chem. A* **9**, 25435–25444 (2021).
243. Li, H. et al. Cooperative catalysis of polysulfides in lithium-sulfur batteries through adsorption competition by tuning cationic geometric configuration of dual-active sites in spinel oxides. *Angew. Chem. Int. Ed.* **62**, e202216286 (2023).
244. Zhang, C. Y. et al. Identifying the role of the cationic geometric configuration in spinel catalysts for polysulfide conversion in sodium–sulfur batteries. *J. Am. Chem. Soc.* **145**, 18992–19004 (2023).
245. Harada, M., Kotegawa, F. & Kuwa, M. Structural Changes of Spinel MCo_2O_4 (M=Mn, Fe, Co, Ni, and Zn) electrocatalysts during the oxygen evolution reaction investigated by in situ x-ray absorption spectroscopy. *ACS Appl. Energy Mater.* **5**, 278–294 (2022).
246. Alvarez, S. & Cirera, J. How High the Spin? Allowed and forbidden spin states in transition-metal chemistry. *Angew. Chem. Int. Ed.* **45**, 3012–3020 (2006).
247. Wang, Y. et al. Preparation and performance of Mg-doped spinel-structured $LiMn_2O_4$ cathode materials. *Mater. Today Commun.* **33**, 104391 (2022).
248. Zhou, S. et al. Engineering electrocatalytic activity in nanosized perovskite cobaltite through surface spin-state transition. *Nat. Commun.* **7**, 11510 (2016).
249. Tyson, T. A. et al. Valence state of Mn in Ca-doped $LaMnO_3$ studied by high-resolution Mn $K_{?e}$mission spectroscopy. *Phys. Rev. B* **60**, 4665–4674 (1999).
250. Csiszar, S. I. et al. Controlling Orbital Moment and Spin Orientation in CoO Layers by Strain. *Phys. Rev. Lett.* **95**, 187205 (2005).
251. Podjaski, F. et al. Rational strain engineering in delafossite oxides for highly efficient hydrogen evolution catalysis in acidic media. *Nat. Catal.* **3**, 55–63 (2020).
252. Dai, C. et al. Chinese knot-like electrode design for advanced Li-S batteries. *Nano Energy* **53**, 354–361 (2018).
253. Zhang, C.-C., Yuan, S., Lou, Y.-H., Okada, H. & Wang, Z.-K. Physical fields manipulation for high-performance perovskite photovoltaics. *Small* **18**, 2107556 (2022).
254. Chaturvedi, V. et al. Room-temperature valence transition in a strain-tuned perovskite oxide. *Nat. Commun.* **13**, 7774 (2022).
255. Varghese, M. et al. Room-Temperature Mixed Spin State of Co^{3+} in $Sr_2Co_{0.02}Ga_{0.98}NbO_6$ Double Perovskites: combined NMR and EPR studies in a potential inorganic pigment. *J. Phys. Chem. C.* **126**, 8450–8460 (2022).
256. Bhattacharya, S. & Kanai, Y. Spin-orbit-coupling-induced band splitting in two-dimensional hybrid organic-inorganic perovskites: Importance of organic cations. *Phys. Rev. Mater.* **7**, 055001 (2023).
257. Du, Y. et al. Quantum spin exchange interactions to accelerate the redox kinetics in li–s batteries. *Nano-Micro Lett.* **16**, 100 (2024).
258. Yu, J. et al. Promoting polysulfide redox reactions through electronic spin manipulation. *ACS Nano* **18**, 19268–19282 (2024).
259. Zhang, Y. et al. Dual-atoms iron sites boost the kinetics of reversible conversion of polysulfide for high-performance lithium-sulfur batteries. *Energy Storage Mater.* **63**, 103026 (2023).
260. Liu, Q. et al. Dilute alloying to implant activation centers in nitride electrocatalysts for lithium–sulfur batteries. *Adv. Mater.* **35**, 2209233 (2023).
261. Kim, J. et al. Atomic structure modification of Fe–N–C catalysts via morphology engineering of graphene for enhanced conversion kinetics of lithium–sulfur batteries. *Adv. Funct. Mater.* **32**, 2110857 (2022).
262. Yu, H. et al. Atomically dispersed and O, N-coordinated mn-based catalyst for promoting the conversion of polysulfides in Li_2S-Based Li–S Battery. *ACS Appl. Mater. Interfaces* **13**, 54113–54123 (2021).
263. Li, Q. et al. High spin-state modulation of catalytic centers by weak ligand field for promoting sulfur redox reaction in lithium-sulfur batteries. *Angew. Chem. Int. Ed.* **64**, e202416176 (2025).

264. Li, C. et al. Balancing electronic spin state via atomically-dispersed heteronuclear fe–co pairs for high-performance sodium–sulfur batteries. *J. Am. Chem. Soc.* **147**, 8250–8259 (2025).
265. Tian, S. et al. Deposition mode design of Li_2S: transmitted orbital overlap strategy in highly stable lithium-sulfur battery. *Adv. Funct. Mater.* **34**, 2309437 (2024).
266. Song, Y. et al. Rationalizing the impact of oxygen vacancy on polysulfide conversion kinetics for highly efficient lithium-sulfur batteries. *J. Energy Chem.* **87**, 51–60 (2023).
267. Larionov, K. V., Pais Pereda, J. J. & Sorokin, P. B. A DFT study on magnetic interfaces based on half-metallic $Co_2FeGe_{1/2}Ga_{1/2}$ with h-BN and $MoSe_2$ monolayers. *Phys. Chem. Chem. Phys.* **24**, 1023–1028 (2022).
268. Ciancio, R. e-DREAM: the European Distributed Research Infrastructure for Advanced Electron Microscopy. *Microsc. Microanal*. **28**, 2900–2902 (2022).

Acknowledgements

This work was financially supported by the SyDECat project from the Spanish MCIN/AEI/FEDER (PID2022-136883OB-C22). The authors acknowledge support from the 2BoSS project of the ERA-MIN3 program with the Spanish grant number PCI2022-132985/AEI/10.13039/501100011033 and from Generalitat de Catalunya 2021 SGR 01581 and European Union NextGenerationEU/PRTR. J. Yu, C. Huang, C. Li, and Y. Ren thank the China Scholarship Council for the scholarship support. G. W. Sun thanks the Fundamental Research Funds for the Central Universities (lzujbky-2023-it36), and the Outstanding Graduate "Innovation Star" Project of Gansu Provincial Education Department, China (No.2023CXZX-058). J. S. Li acknowledges financial support from the Natural Science Foundation of Sichuan province (2022NSFSC1229). The authors also greatly acknowledge the support from the Supercomputing Center of Lanzhou University, China. D.W.Y. acknowledges support from the National Natural Science Foundation of China (NSFC) (Grants No. 22305064). M.E. acknowledges support from 'Departament de Recerca i Universitats: del Departament d'Acció Climàtica, Alimentació i Agenda Rural i Fons Climàtic de la Generalitat de Catalunya' with the grant 2023CLIMA00022. The Catalan Institute of Nanoscience and Nanotechnology (ICN2) acknowledges funding from Generalitat de Catalunya 2021SGR00457. Authors acknowledge the Advanced Materials programme (Project In-CAEM) by the Spanish Government with funding from European Union NextGenerationEU (PRTR-C17.I1) and by Generalitat de Catalunya. The authors are grateful for support from the project AMaDE (PID2023-149158OB-C43), funded by MCIN/ AEI/10.13039/501100011033/ and by "ERDF A way of making Europe", by the "European Union". ICN2 is supported by the Severo Ochoa program from Spanish MCIN / AEI (Grant No.: CEX2021-001214-S) and is funded by the CERCA Programme / Generalitat de Catalunya. ICN2 is founding member of e-DREAM[268].

Author contributions

C.Y.Z. contributed conceptualization and methodology; J.Y. contributed methodology and data curation; C.H. contributed formal analysis and investigation; G.C. contributed data curation; X.D.Q. contributed software and visualization; G.W.S. contributed visualization and resources; C.Q.Z. contributed validation and formal analysis; R.H. contributed Investigation And Data Curation; D.W.Y. contributed formal analysis and writing—review & editing; C.H.L. contributed investigation and writing—review & editing; J.S.L. contributed data curation and resources; X.Q.Qi. contributed conceptualization, supervision and writing—review & editing; J.R.G. contributed supervision and writing—review & editing; M.E. contributed supervision and visualization; J.A. contributed supervision and resources; J.Y.Z. contributed conceptualization, methodology, supervision, and writing – review & editing; A.C. contributed conceptualization, funding acquisition, resources, supervision, and writing—review & editing. C.Y.Z. and J.Y. contributed equally to this work.

Competing interests

Submission of a competing interests statement is required for all content of the journal.

Additional information

Supplementary information The online version contains supplementary material available at https://doi.org/10.1038/s43246-025-00976-z.

Correspondence and requests for materials should be addressed to Javier Rubio Garcia, Marta Estrader, Jin Yuan Zhou or Andreu Cabot.

Peer review information *Communications Materials* thanks Anil D. Pathak, Deyang Qu and Aqsa Nazir for their contribution to the peer review of this work. A peer review file is available.